UNIVERSITÀ DEGLI STUDI DI NAPOLI FEDERICO II

XXIVth PhD COURSE IN INNOVATIVE TECHNOLOGIES FOR MATERIALS, SENSING AND IMAGING

Thin Film and Single Crystal Organic Heterostructure Field Effect Transistors based on Perylene Diimide compounds

PhD SUPERVISOR

Dr. Antonio Cassinese

PhD STUDENT

Flavia Viola Di Girolamo

21 December 2011

Contents

To my parents....

"I love to collect pearls, and your eyes are the purest I have ever seen. If you will weep those eyes away in tears into my waters, then I will take you to the large hothouse where Death dwells and rears flowers and trees, every one of which is a human life." The story of a mother, H.C. Andersen

Introduction

Organic semiconductors offer different advantages respect to their inorganic couterparts, such as the realization of flexible and large area devices, but the electrical properties and the stability are poorer, even if nowadays comparable with amorphous silicon. Several attempts have been made to improve the performances of organic semiconductors; a successful approach in this direction resides in the realization of devices based on junctions between a p-type and a n-type organic semiconductor in which an increase of the density of the majority charge carriers is realized at the interface in both the semiconductors (accumulation heterojunctions).

This approach leads to several advantages, since the electrical properties arising at the interface as consequence of the energy bands alignment can be exploited for innovative applications. Doping, ambipolar operation, improvement of the morphological and structural properties of evaporated thin films are some examples. An increase of the device performances has been experimentally verified, with an improvement of conductivity (even mobility in some cases) in field effect transistors and of quantum efficiency in light emitting devices.

This PhD thesis deals with the study of Organic Heterostructure Field-Effect Transistors, basically realized using two organic semiconductors forming an accumulation junction as the active channel in field effect devices. Organic semiconductors both in the form of thin films and single crystals have been considered. Concerning the thin film heterostructures, this thesis has been developed in Naples, at the Department of Physics of the University Federico II and at the CNR-SPIN, while the single crystal growth and the fabrication of the related micrometric scale devices have been led at the Departement de la Matiére Condensée (DPMC) of the University of Geneva.

In the following, the thesis outline is reported. The first chapter provides some general definitions and concepts which represent the theoretical basis of the experimental results reported

in the following chapters. A fundamental step in the realization of thin film heterostructures is the choice of the most suitable n-type semiconductor. Electrical instability and charge trapping phenomena represented an issue that has limited until recently the realization of n-type devices and of p-n heterojunctions, which represent the building block for a wide class of devices. The second chapter will be consequently devoted to the results obtained from the study and the comparison of three different n-type organic semiconductors belonging to the class of perylene diimides oligomers.

The third chapter is instead dedicated to the experimental results obtained of thin film heterostructure field-effect transistor. The vacuum evaporation and the fabrication procedure have been carefully optimized and the obtained devices have been morphologically, structurally and electrically characterized. The electrical characterization of these devices exhibits several interesting features, such as evidences of a charge transfer phenomenon at the interface, a dependence of the electrical properties on the thickness and an unexpected decrease of the drain source current for increasing negative gates.

The last chapter is dedicated to Schottky gated single crystal heterostructures. In the device configuration the heterostructure is formed by PDI-FCN_2 and rubrene single crystals; rubrene is laminated on a chromium stripe, with which it forms a Schottky barrier. Transfer curves indicates band-like behavior down to less than 150 K, with the electron mobility remaining as high as 1 cm^2/Vs at 50 K in the best devices. Furthermore, the charge carrier density at $V_G = 0$ exhibits a linear temperature dependence. The results can be explained using a simple model accounting for the alignment of the rubrene HOMO band with the bottom of the LUMO band of PDI-FCN_2.

Chapter 1

Organic interfaces and field effect devices: tuning the surface carrier density

This chapter provides some basic concepts, concerning the definition of organic semiconductors and describes the strategies that can be adopted to tune the surface density of carriers in semiconductors: surface doping, for instance, or the application of an electric field. In this regard, two typical field effect device architectures are the Metal Oxide Field Effect Transistor (MOSFET) and the MEtal Semiconductor Transistor (MESFET).

A further way to induce "engineered" modifications in the transport properties of semiconductors resides instead in the realization of heterostructures. The variety of the combinations can indicate innovative solutions to the realization of devices and the requirement of the equilibration of the chemical potential at the interface induces novel and unexpected electrical properties.

In the framework of organic semiconductors, the most interesting application of heterostructures resides in the improvement of the electrical performances and stability of the devices, while the most prominent physical findings have been observed in heterostructures realized with organic semiconductors in a single crystal form. Organic single crystals represent indeed a perfect subject to the clarification of the origins of the charge transport properties in organic semiconductors, due to the high stability and reproducibility of their electrical properties.

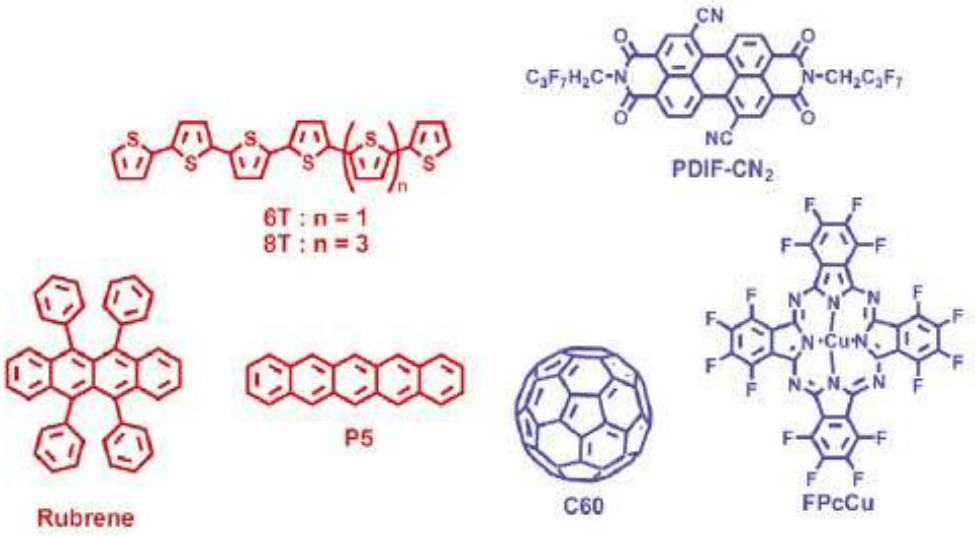

Figure 1-1: Some examples of p-type (in red) and n-type (in blue) organic semiconductors oligomers [3].

1.1 Organic semiconductors

Organic semiconductors are characterized by the presence of several conjugated (π) bonds, like in the case of benzene or thiophene rings, which justifies their label of "conjugated" compounds (Fig. 1-1). In this framework we can distinguish between polymers and oligomers, depending on the molecular weight. Films of organic semiconductors can be obtained through high vacuum deposition (see 2 and 3) or from solution, while single crystals are grown through condensation from a vapour phase (see 4).

Each conjugated chemical bond provides one unpaired electron (the π electron) per carbon atom, due to the delocalized nature of the π orbital wave function (sp_2pz configuration, see for instance Fig.1-2 a)). The overlapping between π orbital wave functions of successive carbon atoms leads to electron delocalization along the molecule, which provides the route for charge mobility. Of course, closer the π orbital wave functions, more efficient the overlapping, higher the electrical properties; symmetry and crystalline order thus play a striking role, since as higher they are, as higher electrical properties arise [1] [2].

The features of these systems can be summarized as follows: orbitals instead of atomic

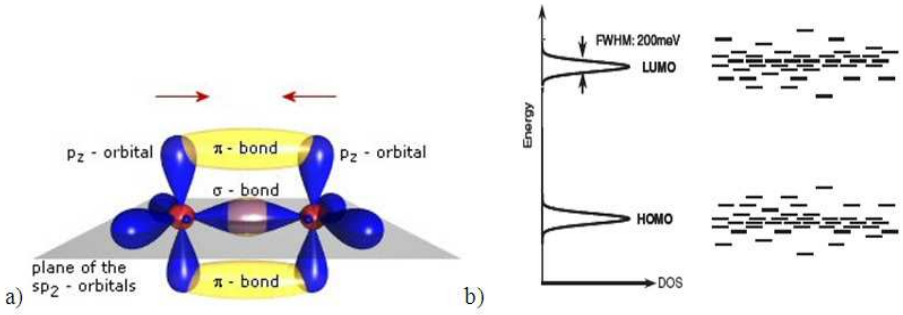

Figure 1-2: a) and bonds in a methane molecule. b) LUMO and HOMO level with the relative Gaussian distribution of states.

wave functions overlap; the carriers involved in the electrical conduction cannot be considered as "free", in the sense that the free electron model cannot be applied since the charges are not sufficiently localized; the number of carriers involved is less than in inorganic compounds, since we have only one per molecule, instead than per atom. Consequently, nor the classical band model, neither the concepts of valence and conductance bands can be applied.

Instead of atomic bands, it is possible to introduce the concept of molecular bands, and the Lowest Unoccupied Molecular Level (LUMO) and Highest Occupied Molecular Level (HOMO) will play the role of the minimum of the conductance band and the maximum of the valence band, respectively (see Fig.1-2 b)). Moreover, since these organic semiconductors have not "free" carriers, they come from the electrodes; as a consequence, the electrical properties are strongly affected by the energy difference between the Fermi level of the electrodes metal and the energy of the closest molecular level. Indeed, higher is the difference, more the device will suffer from contact resistances; moreover, depending on which molecular orbital is closer in energy, the semiconductor will behave as an p-type (if the closer level is the HOMO) or as a n-type (LUMO) [4]. Actually, most of the organic semiconductors tend to exhibit just unipolar behaviour, in particular p-type, for reasons linked to trapping of charges (see for instance [5] and further).

They can be included in the definition of "compensated" semiconductor, in the sense that they are not intrinsic but that they have an equal concentration of p and n dopants, even if the concept of doping is completely different from the case of inorganic semiconductors.

Figure 1-3: Fig. Bracelet with an organic light emitting display [9].

1.1.1 Electron transporting organic semiconductors

Since the beginning of the research on organic semiconductors, the study concerning charge transport and the device realization has been mostly devoted to hole transporting compounds, since electron transport was rarely observed and the performances of the devices were poorer [6].

One of the reasons behind this occurrence basically consists on the misalignment between the LUMO level of n-type compounds (around – 2 / -4 eV) and the workfunction of the electrodes (i.e. the Fermi level of gold is around 5 eV) [7] [8] ; consequently, the first generation of transistors with n-type semiconductors was realized with low workfunction electrodes (i.e. Ca). Electron conduction has been also observed in compounds with a higher LUMO level [5], or using surface treatments [10]. The last two observations, in particular, suggested an alternative picture behind the behaviour of n-type compounds, related to an higher susceptibility of electrons to be trapped.

de Leeuw et al. [5] have considered redox reactions involving the electron transporting compound and oxygen or water and have determined the ranges of redox potential in which redox reactions are less favourites and compounds are consequently expected to be more stable

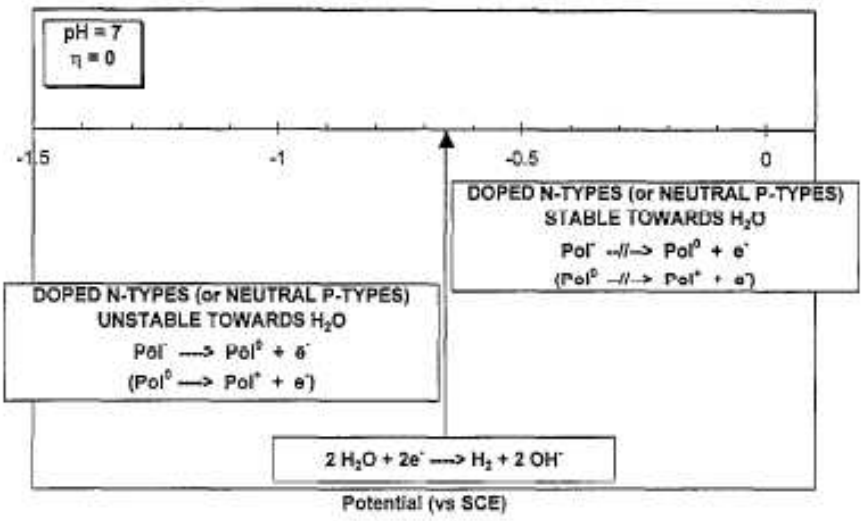

Figure 1-4: Table illustrating the stability conditions of n-type towards water redox reduction [5].

(see the table in Fig.1-4). This study indicates the way to be covered to synthesize stable n-type compounds, also encouraged by good agreement with experimental results.

Field effect transistors have been realized with opportunely treated substrate before organic semiconductor deposition and the electrical properties measured. The occurrence of electron transport only in transistors with surface treatments passivating hydroxyl (Si-OH) groups suggested an interface trapping phenomenon: the injected electrons can indeed be electrochemically trapped as immobile surface Si-O- ions following the subsequent reaction (see in Fig. 1-5) [10]:

$$\mathrm{Si}\,OH + e^- \Rightarrow \mathrm{Si}\,O^- + H_2(g) \tag{1.1}$$

Following the indications provided by the works reported above, novel strategies were developed to realize n-type devices, basically passivating the substrate or functionalizing existing compounds with withdrawing groups. In this case, the treatment is aiming to lower the LUMO level, both to facilitate the injection of charges from higher workfunction electrodes and to increase the redox potential in order to render the compounds less susceptible to reactions with water and oxygen.

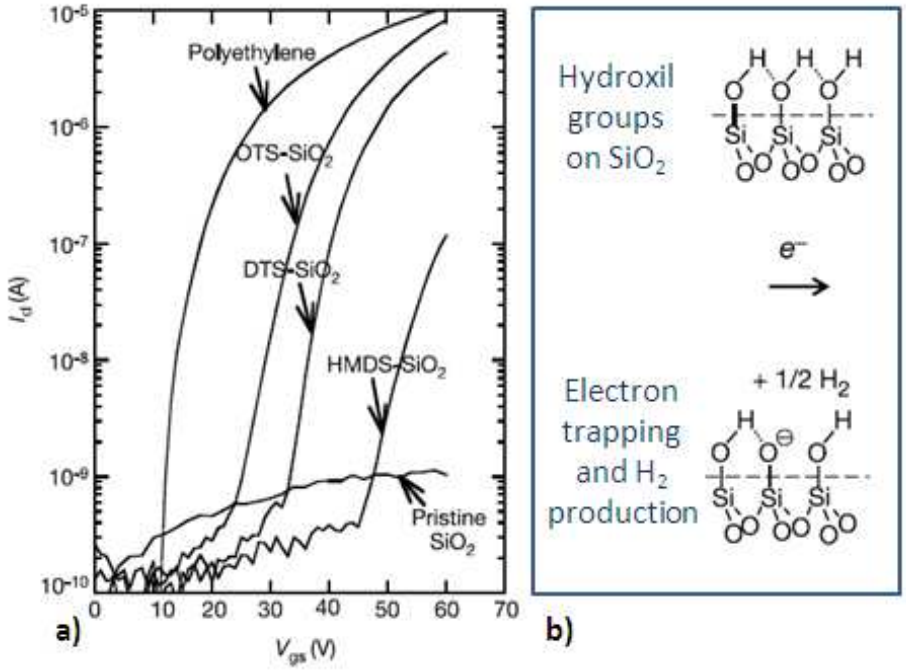

Figure 1-5: The effect of the surface treatment in the stability of n-type semiconductors [10]; a) transfer curves for devices with different surface treatments, b) the electron trapping by hydroxil groups on SiO_2.

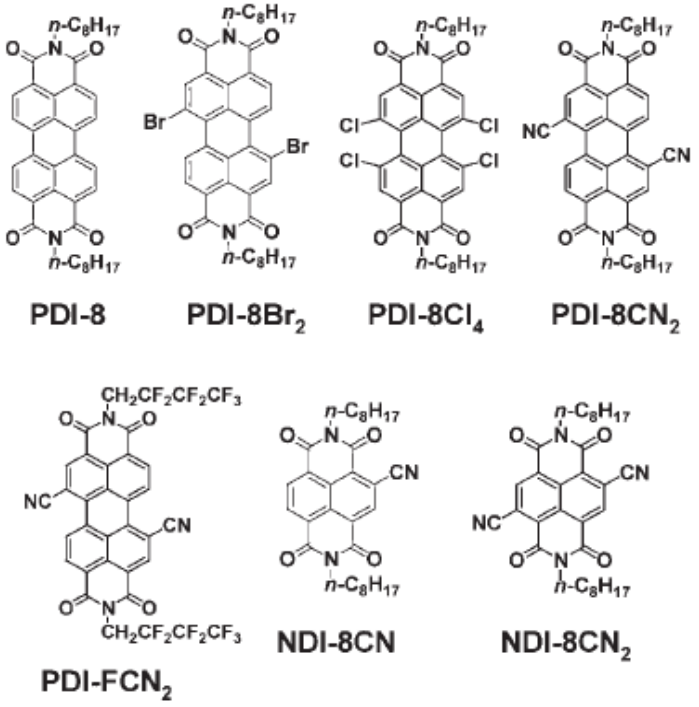

Figure 1-6: Some compounds belonging to the class of perylene diimides [12].

Perylene diimides were found to be an interesting class of electron transporting semiconductors [11], since they exhibited high stability owing to the presence of withdrawing groups [12], such as fluorinated [13] [14] or cyanated [15] ones. The absence of functionalizing groups, can be compensated by surface treatments [16].

Jones et al. [17] have obtained several arylene – based compounds (Fig. 1-6), functionalizing the molecules with suitable withdrawing groups; a comparison has been performed between the LUMO, the molecular geometries, the electronic properties and stability of the devices realized (see Fig.1-7 a)) . They also suggested a further possible origin of instability, residing in geometrical distortions of the molecule, which reduce the $\pi - \pi$ overlap and create free space between two molecules, which represents a preferential channel for oxygen and water diffusion (see Fig.1-7 b)). The results confirm that core – substituting groups should be chosen in order to minimize the reaction with oxygen and water, but also the geometrical molecular distortions.

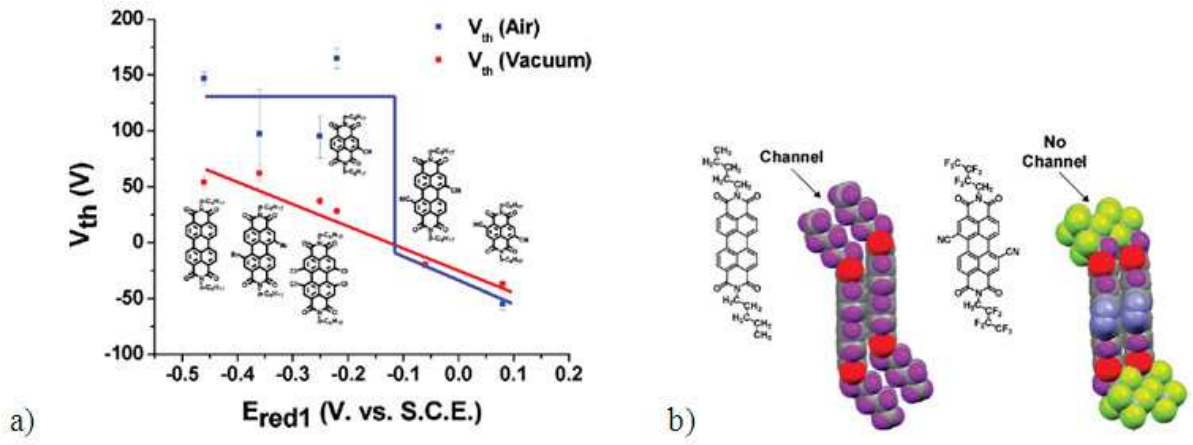

Figure 1-7: Fig. a) The comparison between the electrical performances in vacuum and in air with the chemical properties; b) the illustration of the mechanism which explains the air instability in some n-type semiconductors [17].

1.2 Tuning the carrier density at organic surfaces and interfaces

The manipulation of the electronic properties of a semiconductor offers the possibility to control the electronic transport and the device performance, and consequently it represents an unavoidable step in the realization of efficient electronic devices [18]. There are several strategies to modify the carrier density, by introducing chemical dopants (i.e. chemical doping), by applying an electric field (i.e. electrostatic doping) and by the Fermi level alignment at metal-semiconductor and semiconductor-semiconductor interfaces (i.e. modulation doping, surface doping, Schottky contacts, energy band engineering at heterointerfaces).

The common strategy used to modify the carrier density is the chemical doping, which instead results not to be the more suitable one when an increase of mobility is required, since introducing impurities carries unavoidably to an increase of disorder, at least in the case of disordered systems such as organic semiconductors [19]. An alternative method of doping, for instance, is the surface doping, which basically consists of an heterojunction of semiconductors with different Fermi level and gap. Their choice can be made in such a way that the alignment of the Fermi levels and the consequent charge transfer at the interface leads to an increase rather than a decrease of the density of carriers and consequently to an accumulation rather than a depletion junction. This is the case of the High Electron Mobility Transistor (HEMT),

in which an increase of mobility, and in particular a more pronounced metallic – like behaviour of the mobility is found. The absence of impurities introduces less disorder and makes possible the formation of a 2D electron gas and the observation of a metallic-like behaviour. Indeed, the doping material and the doped region are spatially separated [20], introducing the concept of modulation doping [21]; a bidimensional electron gas forms at the interface and can be tuned by the application of an electric field [22].

Chemical and modulation doping induce an irreversible modifications in the carrier density of the semiconductors. Conversely, the space charge regions consequent to the accumulation or depletion of charges after the application of an external electric field, return again neutral when the electric field is removed. Electrostatic doping consequently represents a "clean" (since it does not introduces impurities) and the sole reversible doping strategy available. Electronic properties of materials and interfaces can be tuned by electrostatic doping, even inducing, in the best cases, phase transitions between different states of the matter, destruction or formation of energy gap at Fermi level, modification in the value of magnetic or superconducting temperatures [19].It represents the working principle of field effect devices, such as Metal Oxide Semiconductor Field Transistor (MOSFET) and Metal Semiconductor Field Effect Transistor (MESFET).

In the following subparagraphs, some aspects of the tuning of carrier density in organic semiconductors will be discussed, referring in particular to surface doping, organic field effect transistor and organic MESFET. Issues linked to the modification of the carrier density in heterostructures require more space and will be the subject of the following paragraphs.

1.2.1 Doping

Surface doping represents the most promising way to modulate the electrical properties of organic semiconductors (and not only, see for instance [23]) without inducing a high level of disorder. It has been demonstrated that it can also allow a control of the degree of doping depending on the area of the semiconductor covered by the dopant: as higher the coverage, as higher the doping effect [24].

The main principle of the doping effect is basically the deposition of a dopant (usually insulating molecular compound) on the surface of the material to be doped. For a schematic picture of the phenomenon, see for instance the Fig 1-8 [23] where the energy level alignment

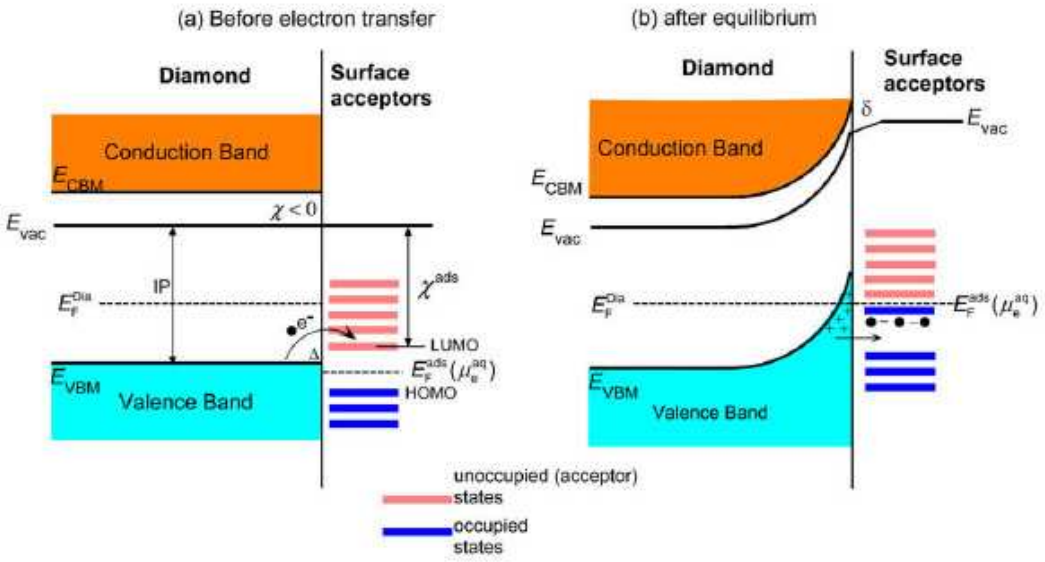

Figure 1-8: A picture illustrating the surface doping phenomenon [23].

induces the transfer of an electron from the valence band of diamond to the LUMO level of the dopant; this causes an increase of the density of holes, band bending in the diamond, an increase of electron density and the formation of an interface dipole in the insulating dopant. Of course, the vice versa happens for a n-type dopant.

This qualitative picture is enough to understand that an analysis of the energy levels at the interface is necessary to assess the magnitude of the doping and eventually distinguish between contributes due to band bending and to the formation of an interface dipole. This analysis can be developed through photoelectron spectroscopy, a family of techniques which have been widely used to understand the phenomena arising at the semiconductor interfaces [25]. Efforts in clarifying the energy levels alignment at organic – organic and organic – inorganic interfaces, to understand the nature of the doping effect, and Ultraviolet Photoemission Spectroscopy (UPS) and related techniques have been widely used for this purpose [26] [27] [28] [29] [30].

1.2.2 Organic Thin Film Transistor

A transistor is a three terminal device and can be simply viewed as a variable resistor. The basic architecture is composed by a gate electrode separated from the semiconductor by a

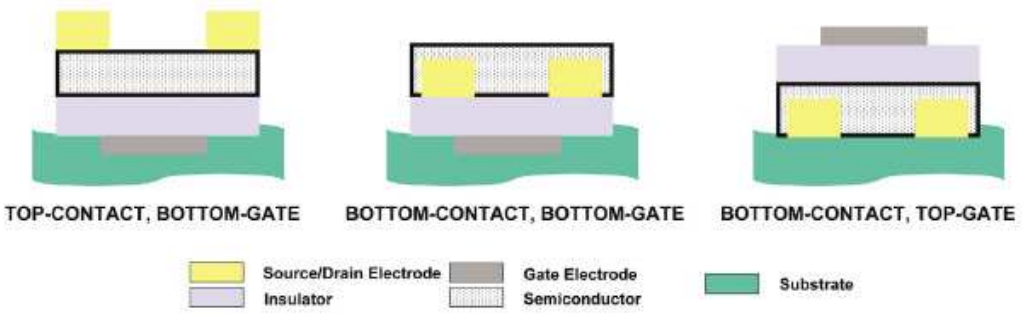

Figure 1-9: Schematic of the three TFT configurations [3].

dielectric layer, drain and source contacts of lenght L separated by a distance W. Provided these four components, there are three different possible configurations, reported in Fig.1-9. The resistance of the semiconducting channel can be varied depleting or accumulating charges at the interface with a dielectric by applying the potential to the gate (V_{GS}). Charges are injected from source (usually grounded, $V_S = 0$), while the potential applied to drain (V_{DS}) regulates the current flowing through the device (drain source current, I_{DS}).

In order to have the formation of the conductive channel between source and drain and consequently conduction between the two electrodes, a sufficient drain voltage has to be applied, and the gate voltage has to be greater than a specific voltage value named as threshold voltage (V_{th}). This value is associated to the presence of traps in the gap of the organic semiconductor and is commonly defined as the value of the potential at which all the traps in the gap are filled and the conduction takes place through delocalized states.

The principle of operation is the following. As a potential to the gate is applied, charges are accumulated in the channel, at the interface with the dielectric. If $V_{DS} = 0$ the potential is in the channel uniform, while applying a potential to the drain contact, an electric field arises between the source and the drain contact and potential vary linearly. At high V_{DS} voltages (i.e. satisfying the condition $V_{DS} > V_{GS}$ - V_{th}) a depletion region is formed near the drain (pinch-off condition); a space charge limited current flows through the depletion region which is now no more dependent on V_{DS}. The current, consequently, does not increase anymore with V_{DS}.

The current voltage characteristics can be distinguished depending if the drain or the gate

voltage is swept. If the variation of the drain current respect to the drain voltage at a fixed gate is considered, than we are measuring an output curve, conversely a transfer curve (Fig. 1-10).The transfer-curves can be modelled by using the standard MOSFET equations in linear and saturation regimes, respectively:

$$I_{DS} = \frac{W\mu C_D}{L}\left(V_{GS} - V_{th}\right)V_{DS}$$

$$I_{DS} = \frac{W\mu C_D}{2L}\left(V_{GS} - V_{th}\right)^2 \tag{1.2}$$

where W and L are, respectively, the channel width and length, C_D is the dielectric barrier capacitance per unit area and V_{th} is the threshold voltage. Based on these expressions, the field effect mobility (μ) can be easily evaluated both in linear and saturation regions by the relations, respectively:

$$\mu_{lin} = \frac{\partial I_{DS}}{\partial V_G}\frac{L}{WC_D V_{DS}} \tag{1.3}$$

$$\mu_{sat} = \left(\frac{\partial\sqrt{I_{DS}}}{\partial V_G}\right)^2 \frac{2L}{WC_D} \tag{1.4}$$

The conductance of organic semiconductors is fairly lower than that of inorganic semiconductors; a specific device architecture designed on purpose has been consequently used. This configuration is the Thin Film Transistor (TFT) [31] and differs from MOSFET in several features.

Since the organic semiconductor are unintentionally doped, the conducting channel is induced in the accumulation regime rather than through the formation of an inversion layer. This simplifies the modelling of the device, in that a further simplification is possible in obtaining the MOSFET equations. In order to maintain the validity the Shockley assumption that the transversal field (i.e. the one applied by the gate) should be greater than the longitudinal one (i.e. applied at the drain) the thickness of the dielectric layer is required to be lower than the channel length, which justifies the name of the device.

The principle of operation of the device has been widely studied [32], and several non-ideal behaviours have been found, such as the gate dependent mobility and the bias stress instability. The dependence of the mobility on the gate is a consequence of the unconventional distribution

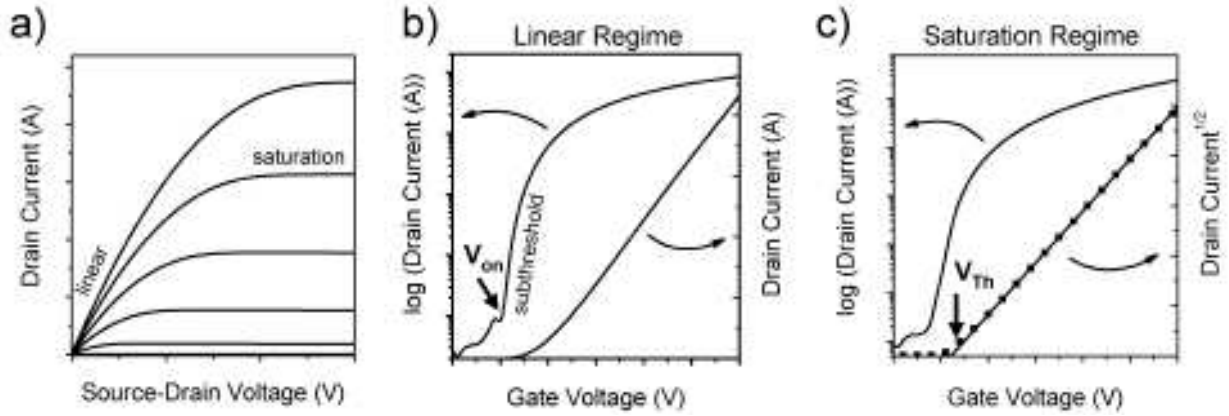

Figure 1-10: Representative current-voltage characteristics of an n-channel organic field-effect transistor: (a) output characteristics indicating the linear and saturation regimes; (b) transfer characteristics in the linear regime (Vd , Vg), indicating the onset voltage (Von) when the drain current increases abruptly; (c) transfer characteristics in the saturation regime (Vds > Vg - VTh), indicating the threshold voltage VTh, where the linear fit to the square root of the drain current intersects with the x-axis [7].

of carriers in organic semiconductor layers [33] while the dependence on the temperature is due to the transport properties in the organic layer, and in particular to the presence of traps in the gap [34].

Bias Stress Effect

One of the main issues affecting the operation stability of Organic Field Effect Transistors (OFETs) concerns the so-called Bias Stress Effect (BSE). This phenomenon is caused by the prolonged application of the Gate-Source (V_{GS}) voltage and consists in the time decay of Drain-Source (I_{DS}) current at any fixed Drain-Source (V_{DS}) voltage [35] [36]. So far, two main experimental approaches, both in DC regime, have been used to investigate the BSE occurrence. The former relies on the analysis of time shift of the transistor threshold V_{th} voltage, which can be determined from the plot of the transfer-curves through geometrical criteria [35]. The latter is based on the direct observation of transistor I_{DS} time decay upon static voltage polarization (fixed V_{DS} and V_{GS}) [37]. In both cases, the time behaviour of the measured parameters can

be modelled by formulas based on the stretched exponential function [38] [39]:

$$I = I_0 + I' \exp\left[-(\frac{t}{\tau})^{\beta}\right] \tag{1.5}$$

This occurrence reflects the dispersive nature of BSE, basically accounting for a wide distribution of characteristic times in the elementary trapping processes.

The physical origin of BSE has been mainly ascribed to the presence of active trapping sites. Traps are related to intrinsic structural defects (e.g. grain boundaries [40] , organic – dielectric interface [41]) and/or to defect-attracted impurities (e.g. water or oxygen) [42]. Nevertheless, the physical localization (e.g. at the interface with dielectric [41], in the film bulk or at the contact regions near the Source-Drain electrodes [43] [44]) and the basic mechanism behind the bias stress phenomenon in organic field effect transistors has been not completely clarified yet.

The origin of the trapping phenomenon is under discussion; for p-type semiconductors, Sharma et al. [45] [46] invoke a proton migration mechanism involving water, whereas Lee et al. [47] assume direct drift/diffusion of holes into the dielectric.

The mechanism proposed by Sharma is based on the observation of the production of H_2 ions for electrolisys from water on SiO_2. Scanning kelvin probe measurements on bare SiO_2 substrates provided of gold electrodes (i.e. the basic structure of an OFET device but without the organic semiconductor) have indeed demonstrated the arising of a potential profile after the application of a drain bias; the time evolution of the potential profile is independent from the sign of the drain voltage, suggesting that always the same type of charge carriers are involved [48]. Furthermore, the potential increases with the level of humidity while decreasing using hexametyldisilazane (HMDS) surface treatment. This result can be explained accounting for a motion of protons, present on the surface of SiO_2 because of the reaction

$$\mathrm{Si}\,OH \Leftrightarrow \mathrm{Si}\,O^- + H^+ \tag{1.6}$$

When a positive voltage is applied to the drain, oxidation of water occurs in the proximity of the electrodes

$$H_2O \Rightarrow 2H^+ + 2e^- + \frac{1}{2}O^2(g) \tag{1.7}$$

provoking a diffusion/drift of protons toward the source and a positive potential profile. Con-

versely, when a negative voltage is applied a deficit of protons arises

$$2H^+ + 2e^- \Rightarrow H_2(g) \tag{1.8}$$

which causes the motion of protons from the source and a negative potential.

When a p-type semiconductor is deposited on the SiO_2 substrate, the protons present on SiO_2 surface and moved by the application of a drain bias react with holes (OS^+) producing neutral species (OS) following the reaction

$$2H_2O + 4OS^+ \Leftrightarrow 4H^+ + O_2(g) + 4OS \tag{1.9}$$

This last equation, with the production of neutral species from holes corresponds indeed to a trapping phenomenon. In the SiO_2, protons in the bulk are naturally present, which concentration is in equilibrium with that on the surface. Once the concentration on the surface increase by consequence of the 1.9, a diffusion of protons in the dielectric arises. The proton migration can explain the exponential behaviour exposed above, following the derivation reported in [45] and neglecting the protons drift contribution.

The model proposed by Lee et al. instead, does not involve the presence of water and as an "intrinsic" bias stress effect is cosidered. They study the bias stress effect in single crystals, in transistors realized with a polymeric dielectric (parylene); in this case, a migration of holes from the conduction channel of the OFET into the localized states of the dielectric is involved. The rate of trapping results consequently to be directely dependent on the energetic overlap between the tail of the semiconductor HOMO and the localized states in the insulator (indicated by the parameter δ_0). When the diffusion of holes into the insulator dominates over the drift, the bias strass is proportional to n_{ch} (the density of mobile holes present in the channel) or V_G and the current decay is described by an exponential relation identical to the one reported above (1.5). τ is V_G independent and is given by

$$\tau = \tau_{ins} \bullet [\frac{\lambda_0 \beta}{\chi_0 D_0 \delta_0 \tau_{ins}}]^{\frac{1}{\beta}} \tag{1.10}$$

where τ_{ins} is the characteristic trapping time in the insulator, λ_0 is a characteristic width of the spatial distribution of holes in the insulator near the interface, χ_0 is a cross section of the

charge tranfer process in square centimeters. Conversely, if the drift dominates over diffusion, the rate will be proportional to n_{ch}^2 or V_G^2 and the phenomenon is described by a stretched hyperbola

$$I_{SD}(t) = \frac{I_0}{1 + (t/\tau)^{\beta}} \tag{1.11}$$

where τ is instead V_G dependent

$$\tau = \tau_{ins} \bullet [\frac{\beta d}{V_G \chi_0 \mu_0 \delta_0 \tau_{ins}}]^{\frac{1}{\beta}} \tag{1.12}$$

where d is the insulator thickness.

1.2.3 Schottky contact and Metal Semiconductor FET

The surface carrier density can be tuned by the application of an electric field in devices with different configurations and using different principles of operation to induce charges at the interface between two different material layers.

In the previous section, we have seen that in the most common FET configuration this goal is achieved by means of a capacitive architecture. In a Metal Semiconductor FET (MESFET), instead, the carrier density is regulated by extending or reducing the depletion layers that forms at a metal-semiconductor interface (Schottky contact) by the application of an external voltage. The basic architecture of the device (n.b. with an organic semiconductor) is illustrated in Fig. 1-11 a).

A Schottky contact differs from a conventional ohmic contact in that the current magnitude depends on the polarity of the voltage applied and the contact is consequently recifying. Due to the Fermi level difference between the semiconductor and the metal, a barrier forms (i.e. see Fig.1-12). The barrier length equals the difference between the Fermi level of the metal and the conduction band edge for a n-type semiconductor, while it is given by the gap minus the difference between the Fermi level and the valence band edge for a p-type one. In the first case, the contact is rectifying for positive voltage applied to the semiconductor, conversely we have the opposite.

As a consequence of the alignment of the Fermi levels at the interface, also a depletion region arises. When a voltage is applied, its width can either increase or decrease, depending if

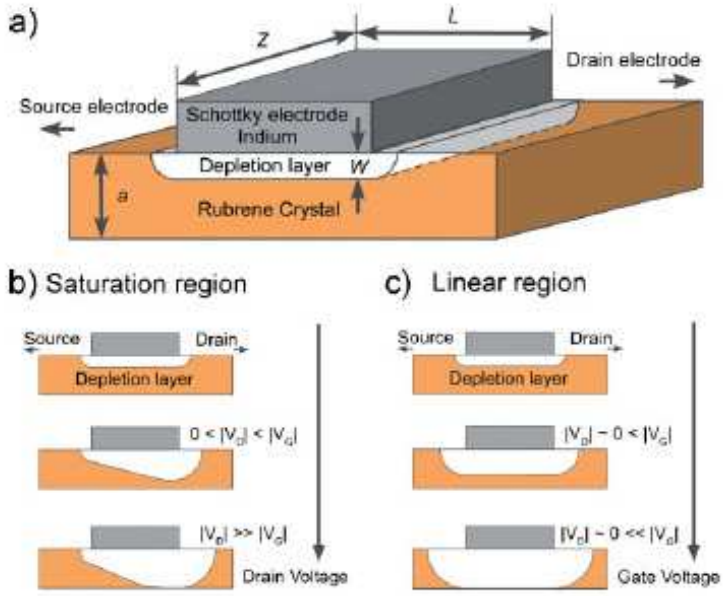

Figure 1-11: Schematic of the device structure and of the working principle of a MESFET [49]

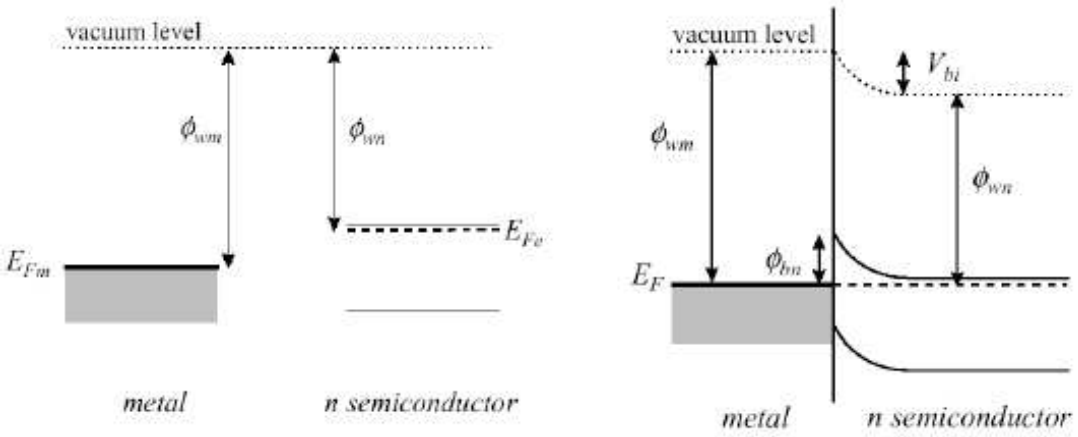

Figure 1-12: Schematic of the energetics before and after the formation of the contact for an n-type semiconductor.

a forward or a backward potential is applied. The barrier height, as we have discussed before, only depends on the energetic of the materials involved, thus is supposed to be independent by the applied voltage. Actually the situation is different, since a barrier lowering effect due to an image force effect is noticed. Also the interfacial impurities play a striking role in the effective value of the Schottky barrier height, in that they form an interface dipole which became an additional unexpected contribute.

After the application of a reverse bias the Schottky barrier hinders the conduction. Nevertheless, also in this last case a conduction is observed, due to several contributes, such as tunnelling or thermoionic emission.

These concepts turn out useful in the description of the principle of operation of a MESFET, which is the main purpose of this section. The basic configuration of a MESFET is (in order) a metal layer, a doped semiconductor layer and source and drain contacts. The metal and the semiconductor are chosen in such a way that a Schottky contact forms at the interface.

Basically we know that varying the potential applied to the metal, the width of the depletion layer can be varied, and so the density of carrier on the surface of the semiconductor. It is worth to mention that the semiconductor has to have free carriers, and has to be necessarily doped. Consequently, the MESFET results to be an always on transistor, depleting carriers rather than accumulating them. Apart from that, the current voltage characteristic are completely the same than in a traditional MOSFET.

1.3 Heterostructures

Heterojunctions are combinations of two or more semiconductors with different gap; the combination of two semiconductors offer several advantages, since the novel electrical properties arising from the alignment of the Fermi levels at the interface can be exploited as the operation principle of innovative electronic devices.

Diodes, for instance, but also lasers, light emitting diodes (LEDs), solar cells, are based on heterostructures [18]. The alignment of the energy level at the interface has been used to engineer the electronic properties of the devices, in that carriers are driven and eventually accelerated from the field arising at the heterointerfaces in order to improve the performances of lasers and transistors [50] [51] [52].

Organic semiconductors are narrow band materials as the electronic interaction and long-range coupling between the molecules is much weaker than those between atoms in inorganic semiconductors. Due also to the strong localization of charges [53] [54], the application of standard theoretical frameworks, usually employed for the inorganic semiconductors, may reveal to be somewhat inadequate to describe the electronic properties of organic semiconductors. Indeed, in many cases, the Fermi level alignment between two organic compounds (which represents the basic process characterizing the properties of semiconductor heterojunctions at equilibrium) can be hindered by the strong localization of charges and by the lack of sufficient number of mobile charges [26].

On the other hand, the results discussed in the recent literature give instead a clear indication that the 'classical' picture based on the Fermi level alignment can work, such as in phenomena of charge transfer, band bending, interface reconstruction (electronic as well as structural) and surface transfer doping [24], which represents a tool for the controlled and non-destructive doping of organic semiconductors. It was experimentally found that these processes can induce a noticeable enhancement of the electrical conductivity in the investigated systems and even insulator to metal transitions, as remarkably shown in the case of the interface between Tetrathiofulvalene (TTF) and 7,7,8,8-tetracyanoquinodimethane (TCNQ) single crystals [55] [56].

On the other hand, the alignment of Fermi levels at organic interfaces reveals to be not expectable neither easily explainable. Indeed, several examples of heterostructure field-effect transistors which do not exhibit interface charge transfer signatures have been reported [57] [58], such as the absence of molecular level bending upon metal deposition on a para-sexiphenil film [59] and flat band condition after contact between materials with different work functions [60] [61]. Several attempts to clarify the charge transfer physics [62] [63] and mechanisms [64] at the organic-organic interface have been made, but the overall picture is not clear yet [65].

1.3.1 Ambipolar transistor

The ambipolar or bipolar FET (n.b. the definition of the term results quite misleading, see for instance [66]), is basically a device in which both electrons and holes can be accumulated by field effect in the operation channel, thanks to particular properties of the semiconductor or to a specific architecture of the device (i.e. a p-n heterostructure composing the active channel of

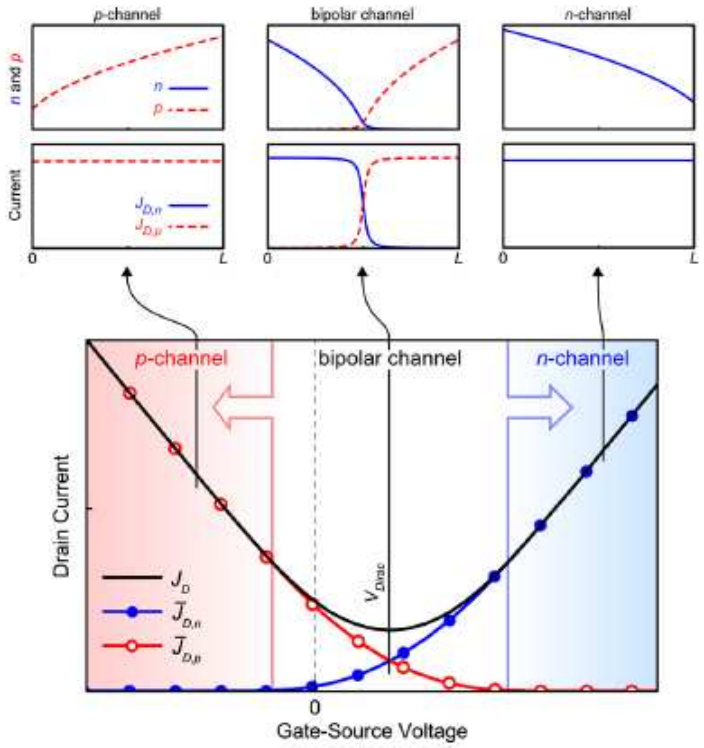

Figure 1-13: The ideal transcaracteristic of an ambipolar FET [66].

the device). Consequently, an ambipolar FET can operate in both n- and p- channel mode [7]. Complementary logic circuitry leads to less power consumption [7] and is usually built using two separated unipolar transistors (such as in [67] [68] [69]); in this framework ambipolar FETs are interesting from the applicative point of view since just one transistor type is needed [70] [71].

The ideal transcaracteristic of an ambipolar transistor is shown in Fig.1-13 [66]. It is possible to observe that the overall behaviour is a combination of a p- and an n- channel operation mode, since for positive gate applied electrons are accumulated while holes for negative ones. Moreover, depending on the threshold voltage for both n- and p- channel operation a bipolar channel can arise, since both the carriers type are present in the operation channel.

The architecture of the device offers also different possibilities, depending on the position of the electrodes; the three typical configurations realized are shown in Fig. 1-14(a), (b), (c) [72].

The electrodes can be positioned: a) below the heterostructure, in contact with the insu-

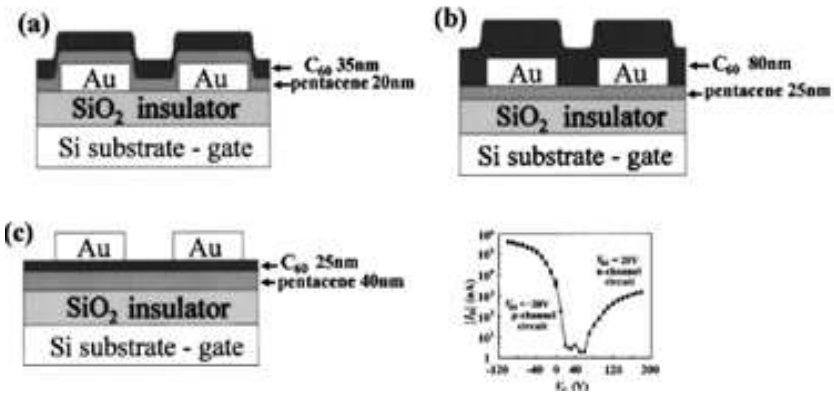

Figure 1-14: Different configurations for ambipolar field effect transistors [72].

lator (indicated as bottom contact/bottom gate or coplanar configuration); b) in the middle between the two semiconductor layers (middle contact); c) above the heterostructure (labelled as top contact/ botton gate or staggered). The configuration greatly influences the electronic properties: for instance, a staggered geometry reduces the contact resistances and facilitate the injection of charges respect to a coplanar. Kuwahara et al. [72] have instead demonstrated that for C60 – pentacene field effect transistors, the middle contact configuration was the most preferable to gain a balanced ambipolar behaviour.

This bipolar channel condition has been widely explained in the papers from Dodabalapur et al. [58] and from Paasch et al. [73]. At low gate voltages (lower than the majority carriers threshold voltage) and only when $V_{DS}>V_{GS}$, injection from the source of the minority carriers can happen (see also Fig. 1-15(a), (b)). As a consequence, the device can never been switched off; moreover, the transfer and output curves can exhibit a "non ideal" shape, as shown in the Fig.1-15 (c), (d) (modified from [58] and [7]). The output curves does not saturate when both charge carriers are present (see curves indicated with 1, 2, 3 in the picture (c)) while the transfer curves show a characteristic v-shape indicating that at low gate voltages minority charge carries are depleting.

The term organic heterostructure field effect transistor was introduced for the first time referring to a C60 – T6 heterostructure behaving as an ambipolar FET, as shown in the Fig.1-16 [57].

The performances of n-type organic semiconductors have been optimized (see for instance

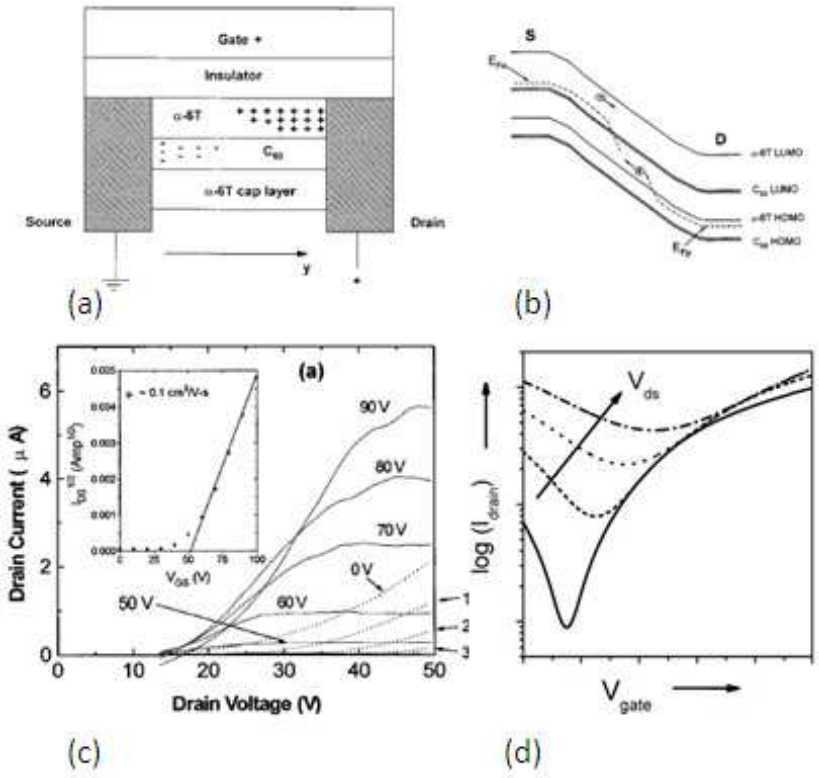

Figure 1-15: a) a schematic of the charge accumulation in an ambipolar FET, b) bipolar channel, c) output curves illustrating the condition of bipolar channel, d) transfer curves with the typical v-shape (modified from [58] and [7]).

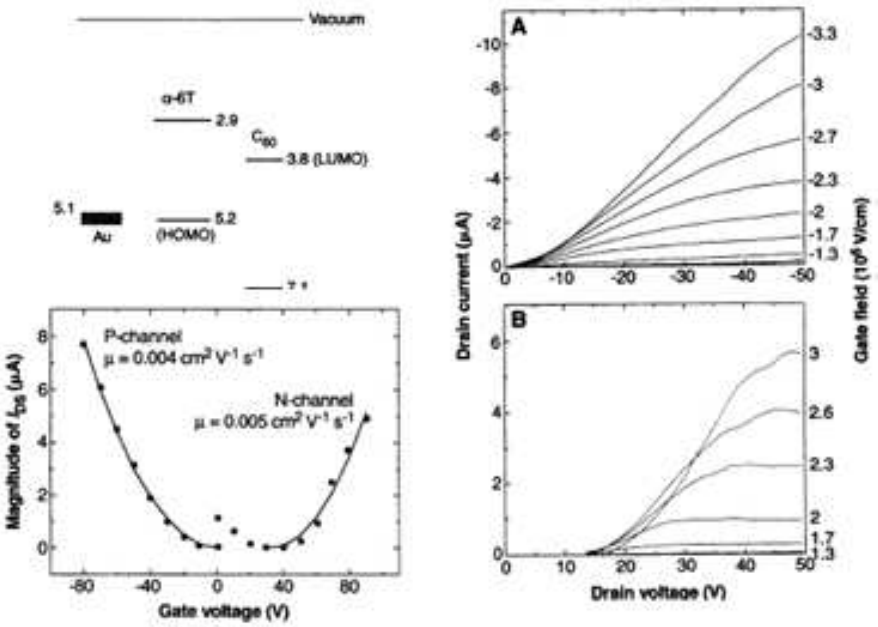

Figure 1-16: Energy levels of the semiconductors composing the heterointerface and its operation [57].

[3] [74] and further) through several strategies, depending on the characteristic of the active layer, the electrodes and the architecture of the device. The active layer, indeed, can be realized with a bilayer but also a coevaporated layer. In this way blend ambipolar transistors have been easily fabricated. although the electrical properties usually suffer from a reduction due to an increase of structural disorder (see for instance [75]).

The issue of the high contact resistances revealed to be the most serious obstacle for the realization of ambipolar devices, since the injection of one charge carrier, mostly electrons, was hindered. A solution resides into the use of asymmetric electrodes, in the sense that different metals were used to fabricate electrodes. This approach revealed to be a successful strategy to induce bipolar transport in an unipolar semiconductor [76].

Another interesting application of ambipolar transistors resides in the realization of light emitting devices. The so- called Light Emitting Field Effect Transistors (LFETs) offer an interesting technological advantage, residing in the possibility to combine the transistor and the light emitting operations in the same device. This phenomenon has been observed both in blends and in heterostructure transistors; even the position of the recombination zone in the channel has been detected and observed [77].

1.3.2 Accumulation heterojunction

The combination between a p-type and n- type semiconductors can form a depletion or an accumulation junction at both sides, depending on the relation existing between the workfunction of the two semiconductors [78]. If $\phi_P < \phi_N$, a traditional p-n depletion junction is realized. The valence band bends downward, while the conduction band upward; the built-in potential points toward the p-type semiconductor, provoking a rectifying behaviour. It is formed by immobile ions and, consequently, exhibits a high resistance.

The only possibility to increase the performances of the devices, such as carrier density at the interface and conductivity, consequently resides in the accumulation heterojunction (Fig. 1-17) . Indeed, only in this case (i.e. when $\phi_P > \phi_N$) the alignment of the Femi levels implies the transfer of electrons from the p-type to the n-type material and vice versa, consequently leading to an accumulation of the majority charge carriers in both the semiconductors and to an increase of the density of charges. The band bending, the built-in potential sign and the rectifying behaviour are reversed. The main features of field effect devices realized with

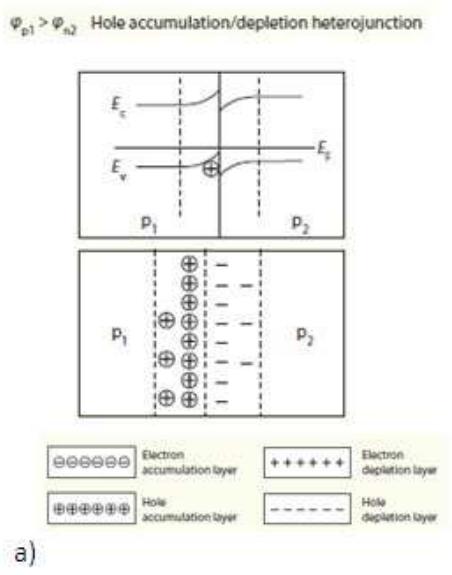

Table 1. Comparison of CuPc/F_{16}CuPc heterojunctions with silicon p–n homojunctions

	p-Type CuPc and n-type F_{16}CuPc heterojunction	Typical silicon p–n homojunction
Space–charge region	Mobile electrons in n-type layer; mobile holes in p-type layer	Immobile negative ions in p-type semiconductors; positive ions in n-type
Build-in potential	From p-type CuPc to n-type F_{16}CuPc	From n-type to p-type
Band bending	Upward in p-type layer; downward in n-type layer	Upward in n-type layer; downward in p-type layer
Conductivity[a]	High conductivity, due to mobile carriers in space–charge region	High resistance, due to immobile ions
Current–voltage characteristic[b]	Reverse-rectifying	Rectifying

[a] Parallel to the heterojunction interface. The high conductivity of the organic heterojunction overcomes the limitations of single-semiconductor material devices, allowing better utilization in organic electronic devices.
[b] Perpendicular to the heterojunction interface.

b)

Figure 1-17: a) Accumulation Heterojunction; b) table comparing silicon p-n junctions with organic accumulation heterojunctions [78].

accumulation heterojunctions are an increased conductivity, even at gate zero, respect to the single layers composing the heterostructure, a normally on behaviour and consequently a shift of the threshold voltage.

The first system exhibiting this behaviour was the heterostructure formed by the combination of p-type copper phthalocyanine (CuPc) and n-type hexadecafluorophthalocyaninatocopper (F16CuPc) [79]. It exhibited almost doubled conductivity and four times higher mobility respect to the single layers, while the threshold voltage shifts from -17 to -19 V, and of course implies normally on behaviour (see Fig. 1-18).

Since then, the proposed explanation for this phenomena was the presence of an accumulation heterojunction, which was later actually verified through UPS [80], Hall effect [81] and transverse (i.e. diode – like measurements) [79].

UPS measurements have been performed on samples with increasing thicknesses on one of the semiconductor layers, for both the two possible configurations (see Fig.1-19 in which the electronic structure is shown). Measurements clearly indicate the shift of the CuPc HOMO towards lower energy while F16CuPc LUMO shifts towards higher energy. The shift results to

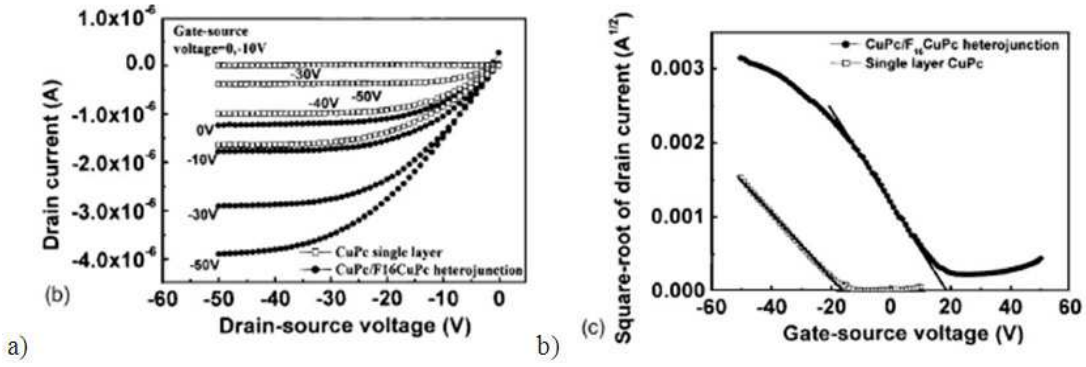

Figure 1-18: a) output and b) transfer curves evidencing the heterojunction effect [79].

be composed by a contribution due to the formation of an interface dipole (which is the same in both the configurations) and another due to band bending. From the solution of Poisson equation, a carrier density of 10^{18} cm^{-3} has been calculated, which is 6 order of magnitudes higher than the upper limit of the intrinsic carrier concentration for pure organic films.

Hall effect measurements were performed also in this case on samples in two different configurations. Hall effect has been observed at room temperature in both, and the mobilities of the carriers has been determined. The manifestation of the Hall effect at room temperature indicates the presence of free carriers in delocalized states of both signs. Measurements at lowering temperature indicates a decreasing conductivity due to the lowered density of carriers; the exponential decrease is agreement with the Multiple Trapping and Release Model (MTR).

The same heterostructure has been further investigated by transversal measurements, realizing a diode-like configuration a) The transversal measurement revealing the sign of the built in field, b) the extraction of the accumulation width [79] (see Fig. 1-20). The current flowing in the direction perpendicular to the interface was measured and the direction of the built-in field arising at the heterointerface due to the accumulation of charges. The result indicates a reverse rectifying behaviour, completely opposed sign respect to a p-n junction. A large current is indeed observed for a forward bias, while the current is greatly reduced in the reverse bias. This suggest that in the first case the applied field is in the same direction of the built-in field and the potential barrier for carrier flowing is increased and vice versa.

In the same paper, a method to determine the length of the accumulation region through

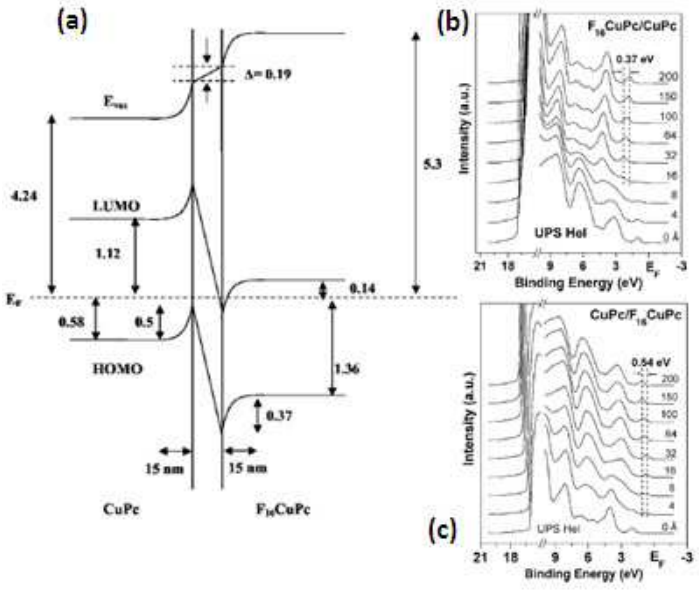

Figure 1-19: a) the energetic and b),c) the UPS measurements for a CuPc - F16CuPc [80].

the threshold voltage shift is also proposed, considering that the threshold shift is a consequence of the formation of the accumulation junction due to trap filling from the accumulated charges. Different devices in the same configuration have been realized with an increasing thickness of one of the two layers, and the transfer curves have been measured, experiencing an increase of the shift with the thickness which ends with a saturation; the thickness corresponding to the saturation should be equal to the width of the accumulation region, as a consequence of the above reported considerations .

As a conclusion, we have to mention that in addition to the CuPc/F16CuPc heterostructure, also other systems have shown the heterojunction effect, such as the heterojunction formed by a poly-p-phenylene vinylene derivative (MEH-PPV) hole injection layer with a poly (9,9 -dioctylfluorene) (PFO) hole accepting [82]. A "sandwich-type" and a "lateral" configurations with 4,4',4"-tris [3-methylphenyl (phenyl) amino] triphenylamine (m-MTDATA) organic donor and a hexadecafluoro-copper-phthalocyanine (F16CuPc) acceptor have been also realized and compared in [83] with the purpose of demonstrating the presence of a double layer of carriers. Moreover, measurements in situ during the heterojunction realization, have been performed, clearly indicating an increase of the current flowing in the device with increasing thickness of

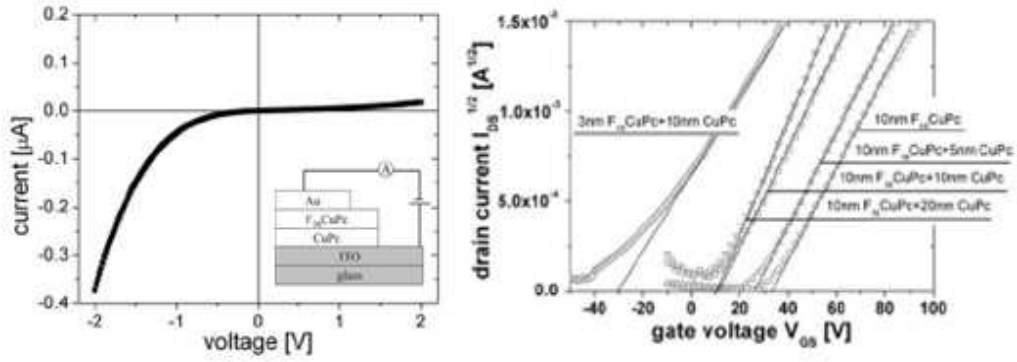

Figure 1-20: a) The transversal measurement revealing the sign of the built in field, b) the extraction of the accumulation width [79].

the upper semiconductor layer.

1.3.3 The influence of the morphology

The attention to the growth of organic films, especially by vacuum evaporation, has been motivated by the strict relation established between the morphological and the electrical properties. It has to be pointed out that organic semiconducting molecules are strongly anisotropic, which has important consequences in the growth mode and also in the electronic properties; the ionization energy of the molecule also depends on the orientation [84].

A direct correlation has been established by Shi et al. [85] between the morphological properties of the lower layer of a 2,5-bis (4-biphenylyl) -bithiophene /copper hexadecafluorophthalocyanine (BP2T/F16CuPc) heterostructure and the mobility of the resulting device. As shown in the Fig. 1-21 the devices exhibit two transitions from unipolar to ambipolar transport depending on the thickness of the lower layer; a proposed explanation resides in the continuity of the film. Analysis by Atomic Force Microscopy (AFM) of the lower layer suggest that a continuous film represents the unavoidable condition to gain ambipolar transport.

It is widely known that, improving the conditions of the deposition surface, higher quality films and devices with better performaces are obtained; self assembled monolayers (SAMs), already mentioned in the paragraph about doping, can serve to this aim, without affecting the electronic properties of the upper layer [86] [87]. Weak Epitaxy Growth (WEG) introduces an

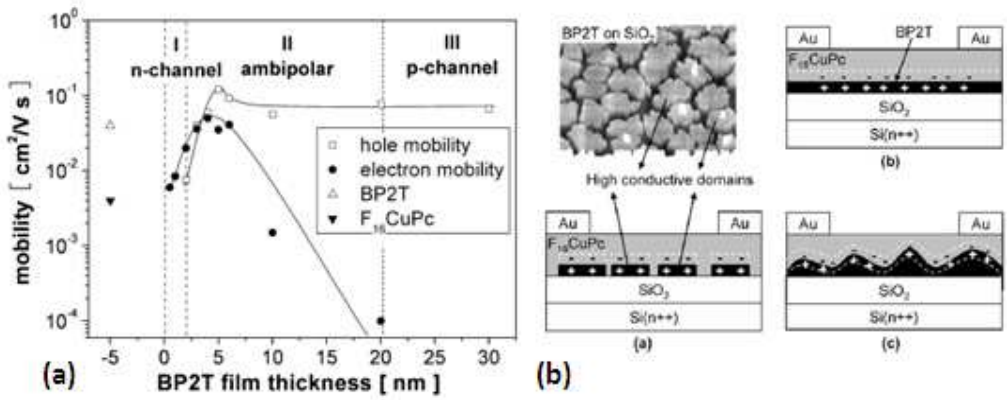

Figure 1-21: The influence of the morphology on a) the ambipolarity, b) the charge transport at the interface [85].

highly ordered ultrathin film (e.g. p- 6P) with the aim of inducing, on his turn, the formation of a highly ordered film which is comparable to single crystals [88]. The heterostructure also exhibits ambipolar transport depending on the thickness of p-6P [89]. Ambipolar transport has been also obtained by Wang et al. [90] and Zhu et al. [91]. It is worth to mention that a high control of the morphological properties represents also the building block for the realization of superlattices [92] [93].

1.4 Tuning the carrier density at organic single crystals surfaces and interfaces

Single crystals are ideal systems for studying the intrinsic physics and improving the electrical performances of organic semiconductors [94] [95]. Band-like transport and a weaker localization of charges have been observed repeatedly in different materials and configurations and have been also theoretically described [53]. Even if the electrical performances are much better than those of thin films, the crystal intrinsic fragility makes difficult their use in applications, although efforts in this directions have been done [96].

Due to the weaker localization of the charges, a high level of reproducibility is achieved and the traditional physical frameworks can be successfully applied to model theoretically the behaviour of single crystals and of the devices realized. In this regard, several studies have been

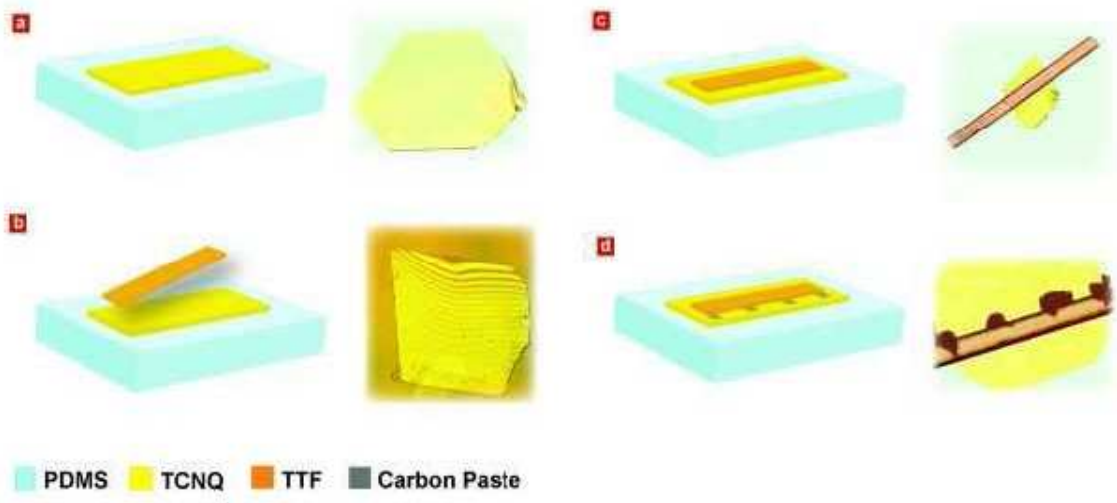

Figure 1-22: Assembly of TTF-TCNQ charge transfer interfaces. a) a TCNQ single crystal is placed onto a PDMS substrate; b) a thin TTF crystal positioned on top spontaneously adheres to the TCNQ crystal; c) result of crystal bonding process; d) electrical contacts to the interface fabricated using a carbon paste. Modified from [55].

performed in order to clarify the injection of charges into organic semiconductors from metal electrodes, exhibiting a surprising agreement between theory and experiments.

Field-effect transistors have been obtained with single crystals of pentacene [97], tetracene [98] and rubrene [99]. The comparison between the performances of rubrene FETs on insulators with different dielectric constants [100] has paved the way for a novel interpretation for the origins of the transport properties at the interface between the semiconductor and the dielectric. The decrease of the mobility with increasing dielectric constant has indeed suggested that Frohlich polarons can play a role in the conduction in organic semiconductors [101]. The use of an air-gap configuration, which does not account for the presence of a solid insulator at all, represents, in this framework, an interesting case study and has indeed made possible to observe the intrinsic transport in single crystal FETs [102].

Scaling experiments on rubrene FETs with different channel lengths have demonstrated that the contact resistances vary linearly with the channel length and are weakly depending on the gate voltage [103]. Schottky barriers have been realized with different metals and the electrical behaviour was successfully described through the classical Schottky theory [104].

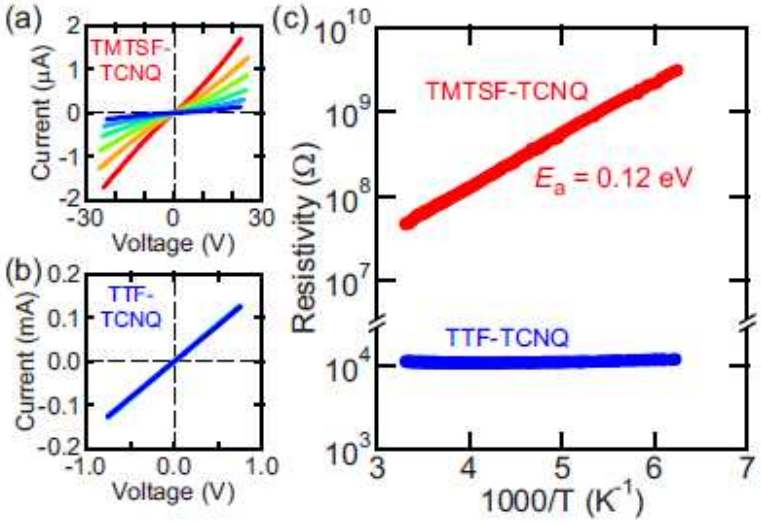

Figure 1-23: for both systems. The resistivity of TMTSF–TCNQ is thermally activated. [56].

The demonstration of the reliability of organic Schottky barriers paved the way to the realization of organic MESFETs [49] [105]. The use of single crystals, in particular, allowed a quantitative analysis of Schottky diodes; the determination of the depletion width in rubrene (2 μm) was achieved simply from transfer curves in linear region [49].

Even more interesting results have been obtained combining two insulators, TTF-TCNQ, and TMTSF-TCNQ, since in this case the transport phenomena arising can be in both cases easily explained in the framework of a simple band alignment picture.

Current-voltage measurements at the interface between TTF and TCNQ evidence the presence of a high density of carriers, an unexpected result taking into account that the two materials are basically insulators [55]. The characterization at different temperatures demonstrates that the resistance stays almost constant with temperature or even increase in the case of the best samples, indicating a metallic-like behaviour. These findings can be explained accounting for an interfacial charge transfer phenomenon.

Once the two crystals are put into contact, the requirement of the uniformity of the chemical potential through the whole structure, basically causes an electron transfer from TCNQ to TTF. An electric dipole consequently arises at the interface, along with the formation of two interfacial layers of accumulated charges, holes in TCNQ and of electrons in TTF. The presence of the

dipole at the interface causes an upward shift in the HOMO level in TCNQ, while an upward one of the LUMO in TTF. As a consequence, an overlapping region between the two bands arises, and the electronic behaviour at the interface basically results metallic.

On the other hand, while combining TMTSF and TCNQ a semiconductive behaviour is obtained. In this case the resistivity increases exponentially at decreasing temperature, indicating the presence of a gap and thermally activated transport [56]. The density of carrier at the interface results lower than the case of TTF-TCNQ, even if higher than that of the single materials composing the interface. These results can be basically rationalized accounting for an interfacial charge transfer phenomenon also in this case, even thou this time the charge transferred results way lower and not sufficient to induce a band overlap; a gap remains between the LUMO level of TCNQ and the HOMO level of TMTSF and a semiconductive behaviour is obtained.

Chapter 2

Perylene diimide field effect transistors

The choice of the most suitable n-type semiconductor for the realization of OFET heterostructures represents even nowadays a delicate and not trivial step. Electron conducting organic semiconductors are indeed more prone to electrical instability and to charge trapping phenomena respect to hole conducting compounds. This issue has limited until recently the realization of n-type devices and of p-n heterojunctions, which represents the building block for a wide class of devices.

I have consequently dedicated the first part of the research work to the study of field effect transistors realized with innovative and high-performance perylene diimide organic semiconductors, both in thin film and single crystal form.The electrical study was performed also in combination with structural and morphological analysis. Concerning the thin films, careful attention was used in the cleaning and in the (chemical) treatment of the substrates, since the strong influence of the surface conditions on the film growth has been widely demonstrated, as it will be shown in the following.

2.1 Field-effect devices realization and characterization

In this paragraph, the fabrication procedure of organic transistors will be reported. It is devided into two sections, the first one devoted to the fabrication of thin film transistors and will

consequently deal with the thin film growth. Analogously, the second one is focused on the single crystal FETs and the growth of single crystal will be described as the first step for the realization of the devices.

2.1.1 Thin film transistors

Thin film growth

Organic thin films were deposited by Joule deposition with Knudsen cells in a high vacuum system, (Fig.2-1 a) (base pressure 10^{-7} mbar). Structural and morphological properties are deeply correlated with the electrical performances [106]. The sublimation temperature, the temperature of the substrate and the deposition rate are the key parameters influencing the morphology of the films; a higher substrate temperature and a lower deposition rate indeed facilitate a more efficient packing of the molecules which tend consequently to occupy the position related to the most favorable energetic minimum [107].

In this regard, also surface treatments exhibit several beneficial functions, like changing of surface energy, improving of the texture of the films, reducing the probability of trapping and degradation of the electrical properties. Among the different surface treatments available, the application of a hydrophobic hexamethyldisilazane (HMDS) substitutes the hydroxyl groups present on SiO_2 surface (which are polar groups) with methyl groups (which are instead apolar) [106]. The hydrophobic nature of the compound reduces the concentration of water molecules on the surface, while the apolar nature of the methyl groups has demonstrated to play an important role in controlling the molecular assembly, attracting for instance the hexyl side chains in poly(3-hexylthiophene) (P3HT), a regioregular polymer [106].

Several techniques are available to check the quality of the films obtained; the most widespread is the analysis of the film surface texture through Atomic Force Microscopy (AFM), which probes the surface of the films and the growth mode can be studied. It cannot give information about the dielectric – organic interface, which instead represents the place where the transport of carriers occurs. AFM measurements are consequently particularly useful in the study of the morphology of thin layers with different thicknesses, with particular attention to the sub-monolayer regimes.

In our work, morphological AFM characterization was performed at room temperature in

air ambient by means of XE100 Park instrument, operating in non-contact mode (amplitude modulation, silicon nitride cantilever from Nanosensor). Film thickness were measured by AFM, scratching the film with a thin hard plastic tip. Root Mean Square Roughness (Rq) values have been obtained through XEI software (Park Systems). Furthermore, the Correlation Length (ξ) and the Root Mean Square Roughness (σ_{sat}) have been extracted through the Gwyddion Scanning Probe Image Processor, by fitting the Power Spectrum Density Function [108]:

$$PSD(f) = \frac{1}{L}\left|\int_0^L dx \cdot h(x) \cdot e^{i2\pi fx}\right| \tag{2.1}$$

where h(x) is the apparent topographical height with respect to the mean height, calculated on images of size L, x is the fast scan direction and f the spatial frequency. Palasantzas et al. [109] have demonstrated that ξ is directly correlated to the effective radius of the surface domains of the film under study, highlighting characteristic features of the film growth mode.

The structural characterization of all the samples have been performed by means of X-ray diffraction (XRD), performed in symmetrical reflection mode at the Cu Kλ wavelength radiation. X-ray measurements result particularly useful to assess the quality of the out-of-plane growth and the molecular arrangement. $\theta/2\theta$ diffraction scans, for instance, provide the spacings in the films, which allows determination of the molecular orientations relative to the substrate surface. The eventual presence of multiple Bragg reflections and Laue oscillations around the first-order diffraction peak indicates a high long-range film order, and, consequently, a high crystalline quality of the polycrystalline organic thin films. Finally, the broadening of the rocking curves is directly related to a good out-of-plane texturing in the films [17].

A complete analysis of several arylene derivatives including also x-ray analysis and AFM measurements [17] has for instance been developed in order to clarify the reasons behind a higher stability of the electrical response and to individuate the most suitable compound for applications. The relationship between the arylene derivatives thin film growth conditions and the electrical performances of the devices realized has been also analyzed in details [12]. In this paper, the influence of the surface treatment (polystyrene, octadecyltrichlorosilane (OTS) and hexamethyldisilazane (HMDS)) and of the growth conditions on the electrical performances of PDI-8CN_2 and PDI-FCN_2 has been also investigated. The morphology of PDI-8CN_2 results

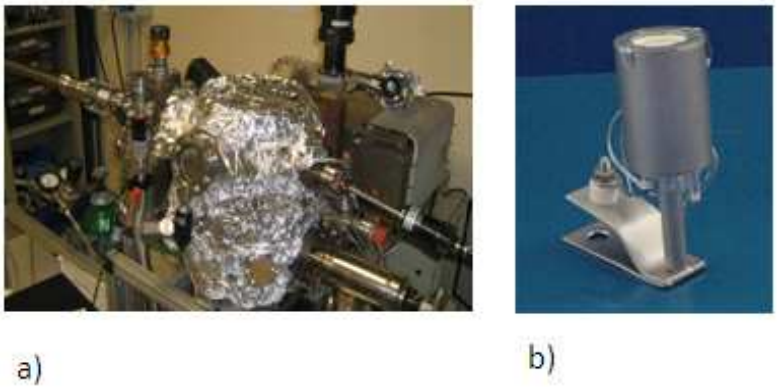

Figure 2-1: a) Organic Molecular Beam Deposition (OMBD) system used for the evaporation of the organic thin film and the realization of thin film transistors; b) a Knudsen evaporation cell.

more affected by the surface treatments than in the case of PDI-FCN_2, exhibiting a change in the size and shape of the grains. The treatments result instead crucial in obtaining high crystalline order in PDI-FCN_2, as the more and narrower peaks in the x-ray measurements suggest, while it is almost not influent for PDI-$8CN_2$.

For each material, an optimization procedure of the evaporation conditions, namely, the substrate temperature and the evaporation rate, has been consequently developed: several thin films have been realized in different evaporation conditions and their structural, morphological and electrical properties subsequently assessed and compared. For all the depositions, the entire vacuum chamber was warmed for 24 hours at the same temperature in order to assure uniform warming of the evaporation ambient and of the substrate (fixed to $\sim 100°C$). During the evaporation, the substrate temperature and evaporation rate was maintained constant [110] [111].

Device fabrication procedure

The devices used for this study are hybrid organic – inorganic bottom contact bottom gate thin film field-effect transistors.

The substrates are composed by a heavily n-doped silicon substrate (working as the gate electrode) covered by a thermally grown 200 nm thick SiO_2 (the dielectric) with multi fingered

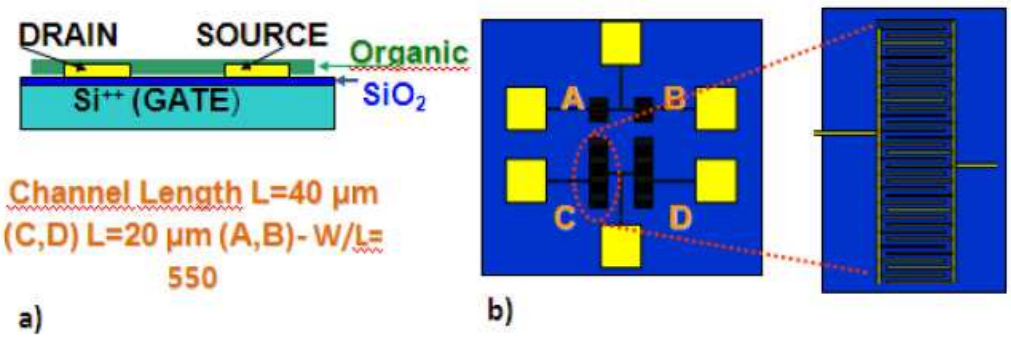

Figure 2-2: Schematic of the substrate used for the realization of the devices; a) cross section,b) top view.

gold source and drain contacts. These electrodes define channel length L = 40 μm and channel width W = 22 mm. Four adjacent devices are realized on the same substrate, two sharing the source contact (see Fig. 2-2). The devices have been finalized by depositing organic semiconductor films. It is worth to mention that the deposition system allows charging two samples during the same evaporation route.

Before the deposition, all $Si^{++}/SiO_2/Au$ substrates were cleaned with a basic procedure consisting of three steps: ultrasonic bath of acetone (5 min), ultrasonic bath of ethanol (5 min), a drying in pure N_2 gas. While some substrates were used without any further treatment (Bare), others were chemically functionalized by the coverage of a hexamethyldisilazane (HMDS) monolayer. Before HMDS vapour treatment, the substrates were further cleaned by placing them in a hot (120°C) Piranha solution (H_2SO_4-H_2O_2 – 50%-50%) for 15 min. Then, they were washed with deionized H_2O, sonicated for 5 min in MeOH (Methyl Alcohol), rinsed in DCM (dichloromethane) and finally dried with N_2. After, substrates (up to 15 for each treatment run) were located on a plastic sample-holder positioned in a home-made glass reactor which was evacuated and filled with Nitrogen (three times) before the addition of 1 mL of HMDS. Substrates were then stored in the glass reactor for 7 days. After the treatment, substrate surface was found to be highly hydrophobic with a water contact angle Θ_c of 108-109°. For un-treated (bare) substrates, Θ_c was about 60°.

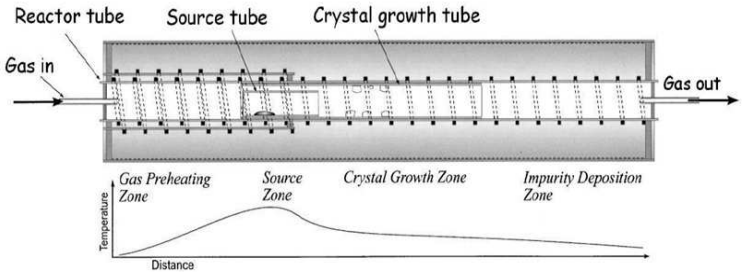

Figure 2-3: A scheme of the crystal growth technique used in this work. Modified from [112].

2.1.2 Single crystal transistors

Organic single crystal growth

The growth of organic single crystals was extensively studied by Laudise et al. [112]. They proposed the use of an horizontal glass reactor tube for the material transport and growth. A gradient of temperature is induced by a resistance wire wounding the tube and the temperature itself regulated by the distance between the spirels. Inner shorter tubes contain the initial powder and the grown crystals.

The ideal gradient of temperature is shown in Fig. 2-3. As can be seen, it firstly experiences a fast increase, reaching the sublimation temperature of the organic powder, then it slowly decreases. Where the grandient reaches the condensation temperature single crystals start to grow. An inert gas flow, in our case Argon, transports the evaporated molecules from the higher temperature region to the lower temperature one. The gas is trapped outside in an oil trap.

The optimal temperature gradient for the growth has to be determined empirically for each furnace and each material, adjusting the shape and the distance between the spirals. The fundamental parameters in the growth are the sublimation temperature and the difference between the sublimation and the condensation temperature, which regulates the dimension, the density and the quality of the crystals obtained.The flow rate can be used to set the transfer rate of the molecules from the sublimation to the condensation zone, and, consequently, can be used to determine the shape, the dimension and the quality of the crystals.

It has been demonstrated that the mobility of the single crystals can be highly improved recycling and re-growing the crystals several times, even if this represents a time-consuming

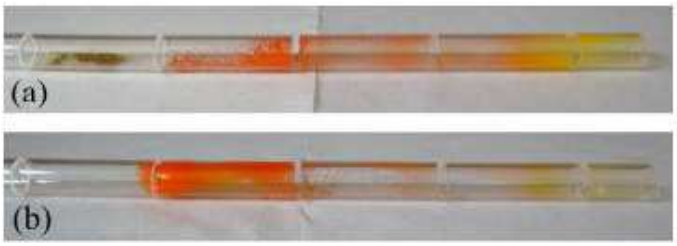

Figure 2-4: Comparison between the result of the growth of a) material as purchased, b) regrowth of the obtained crystals. Only in the first case impurities are present in correspondence of the section were the purchased powder was. This indicates that the growth procedure causes a purification of the crystals[95].

procedure. This seems to reduce the concentration of impurities that are present in the crystals [95], as also shown in Fig.2-4. In our case, even four generation rubrene crystals have been obtained.

Fig. 2-4 the figure illustrates the difference between first generation and second growth in term of the purity of the source material, which, in a second generation growth, is obtained smashing the first generation grown crystals [95].

Device fabrication procedure

Single crystals are free standing and can be manipulated and collocated on a substrate; particular care has to be used since the crystals are extremely fragile and their surface can be easily damaged, thus affecting the electronic properties. There are several strategies for the realization of devices [95]. The free standing single crystals can be collocated on a structure already provided of gate, dielectric and contacts; conversely, the gate can be instead deposited on the surface of the crystal, such as for a thin layer of parylene [99]. Opportunely shaped PDMS stamps can allow the realization of air gap field effect transistors, in which the insulator basically consists of air or a ionic liquid and which have given the highest mobility in n-type single crystals [113].

In our case, the chosen substrate was silicon with a thermally grown SiO_2 layer, in analogy with thin film devices (Fig. 2-5). Nevertheless, given the high environmentally sensitivity of PDI-FCN_2, in this case the oxide was covered by an ultrathin fluoropolymer (Cytop) layer

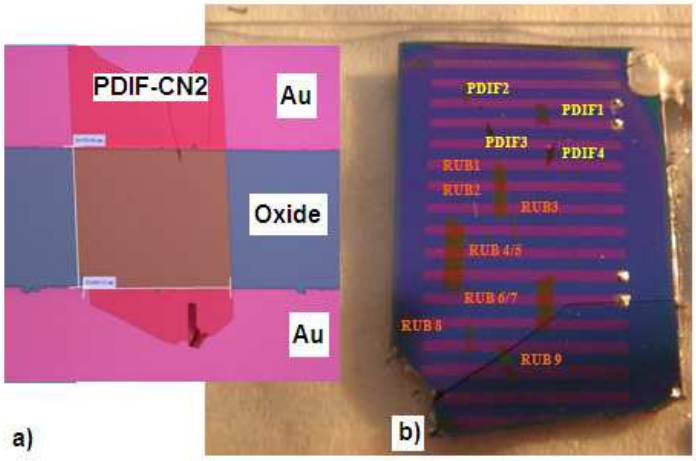

Figure 2-5: Single crystal transistors used for our study. a) a detail of single device, with a PDIF-CN_2 single crystal efficiently sticking on both SiO_2 and gold electrodes, b) a SiO_2 substrate with several gold stripes and devices.

(equivalent dielectric capacitance per unit area: C_{ox} ~5.29 nF/cm^2), which is widely known to reduce the presence of hydroxyl groups at the interface with the dielectric and improve the electrical performances [114]. The interdigitated geometry resulted not suitable for sticking organic single crystals, since the thickness of the electrodes hindered an uniform sticking to the oxide, eventually even causing the cracking of the crystals. The electrode geometry has consequently been greatly simplifyied, with simply parallel gold stripes; the single crystals have been sticked on the gold and on the oxide with the long axis perpendicular to the electrodes.

2.2 Study and comparison of PDI-8, PDI-8CN_2 and PDI-FCN_2 thin film transistors

Among the air-stable organic semiconductors, the class of compounds which exhibits the highest electrical performances is that of the arylene (or either rylene) diimides, which building block is the arylene group, formed by two benzene rings linked together.

This class includes imides substituted oligo naphtalenes, and in particular naphthalene and perylene diimides derivatives [17], such as N,N'- bis (n-octyl) -2- cyanonaphthalene -1,4,5,8- bis (dicarboximide) (NDI-8CN), N,N'- bis (n-octyl) -2,6- dicyanonaphthalene -1,4,5,8-bis (dicar-

boximide) (NDI-8CN_2) , N,N'-bis (n-octyl) -1,7- and N,N'- bis (n-octyl) -1,6- dibromoperylene -3,4:9,10-bis -(dicarboximide) (PDI-8Br_2), N,N'- bis(n-octyl) - 1,6,7,12 -tetrachloroperylene -3,4:9,10- bis(dicarboximide) (PDI-8Cl_4).

Among these compounds, we have focused the attention on N,N'- bis (n-octyl) perylene-3,4:9,10- bis (dicarboximide) (PDI-8), N,N'- bis (n-octyl) -1,6- dicyanoperylene-3,4:9,10- bis-(dicarboximide) (PDI-8CN_2) and N,N'-1H,1H- perfluorobutyl dicyanoperylenediimide (PDI-FCN_2). They have the same core, perylene, but different substituent groups. The cyano core substituent group, in particular, is present only in the last two materials, and is responsible for the environmental stability of these two compounds. PDI-8 and PDI-8CN_2 have in common the same end-substituent group, n-octyl dicarboximide, while PDI-FCN_2 presents a fluorinated end group. The choice of these three similar compounds, consequently, allowed the study of the influence of core and end-substituents on the morphological, structural, electrical and environmental stability of perylene diimide n-type organic semiconductors.

2.2.1 Structural an morphological analysis

Atomic force microscopy (AFM) images in Fig.2-6 1 a) and b) show, respectively, the surface morphology of 30 nm thick PDI-8 and PDI-8CN_2 films on bare SiO_2 substrates [115]. Both films are polycrystalline with the crystallites organized in a ribbon-like grain structure, in good agreement with previous studies [17] [12]. For both PDI-8 and PDI-8CN_2 films, the terrace heights are around 19.5 $\pm$ 0.5 Å. This result is consistent with a film microstructure where the semiconductor molecules grow with the long c axis almost perpendicular to the substrate surface and a molecular tilt angle of $\backsim 40^\circ$, independently from the substrate treatment. The terrace edges of PDI-8 films are preferentially faceted and more elongated in one preferential direction, while PDI-8CN_2 films exhibit more rounded grains. The root-mean-squared-roughness of these films is similar, i.e., 1.7 $\pm$ 0.1 nm for PDI-8 and 1.8 $\pm$ 0.1 nm for PDI-8CN_2. The semiconductor surface is characterized by only 3-4 atomically flat terraces for a 30 nm thick film.

The growth mode of PDI-8CN_2 has been analyzed in details [116]. The evolution of PDI-8CN_2 thin-film morphology as a function of the film thickness has been studied by atomic force microscopy on four samples characterized by different thicknesses. The thinnest film shows quasi-two-dimensional well connected islands, uniformly distributed on the surface. On increasing the film thickness, the molecular solid starts to grow by creating elongated three-

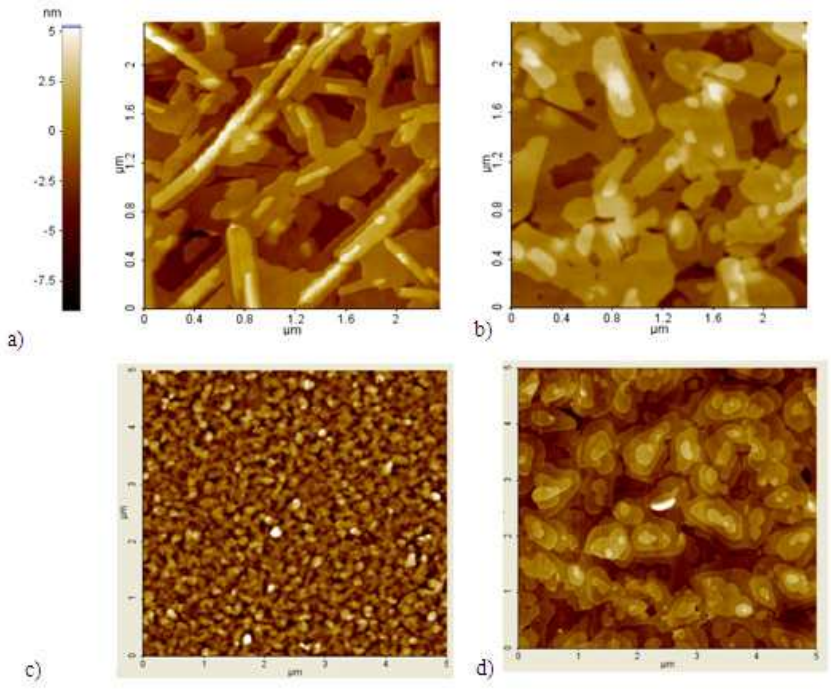

Figure 2-6: 10 nm x10 nm AFM images of a) PDI8; b) PDI-8CN_2; c) PDI-FCN_2 without HMDS surface treatment; d) PDI-FCN_2 with HMDS surface treatment. All the films were grown in the same conditions.

dimensional (3D) islands. The morphology differences exhibited by thin and thick films point out a continuous transition from two-dimensional to three-dimensional growth at increasing thickness.

The growth of PDI-FCN_2 exhibits specific properties in comparison with PDI8 and PDI-8CN_2, because in this case the film structural and electrical (see next paragraph) features result to be strongly affected by the surface treatment. In the following the comparison between the characteristics of PDI-FCN_2 films both grown on a treated and an untreated substrate will be consequently presented. Atomic force microscopy (AFM) images in Fig. 2-6 c and d show the surface morphology of 30 nm thick PDI-FCN_2 both on bare and HMDS treated substrates, respectively. The PDI-FCN_2 film morphology results to be composed by an analogous granular structure, both for films grown on SiO_2 and HMDS. However, in films on SiO_2, the structures protruding from the surface are rounded and smaller, while on HMDS the protruding features become larger and more irregularly shaped. The root-mean-squared-roughness varies from 2.951

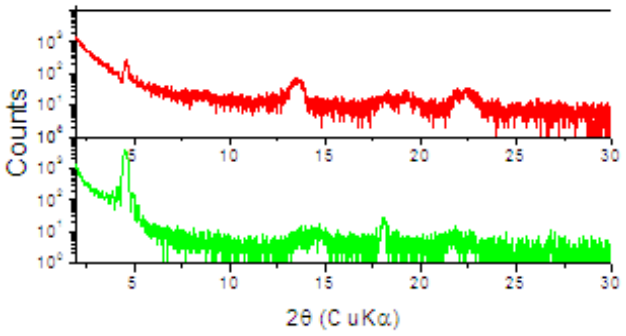

Figure 2-7: $\theta/2\theta$ x-ray spectra of PDI-FCN_2 on HMDS treated substrate (in red) and of PDI-$8CN_2$ on a bare substrate (in green).

nm on SiO_2 to 1.769 nm on HMDS, in agreement with the increased the dimension of the grains [17] [12].

The increased grain dimension suggests the possibility of an improvement of the quality of the film. In order to verify this assessment , X-ray analysis has been also performed. X-ray characterization of PDI-FCN_2 films deposited on untreated substrate and of PDI-8 has not given any considerable result, since the θ-2θ diffraction spectra are basically flat and no peak can be clearly distinguished. This indicates that the z-axis molecular order is very poor, or that the percentage of disordered regions (such as grain boundaries) is much higher than the crystalline domains. In Fig.2-7, we consequently report the X-ray $\theta - 2\theta$ diffraction patterns of PDI-FCN_2 on HMDS treated substrates and of PDI-$8CN_2$. θ-2θ patterns clearly exhibit several (00h) reflections. This result indicates that the layers are well structured, differently from the case of PDI-FCN_2 grown on bare SiO_2 and of PDI-8.

2.2.2 Electrical analysis

Electrical measurements were carried out always in darkness, both in vacuum (about 10^{-4} mbar) and in air, by using a cryogenic probe station, connected to a Keithley 487 picoammeter and a Keithley 2400 voltmeter (Fig. 2-8). The charge transport properties of the fabricated FETs have been assessed by measuring the output (I_{DS} vs V_{DS} at different V_{GS}) and transfer- (I_{DS} vs V_{GS} at different V_{DS}) curves. This analysis was mainly devoted to the determination of the charge carrier mobility μ value. Unless otherwise stated, all electrical tests were performed in

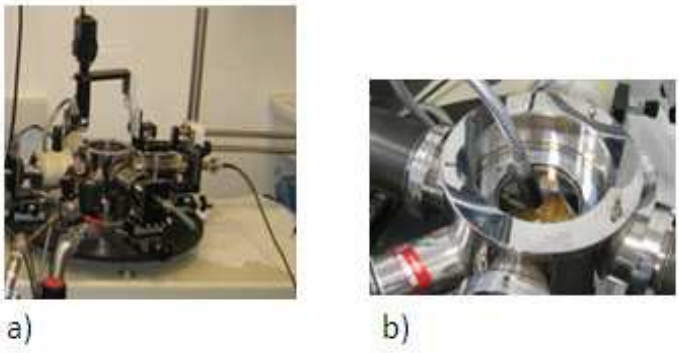

Figure 2-8: a) The cryogenic probe station used for the electrical measurements; b) detail of the probe station.

vacuum (10^{-4} mbar) and in the dark, immediately after the transistor fabrication.The output curves in Fig.2-9a reveal that the electrical response of the PDI-8 transistors is significantly affected by the contact resistance (R_c) contribution, since for drain-source (V_{DS}) voltages lower than 10 V, I_{DS} current displays a marked sublinear behavior, very far from the predictions of the ideal MOSFET model [18]. The charge carrier mobility (μ) of these FETs, evaluated in the saturation region (see the corresponding transfer-curve in the inset of Fig. 2-9 a), is $\backsim$0.1 $cm^2/(V\ s)$, being one order of magnitude higher than that extracted in linear region. For PDI-8 transistors, the onset voltage V_{on}, defined here as the voltage where the device current exceeds the lower limit of the experimental setup (1 nA), is very close to 0 V.

The electrical response of the PDI-8CN_2 devices (see Fig. 2-9 b) presents quite different features. Here, the contact resistance R_c at low biases is lower and the output curves follow the predicted linear behavior at small V_{DS} values. Since the values of the onset voltage V_{on} are largely negative (V_{on} < -20 V), the drain current is not null even when the gate-source voltage (V_{GS}) is zero. Mobility values for PDI-8CN_2 (see the inset in Fig. 2-9 b for a typical transfer-curve in saturation) are similar in the linear and saturation regions, being about 0.02-0.03 $cm^2/(V^*s)$, in good agreement with the results reported by Yoo et al. for PDI-8CN_2 bottom-contact transistors on bare SiO_2 substrates. The gate voltage dependence of the conductivity (σ) extracted from the data reveals, at $V_{GS} = V_{DS} = 50$ V, that PDI-8 σ is about four times higher than that of the core-cyanated perylene. This discrepancy is very similar to the value observed for mobility, and consequently, a contribution coming from different densities of

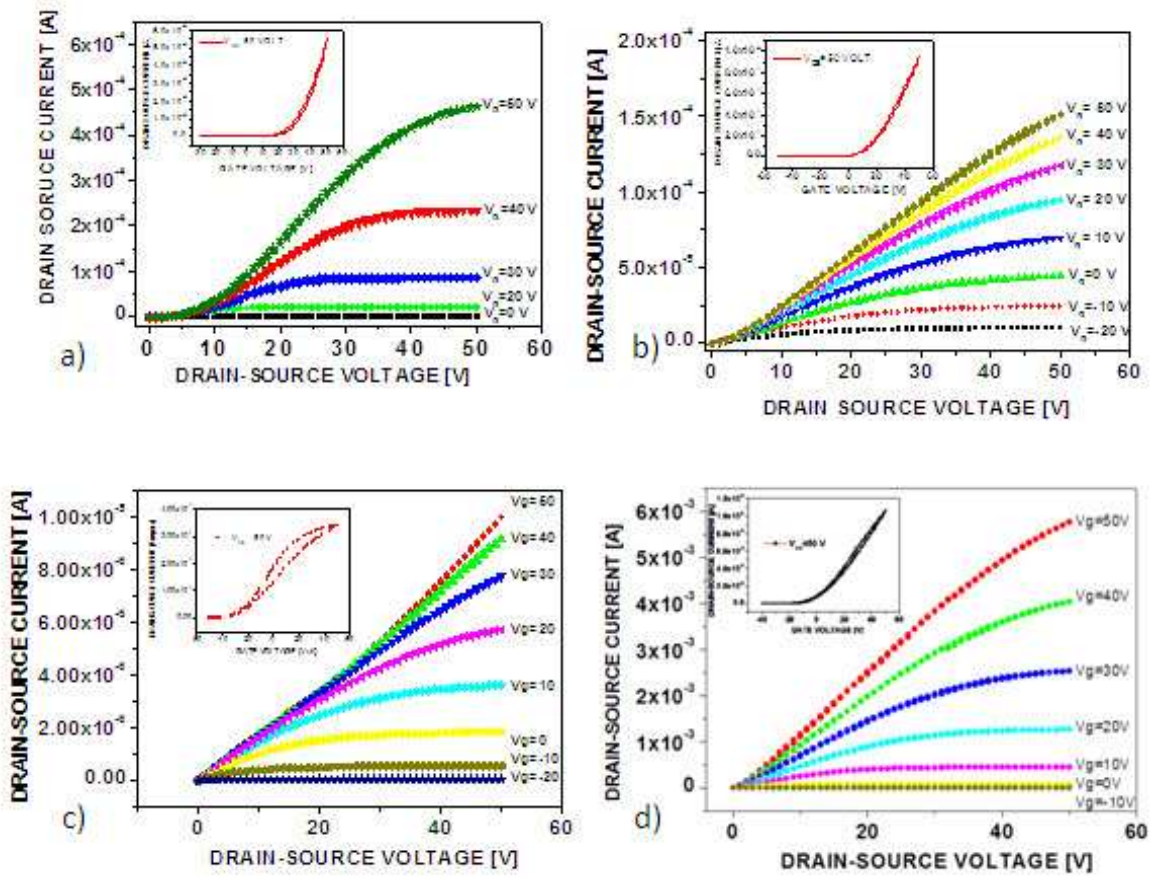

Figure 2-9: The electrical response of typical a) PDI-8, b) PDI-8CN_2 ,c) PDI-FCN_2 on bare SiO_2 substrate, d) PDI-FCN_2 device on HMDS treated substrate field effect transistors.

induced charge carriers should be excluded. Electrical tests performed in air confirm that the PDI-8CN_2 devices are stable in ambient conditions. For this compound, the difference between the mobility values extracted in air and vacuum is in the range of 20-30%. Conversely, PDI-8 FETs are inactive after a few seconds of air exposure, and no detectable I_{DS} current is recorded at any V_{GS} by our experimental setup.

Fig. 2-9 c and 2-9 d report the electrical responses of PDI-FCN_2 on bare and HMDS treated SiO_2, respectively. The maximum drain source current in saturation region increases from 3.37*10^{-5} A for the film on the bare substrate to 0.01 A for the HMDS treated one. The mobility, extracted from the transfer curves reported in the insets, respectively increases instead from 2.31*10^{-3} cm^2/Vs to 0.59 cm^2/Vs, which is the highest value obtainable in polycristalline thin films [14]. The onset voltage also experiences a variation, being largely negative for the film on the bare substrate (-50 V or -30 V, depending on the device), while getting closer to zero (ranging between -35 V and -25 V) for those on treated substrates, suggesting an inferior density of traps at the semiconductor - insulator interface. Electrical response is consequently largely improved by the treatment with HMDS, which can be simply explained by the higher structural quality of the films, as proved by the x-ray measurements and by the increased dimensions of the grains.

The table below summarizes the electrical response of the devices realized with the four perylene diimide compound investigated:

	PDI-8	PDI-8CN_2	PDI-FCN_2	PDI-FCN_2
saturation region	bare SiO_2	bare SiO_2	bare SiO_2	treated SiO_2
I_{DS} max [A]	4.62*$^{-4}$	1.51*10^{-4}	9.91*10^{-6}	0.011
μ [cm^2/Vs]	0.01	0.03	0.002	0.6
V_{ON} [V]	-20	0	-50	-35

2.3 Bias stress experiments on PDI-8CN_2 thin film and PDI-FCN_2 single crystal transistors

In the previous paragraph, PDI-8CN_2 emerged as the best candidate for the realization of thin film heterostructure field effect transistors, since its morphology and electrical response resulted

less dependent from the substrate treatment. Nevertheless, PDI-FCN_2 remains the compound which exhibits the best electrical performances, and it is consequently the most suitable n-type semiconductor for single crystal heterostructures, where the morphology of the semiconductor do not represent an issue, as widely discussed in the previous chapter.

We have consequently focused our attention on PDI-$8CN_2$ thin film transistor and on PDI-FCN_2 single crystal FET. We have analyzed the basic electrical behaviour and the instability, which reveals to be the major issue for electron transporting organic semiconductors, as discussed in the paragraph 1.1.1. Bias Stress effects on OFET operation have been studied by recording the I_{DS} time decay curves upon static polarization (i.e. V_{GS}=40 V, V_{DS}=-5 V). The experimental curves (I_{DS} vs time) have been fitted by the stretched exponential function:

$$I = I' + I_0 \exp\left[-\left(\frac{t}{\tau}\right)^{\beta}\right] \tag{2.2}$$

Since the equation 2.2 is rigorously valid only if any contact resistance effect can be excluded, the aforementioned approach has to be considered suitable to describe the BSE dynamics only in first approximation.

2.3.1 PDI-FCN_2 single crystal transistors

The last study of instability has been led on transistors realized with PDI-FCN_2 single crystals on silicon dioxide substrates covered with a layer of Cytop. This polymer dielectric has been demonstrated to reduce almost to zero the bias stress in p-type single crystals transistors; the findings have been explained suggesting that the hydrophobicity of the Cytop layer avoid the presence of water molecules at the interface with the organic semiconductor [117]. Given the high sensitivity of PDI-FCN_2 to the dielectric substrate, the choice of Cytop as a dielectric was the more indicated (n.d.r. the transistors realized with PDI-FCN_2 single crystals on bare silicon dioxide substrates did not show measurable currents). In the Fig. 2-10 the typical electrical response of a PDI-FCN_2 single crystal transistor is shown, even before and after the bias stress experiment. The maximum mobility results 2.91 cm^2/volt*s, without any significative variation after the application of the bias stress. The onset voltage is about -4 V and shifts towards positive voltages after the application of the bias stress (Fig. 2-10).

In Fig. 2-11 are instead exhibited the drain source current vesus time. After 5000 sec, I(t)

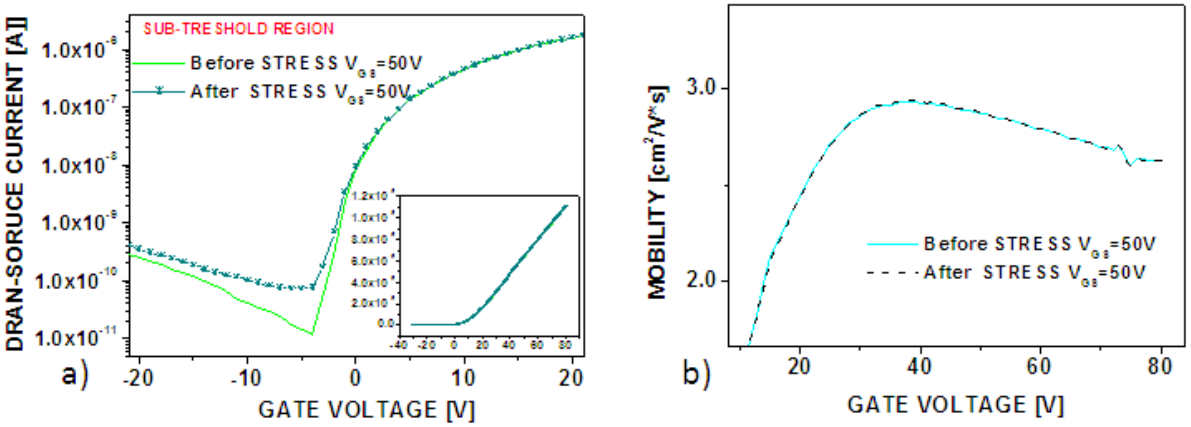

Figure 2-10: Electrical response of PDI-FCN_2 single crystal transistor before and after the bias stress experiment (Cytop on silicon dioxide substrate). a) Transfer curves in logarithmic scale illustrating the shift of the onset voltage after the bias stress experiment; in the inset, the transfer curves in linear scale. b) The respective variation in the mobility extracted.

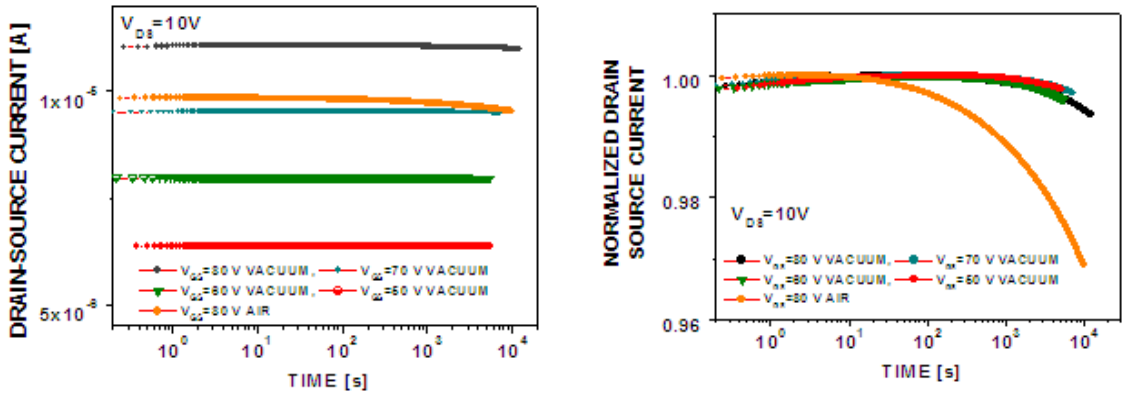

Figure 2-11: a) Drain source current versus time at different fixed gate voltages, b) the respective normalized curves.

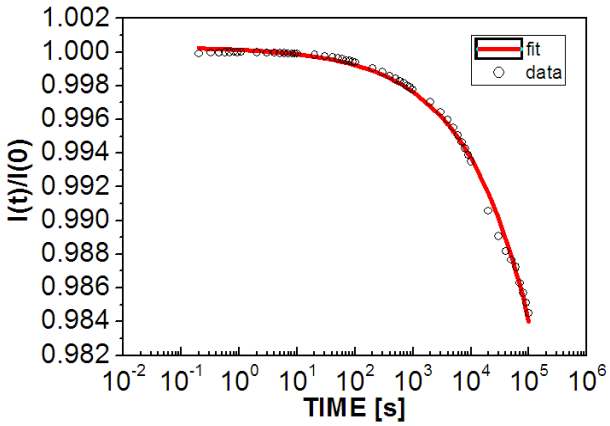

Figure 2-12: Normalized drain source current curve versus time fitted with the stretched exponential relation until $10^5 s$.

curves in vacuum display a decrease of much less than 1% in comparison with the maximum current. We were not able to observe a clear correlation between the amount of decrease and the V_{GS} value applied during the stress experiment. Transfer-curves recorded before and after any I(t) curve confirm that the bias stress effect is very small.

The curves have been fitted as well, with the stretched exponential function until 10^5 sec (Fig. 2-12). As a result β= 0. 35±0.05 while τ=(348±4)*10^7 s with a normalized χ^2 of 4.

2.3.2 PDI-8CN_2 thin film transistors

The devices have been realized depositing PDI-8CN_2 on HMDS treated substrates have analyzed. In Fig. 2-13, the transfer curves and mobility in saturation region are reported. The maximum mobility results 0.026 cm^2/volt*s and the V_{on} -4 V.From the transfer curve recorded after the bias stress experiment, it is possible to extract both the V_{on} and the mobility and compare with the values above reported (Fig. 2-13). The V_{on} shifts towards more positive values, while the maximum value of the mobility does not seem to be deeply affected by the bias stress, as expected.

The instability behaviour after a prolonged application of a gate bias is instead analyzed recording several curves at different gate bias values (Fig. 2-14). In order to clarify the issue, the curves have been fitted through the above reported stretched exponential function and the parameters β and τ have been extracted, resulting, respectively, 0.23±0.05 and 19±3*10^6s (

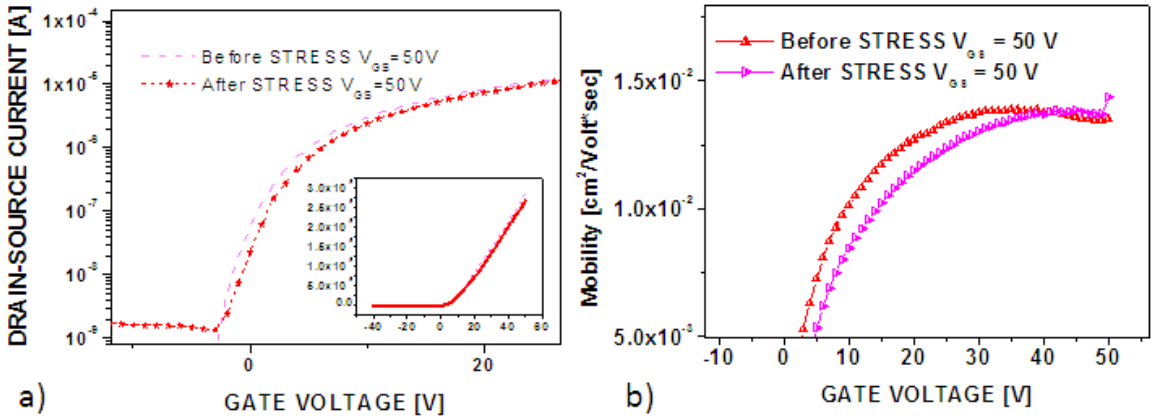

Figure 2-13: Electrical response of PDI-8CN$_2$ thin film transistor before and after the bias stress experiment. a) Transfer curves in logarithmic scale illustrating the shift of the onset voltage after the bias stress experiment; in the inset, the transfer curves in linear scale. b) The respective variation in the mobility extracted.

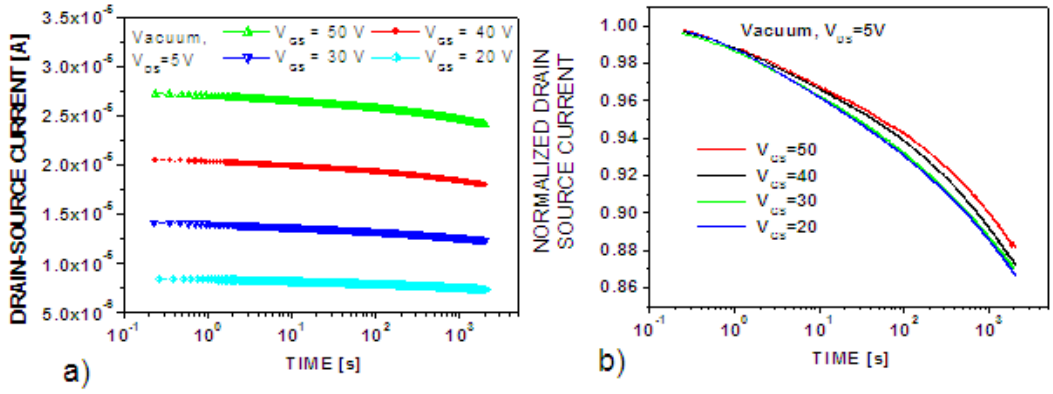

Figure 2-14: a) Drain source current versus time at different fixed gate voltages, b) the respective normalized curves.

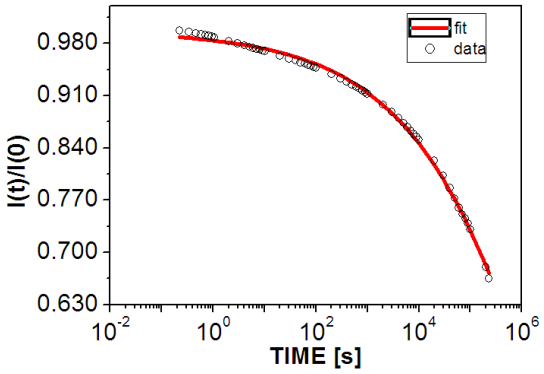

Figure 2-15: Normalized drain source current curve versus time fitted with the stretched exponential relation (Vg = 50 V).

Fig. 2-15).

2.4 Conclusion

The morphological and electrical properties of different types of Perylene Diimide films have been reported, deposited by evaporation with Knudsen cells on SiO_2 substrates. N'–bis (n-octyl) -perylene-3,4:9,10-bis (dicarboximide) (PDI-8), N, N'–bis (n-octyl) -1,6- dicyanoperylene -3,4:9,10-bis (dicarboximide) (PDI-8CN_2) and N, N0-1H, 1H- perfluorobutyl dicyanoperylenediimide (PDI-FCN_2) molecules have been considered. The structural properties of these films have been investigated by AFM and XRD characterizations, while the electrical response of the related transistors has been analyzed by dc transfer and output curves. Our results demonstrate clearly how the presence of specific chemical groups (i.e alkyl, cyano and perfluoroalkyl groups) in the Perylene molecular core is able to strongly modify the final self-assembling properties on both bare and chemically functionalized SiO_2 substrates. At the same time, the different energetics of the frontier molecular orbitals mainly affect the capability of Perylene films to effectively transport electrons even in ambient conditions. The optimization of the growth conditions of the PDI-FCN_2 films on hexamethyldisilazane (HMDS) functionalized substrates allowed the fabrication of bottom-contact transistors displaying charge carrier mobility up to 0.6 cm^2/volt*sec. These values are comparable with the best results ever obtained with this

type of molecule.

The experimental findings above reported suggest that the presence of HMDS is indispensable to obtain outstanding performances of PDI-FCN_2. It indeed guarantees an high molecular order and, as a consequence, increased electrical performances. Heterostructures are although realized depositing an organic semiconductor on another; considering also that the morphology of organic thin films greatly varies with every external condition and with the thickness of the layer, a compound less sensitive to the substrate conditions was needed. On the other hand, the electrical performances and stability of PDI-8 resulted poorer as compared with the other two compounds. PDI-$8CN_2$ consequently was considered as the best candidate for the realization of heterostructure thin film field effect transistors.

Chapter 3

Thin film heterostructure field effect transistors

In this chapter, sexithiophene (T6)/N,N'-bis (n octyl)-dicyanoperylenediimide (PDI-8CN_2) heterostructures, composing the active channels of field-effect transistors, are presented. The electrical and structural characterization of these heterostructures as a function of the T6 layer thickness was performed in a systematic way and by employing different device configurations. The experimental data evidence both the presence of ambipolar charge transport and a large enhancement of the channel conductance, suggesting accumulation of exchanged charge carriers at the T6/PDI-8CN_2 interface.

Moreover, with the application of the gate, ambipolar transport and Negative Transconductance (NTC) phenomena (i.e. a decrease followed by an eventual nullification of the drain-source current at increasing gate voltages) have been observed.

A model has been proposed as a possible explanation of these phenomena describing the energetic levels at the heterointerface at the equilibrium and in presence of a field-effect, and accounting for the band bending promoted by the charge transfer at the interface. In this scenario, the NTC effect can be explained in terms of a further shift of the energetic levels at the interface due to the application of a gate voltage, which in favourable conditions, leads to recombination of charges.

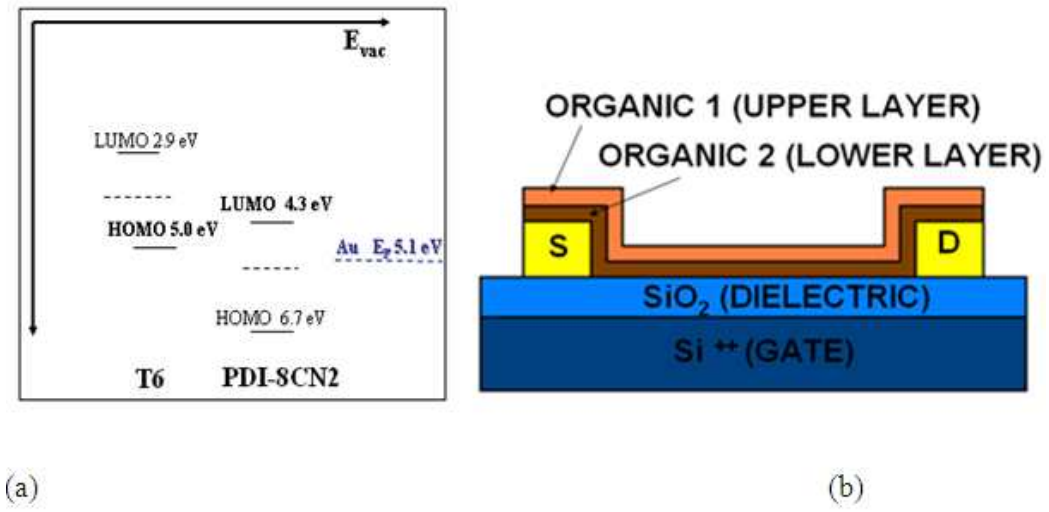

Figure 3-1: (a) The energy levels of the two semiconductors, compared with gold Fermi Level; (b) the double-layered configuration device.

3.1 Device fabrication procedure

T6/PDI-8CN$_2$ double-layered heterostructures have been fabricated using the same substrates and following an analogous procedure to that exposed in 2.1.1. In this case, a sequential deposition of both organic layer was performed and two samples were deposited simultaneously during the same evaporation run. In this work, we fabricated up to 18 devices which exhibited very reproducible experimental results [119].

The choice of T6 (Sigma Aldrich) and PDI-8CN$_2$ (Polyera Corporation Inc.) as hole and electron transport type materials for OFETs is justified by the good match between the work function of the electrode material (gold), the highest occupied molecular orbital (HOMO) of the hole-transporting T6 [118] and the lowest unoccupied molecular orbital (LUMO) level of electron-doped PDI-8CN$_2$ [17] (see Fig. 3-1). Such condition assures a good injection of both holes and electrons from the electrodes, thus allowing ambipolar transport in OFETs [120].

Before the deposition of the organic layers, the substrates were cleaned in ultrasonic baths of acetone and ethanol, followed by drying in pure N_2 gas. The evaporation rate was 2 nm/min for T6 and 1 nm/min for PDI-8CN$_2$. The deposition rates and the thickness of each layer were controlled by a quartz-balance thickness monitor carefully calibrated by atomic force

microscopy (AFM, XE100 (Park instruments)) measurements, by ex-situ ellipsometry and by x-ray diffraction (performed on the Pendellosung finite size effect on the (00l) reflection showed by PDI-8CN_2 films). Some care about the effective thickness of T6 is necessary in the case of ultra-thin films for which, as shown below, a complete coverage is achieved only for thickness higher than 2 nm [121].

Three different device configurations have been realized. Referring to Fig.3-1b, in the first configuration (labelled as configuration A), the T6 layer was directly deposited on the substrate and PDI-8CN_2 was grown on the T6 film. On the contrary, in the latter configuration (indicated as configuration B), the PDI-8CN_2 film was used as the bottom layer. Finally, blend structures (configuration C) based on co-evaporated T6 and PDI-8CN_2 films were also fabricated and characterized in order to evidence phenomena relying only on the presence of bulk heterojunction regions without structural order. In the configuration A, the T6 thickness was changed between 1 nm (incomplete T6 films) and 15 nm, while that of the PDI-8CN_2 layer was fixed at 24 nm; in the configuration B, only samples with 5 nm thick PDI-8CN_2 bottom layers and 22 nm thick T6 top layers were analyzed. In the configuration C, the volume percentages of PDI-8CN_2 and T6 have been found to be approximately the same, by ellipsometry measurements [121].

3.2 Experimental results

3.2.1 Film structural and morphological characterization

In order to achieve an accurate control of the T6/PDI-8CN_2 heterostructures fabrication, we have performed systematic structural and morphological characterizations of the single and double layer structures. In the Fig. 3-2 we report the x-ray θ-2θ diffraction spectra of all the heterostructures, the coevaporated film and also the spectra of the single layers as reference [121]. At lower T6 thickness, θ-2θ spectra clearly exhibit several PDI-8CN_2 (00h) reflections with a d-spacing of 1.98 nm in agreement with the single layer spectrum and with the data reported by Jones et al. [17] regarding PDI-8CN_2 deposited on SiO_2. This occurrence indicates that PDI-8CN_2 layers deposited on T6, well structured way. At high T6 thicknesses, further reflections are evident which have been instead addressed to T6, as confirmed by the spectrum of T6 10 nm thick layer and by previous results [111].

The high crystal quality of the PDI-8CN_2 films is confirmed by the presence of the Laue

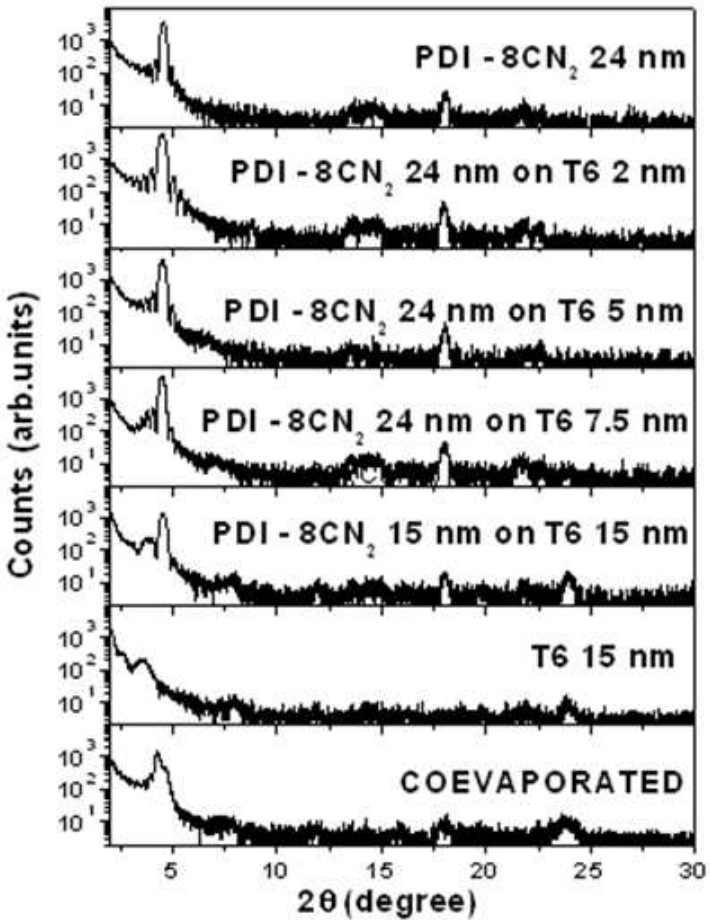

Figure 3-2: Spectra of the heterostructures with T6 thickness ranging between 1 nm and 15 nm and PDI8-CN2 of 24 nm.

oscillations around the first order diffraction, although at increasing T6 thicknesses peaks and reflections are less defined and more rare, indicating a worsening in the structural molecular packing. X-ray diffraction spectra have been also reported for the coevaporated film (configuration B); the reflection peaks present (both addressable to PDI-8CN_2 and T6) result less intense and broad and the Laue oscillations at low angles are absent, suggesting a lower crystallographic order compared to the heterostructure one. Nevertheless, the presence of the same peaks as measured in configuration A, indicates that the molecules are still oriented perpendicularly respect to the substrate.

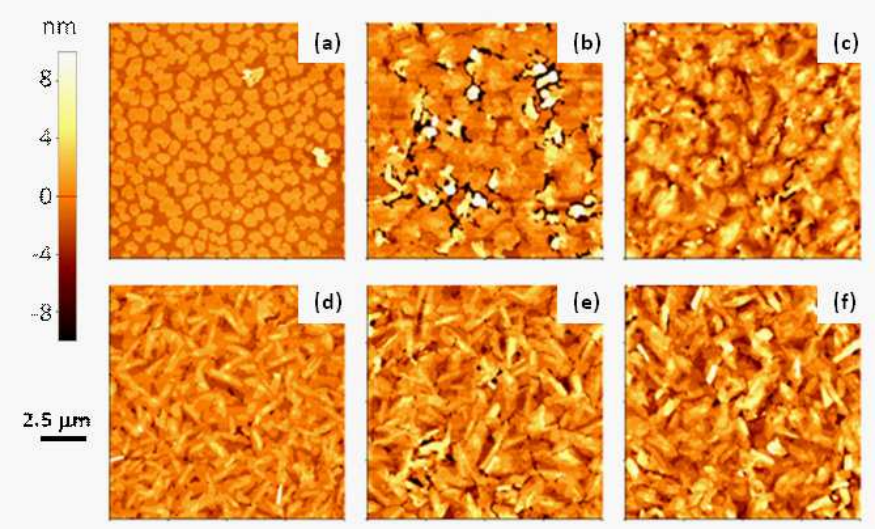

Figure 3-3: (a)-(c) 10 μm x 10 μm^2 non contact AFM images of T6 films deposited on SiO_2 and (e)-(f) of T6/PDI-8CN_2 at increasing thickness of T6 bottom layer. From left to right (a) 1nm, (b) 2 nm (c) 15 nm thick T6; 24 nm thick PDI8-CN_2 on (d)1 nm , (f) 4.5 nm, (g) 15 nm thick T6.

T6 thickness	T6 σ_{sat}(nm)	T6 ξ (nm)	PDI-8CN_2 σ_{sat} (nm)	PDI-8CN_2 ξ (nm)
0			1.87±0.01	201±1
1	1.29±0.01	133±1	1.60±0.01	168±1
2	0.98±0.01	107±1	1.60±0.01	233±1
4.5	3.18±0.01	141±1	2.33±0.01	165±1
7.5	3.35±0.01	145±1	2.73±0.01	163±1
15	2.44±0.01	185±1	2.75±0.01	195±1

The surface morphology of the samples was analyzed by a XE100 Park AFM microscope operating in air. Images were acquired using silicon-doped cantilevers (resonance frequency around 300 KHz) provided by NanosensorTM, in non-contact mode. Focusing the attention on the AFM images, it is possible to note that the T6 morphology (Fig.3-3 (a), (b), (c)) is generally characterized by a disk-shaped island growth. In Fig.3-3, we show the evolution of the AFM morphology of T6 and T6/PDI-8CN_2 (configuration A) films deposited on Si/SiO_2 as a function

of the T6 thickness. In the table, we report the root mean square deviation (RMSD) and the correlation length determined by fitting the power spectrum density distribution, obtained from data acquired on 10 x 10 μm^2 area. It is worth noting that a direct observation of the T6 morphology in T6/PDI-8CN_2 double layer structure was achieved by covering, with suitable shadow masks, selected regions of the substrate surface during the deposition of the PDI-8CN_2. This method allows to investigate the variances in the growth mode of PDI-8CN_2 on T6.

T6 ultrathin films exhibit a 2D-island growth forming one unit cell (uc) high terraces (1 uc = 2.4 nm), as reported also by Dinelli et al. [122]. At low nominal thicknesses (below 2 nm), the 2D islands are not completely connected. The data analysis shows that the critical percolation threshold in T6 island coalescence corresponds to a 70% covering of the substrate surface. In particular, the 1 nm thick T6 film Fig. 3-3 a) is characterized by a sub-monolayer coverage, where the islands do not form a continuous percolating path and, as it will be also pointed out in the following discussion, the T6 layer cannot support the transport of charges.

Conversely, at increasing T6 coverage, islands start to coalesce forming a continuous layer on the surface. T6 films with nominal thickness of 2 and 4.5 nm Fig. 3-3 b) considered in this study correspond approximately to one and two complete T6 molecular monolayers (ML). Above 2 ML Fig. 3-3 c), T6 growth begins to occur mainly through the formation of 3D islands and the films are characterized by a slight increased roughness.

PDI-8CN_2 films with fixed 24 nm thickness Fig. 3-3 d), e), f) exhibit a needle-like surface and two-dimensional, well connected, few unit cells (1 uc of PDI-8CN_2 = 1.9 nm [17]) thick islands, uniformly distributed on the surface. Despite their relatively large thickness, these heterostructures display a quite smooth surface with a lower roughness with respect to the one of a single T6 layer. The morphology of PDI-8CN_2 top layers is not dramatically affected by the underlying T6 morphology and, as confirmed by X-ray analysis [121], the molecular assembly retains the same structure of the one deposited on SiO_2 substrates, with the molecules growing with the long c-axis almost perpendicular to the surface of the bottom layer. From this analysis we conclude that the changes in the electrical response of T6/PDI-8CN_2 field-effect devices, as discussed below, cannot be simply associated to differences in PDI-8CN_2 morphological features.

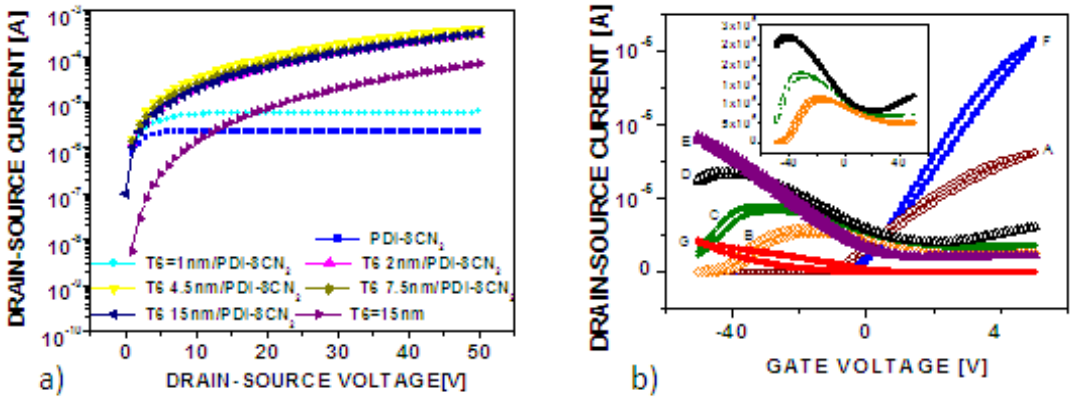

Figure 3-4: a) Output curves ($V_{GS} = 0$ V) measured for heterostructure devices (configuration A) with different T6 thicknesses. b) Transfer-curves ($V_{DS} = 5$V) measured for heterostructure devices (configuration A) with different T6 thicknesses (T6 1 nm open brown circles, A, T6 2nm open orange diamonds, B, T6 4.5 nm green circles, C, T6 7.5 nm open black triangles, D, T6 15 nm filled violet triangles, E) compared with the ones of unipolar transistors based on PDI-8CN$_2$ (filled blue squares) and T6 (filled red circles) single layers. In the inset, the transfer-curves of three of the devices realized in the configuration A, evidencing the NTC effect.

3.2.2 Electrical response of T6/PDI-8CN$_2$ heterostructure transistors

The electrical characterizations were performed in vacuum (10^{-5} mbar) and in dark conditions, using a Janis probe station. I_{DS} vs V_{DS} (drain-source current vs drain-source voltage at fixed gate-source voltages) output curves and I_{DS} vs V_{GS} (drain-source current vs gate-source voltage at fixed drain-source voltages) transfer-curves were recorded using a Keithley 487 picoammeter and a Keithley 2400 voltmeter.

Fig. 3-4 a reports the output characteristics (I_{DS} vs V_{DS}) of the T6/PDI-8CN$_2$ heterostructures in field-effect transistor configuration A, as a function of T6 layer thickness (from 1 nm to 15nm) and with fixed PDI-8CN$_2$ thickness (24 nm). For comparison, the electrical response of single layer PDI-8CN$_2$ (24 nm thick) and T6 (15 nm thick) devices are also reported. The output curves have been recorded with V_{GS}=0 V and V_{DS} sweeping from 0 to 50 V; the main feature observed in each of these curves are discussed in detail in the following.

The single layer PDI-8CN$_2$ device and the double layer T6 (1 nm)/PDI-8CN$_2$ heterostructures display a typical n-type behaviour, with unipolar electron current saturating at high V_{DS} voltages. This behaviour is expected, since a nominal 1 nm thin T6 film is unable to carry a

current (of hole carriers), since the islands are physically disconnected.

In the single layer (p-type) T6 device, we observe that the output curve does not saturate at high positive V_{DS}; this occurrence indicates the injection of mobile holes from the drain electrode at high positive V_{DS}, when the voltage between gate and drain becomes negative. In this case, a maximum current of about 70 μA is achieved.

Finally, the output current of all the other devices, the T6/PDI-8CN_2 heterostructures having T6 thickness higher than 1 nm, increases at high V_{DS} without saturation. This experimental occurrence confirms the capability of these devices (being based on continuous T6 films) to support the flow of holes from source to drain. Moreover, the maximum current values at V_{DS}=50V ranged between 300 and 400 μA, values much higher than those supported by a single layer T6 transistor. This current enhancement (in an operation region of the transistors where the electron currents saturate, getting values not higher than few μA, as shown above) can be justified only by considering an increase of mobile hole conductivity, promoted by the presence of T6/PDI-8CN_2 interface.

The specific features of the electrical response of these devices are further analyzed in Fig. 3-4 b, where their transfer-curves recorded in linear regime (V_{DS}=5 V) are presented. A mobility value was extracted from the MOSFET equations in the V_{GS} driven accumulation regions, where the carrier density is modified by the field-effect with respect to the basic equilibrium configuration. We followed the procedure used in [79] and [24], with the goal to allow the reader to compare, on the base of mobility values, the performances of our devices with the one of other transistors discussed in literature.

The n-type single layer PDI-8CN_2 transistor exhibits a mobility of 0.03 cm^2/volt*sec in good agreement with the performances reported for similar bottom-contact devices [111]. The onset voltage V_{on} (defined as the voltage where the drain-source current starts to increase, exceeding the lower limit of our experimental set-up) is largely negative (V_{on} -13 V). As already observed from the output curves, the T6 (1 nm) / PDI-8CN_2 heterostructure behaves exclusively as a n-type transistor and only the electron accumulation region can be detected. Despite the inability of the 1 nm thick T6 bottom layer to support the hole current, its presence affects deeply the overall transistor operation. Indeed, in this case, the extracted mobility and the onset voltage are equal to about 0.015 cm^2/volt*sec and -17 V, respectively.

The occurrence of the negative V_{ON} voltage in the single layer PDI-8CN_2 device is due

to the large electron affinity of the cyanated perylene derivatives, providing an unintentional material doping due to the interaction with the chemical functional groups (i.e. silanol and carbonyl) present on the bare SiO_2 surface [115].

In the T6(1nm)/PDI-8CN_2(24nm) heterostructure, V_{ON} has a tendency to shift (of about -4V) towards more and more negative values, even if the contact area between PDI-8CN_2 film and SiO_2 surface is reduced. These experimental finding seems to suggest again that the formation of the organic-organic interface is able to provide a not negligible increase of the free charges density in the transistor channel.

The T6(15 nm)/PDI-8CN_2 device operates basically as a p-type transistor with a mobility of 0.015 cm2/volt*sec [123]. If compared with the single layer (15 nm thick) T6 transistor, a considerable enhancement of the mobility and of the overall current is detected. Indeed, the mobility of a single layer T6 transistor is about 0.005 cm^2/volt*sec (three times lower than the T6(15 nm)/PDI-8CN_2 device one) and the minimum current at V_{GS}=0 in the transfer-curve of T6(15 nm)/PDI-8CN_2 device is 4 μA, i.e. three order of magnitude higher than the off-current values measured for the single layer T6 transistor. This current enhancement is also present by considering different thicknesses of T6, and it is almost gate independent.

The T6(7.5nm)/PDI-8CN_2 device displays instead very clear evidences of ambipolar transport, since well defined accumulation regions are achieved for both charge carrier types [7]. Hence, the best balance for the electron and hole mobility, equal to 0.0035 and 0.0095 cm^2/volt*sec, respectively, is found. However, in the transfer curve of this device, a peculiar electrical feature is observed at large negative V_{GS} values, where the current (dominated by the hole contribution) unexpectedly begins to decrease and gives rise to a peak. This phenomenon, usually named negative transconductance (NTC) effect, is still more evident in T6/PDI-8CN_2 heterostructures with T6 thickness of 2 and 4.5 nm as magnified in the inset of Fig. 3-4. Here, the device current seems almost to cancel out at highly negative V_{GS} and the overall transfer-curves are strongly affected by the NTC effect.

From our experiments, we conclude that the NTC occurrence is unambiguously related to the T6 thickness, since its gate voltage position depends on the T6 thickness and increases when this thickness increase from 2 nm to 7.5 nm. For thicker T6 films, the position of the NTC peak could eventually exceed the value of V_{GS} = -50 V, which is the maximum gate voltage investigated (in order to avoid dielectric breakdown phenomena in our devices). This is the

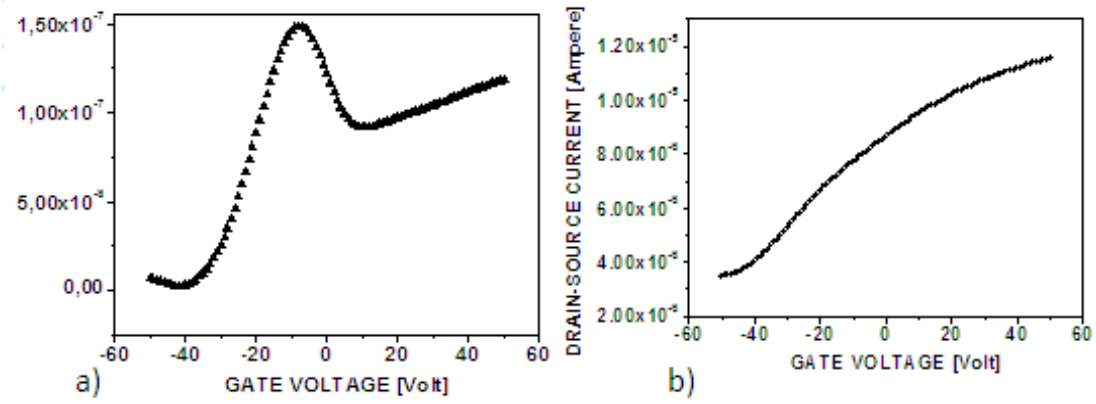

Figure 3-5: a) Transfer-curves recorded in linear region (V_{DS}=5 V) for the PDI-8CN_2 5 nm/ T6 22 nm bilayer device (configuration B). b) Transfer-curves recorded in linear region (V_{DS}=5 V) for the co-evaporated (configuration C).

reason why the NTC effect is not observed in T6(15nm)/PDI-8CN_2 heterostructures.

To gain further insights about the physical origins of the NTC phenomena, we fabricated and characterized electrically field-effect transistors in configuration B (T6 and PDI-8CN_2 as top and bottom layer, respectively) and configuration C (co-evaporated).The transfer-curves of the PDI-8CN_2 (5 nm)/T6(22 nm) bilayer (Fig. 3-5 a) also exhibits a NTC effect which, very interestingly, occurs again for negative gate voltages. On the other hand, the transistor with the co-evaporated active channel (Fig. 3-5 b) displays mainly a n-type behaviour with only a moderate current modulation as a function of the gate voltage (ON/OFF current ratio is lower than 4). Moreover, no NTC effect can be observed in this case.

Transfer (Fig. 3-6) and output (Fig. 3-7) curves at different temperatures have been also recorded in order to deepen the effect of current decrease; the attention has been focused on four samples: a device with a layer of PDI-8CN_2 alone; a 2 nm T6/ 24 nm PDI-8CN_2 bilayer exhibiting the above exposed effect; a 7.5 nm T6/ 24 nm PDI-8CN_2 bilayer which substantially shows an ambipolar behaviour, a 15nm T6/ 24 nm PDI-8CN_2 bilayer with a predominantly a hole transport. In Fig. 3-8 mobility and conductance are extracted from the data in Fig. 3-6 and 3-7.

In the case of PDI-8CN_2, n-type transfer curves exhibit a shift versus lower negative voltages, such as the 15nm T6/ 24 nm PDI-8CN_2 bilayer, while for the 7.5nm T6/ 24 nm PDI-8CN_2

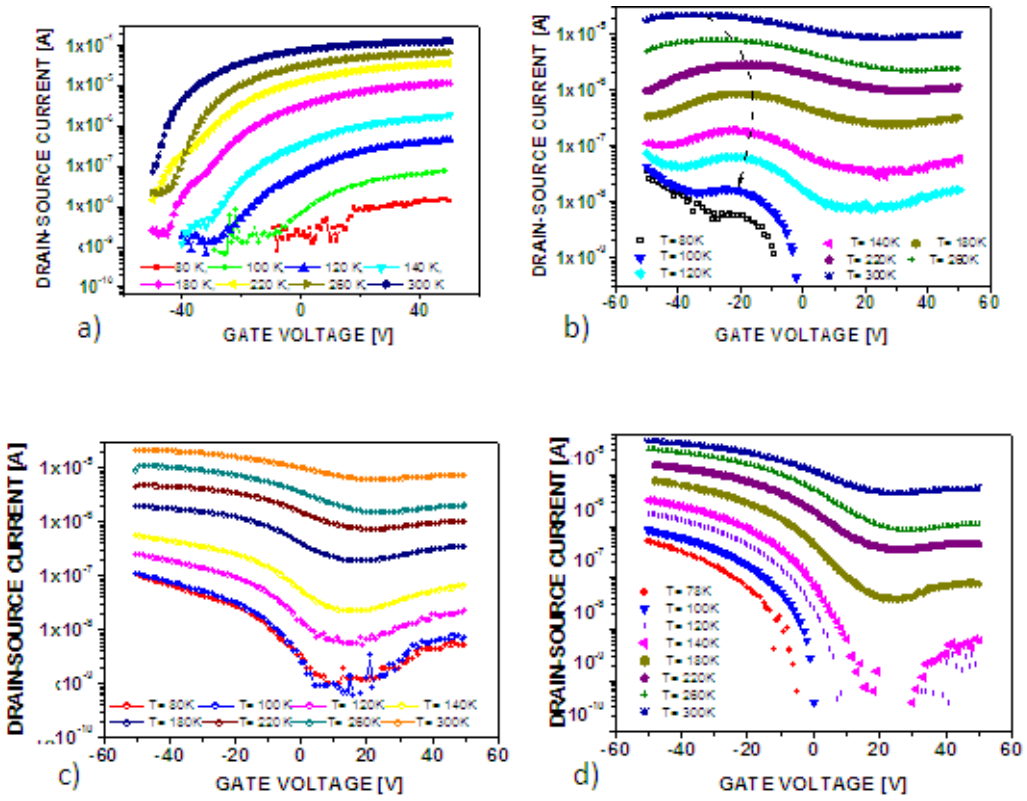

Figure 3-6: Transfer curves recorded at different temperatures for the four samples considered: a) PDI8CN2, b) 2 nm T6/ 15 nm PDI8CN2 bilayer, d) 7.5nm T6/ 15 nm PDI8CN2 bilayer, c) 15nm T6/ 15 nm PDI8CN2 bilayer.

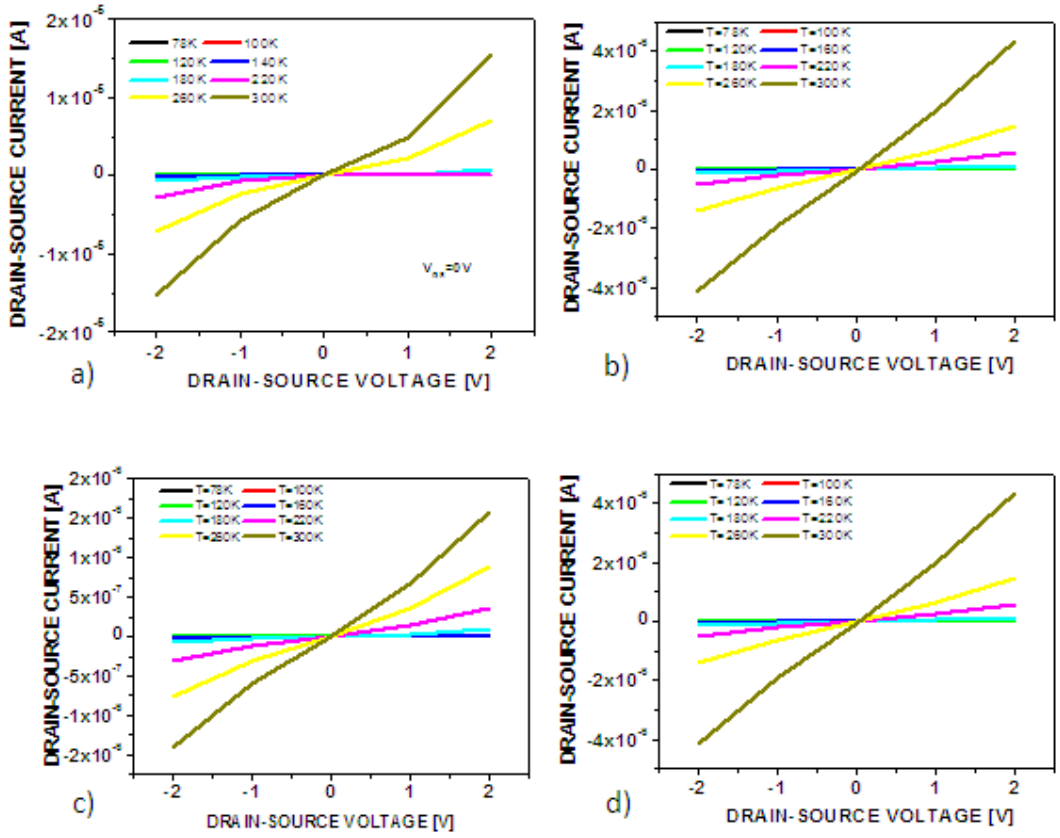

Figure 3-7: Output curves recorded at different temperatures for the four samples considered: a) PDI8CN2, b) 2 nm T6/ 15 nm PDI8CN2 bilayer, d) 7.5nm T6/ 15 nm PDI8CN2 bilayer, c) 15nm T6/ 15 nm PDI8CN2 bilayer.

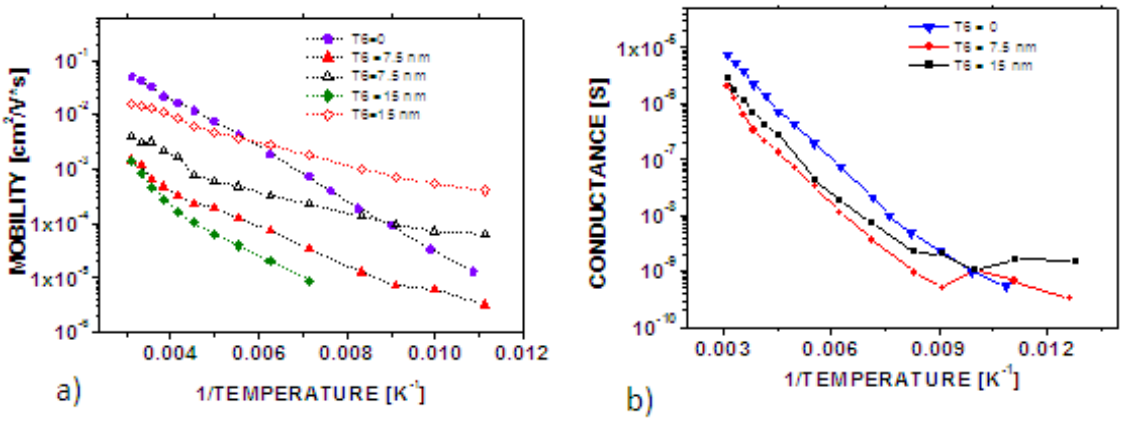

Figure 3-8: a) Mobility and b) conductance versus temperature extracted from the data in 3-7 and 3-6.

bilayer the v-shaped curve shows a downward shift, and the minimum of the curve becomes more and more evident at decreasing temperature. The 2 nm T6/ 24 nm PDI8CN$_2$ bilayer exhibits the more peculiar features. At decreasing temperatures the decreasing of the hole current at high negative voltages become more and more evident, accompanied by a shift of the maximum of the peak toward less negative voltages, such as in the case of the sole PDI-8CN$_2$.

As mentioned in the experimental section, the evaluation of the field effect mobility was not possible in all cases, such in the case of the 2 nm thick T6 bilayer. The mobility of the heterostructures exhibits thermally activated behaviour, which implies a conduction mechanism dominated by hopping transport defect states.

Only in two cases the mobility temperature behaviour obeys to the so called Arrhenius law, as predicted by the Multiple Trapping and Release (MTR) model, for the sole PDI-8CN$_2$ and for the 15 nm T6/ 24 nm PDI-8CN$_2$ bilayer, which behaviour is almost unipolar. They consequently follow the subsequent relation

For PDI-8CN$_2$ the activation energy (E$_a$) results to be equal to 91 meV in the linear regime. On the other hand, in saturation there are two regimes, the first, between 90 and 160 K, corresponding to an activation energy of 95.7 meV, while the other, between 160 and 320 K, giving an activation energy of 77 meV.

In the case of T6, in linear region two different regimes have been found, one comprised

between 78 K and 160 K and the other between 160 K and 320 K with activation energies respectively equal to 52 meV and 37 meV, both quite lower than the case of PDI-8CN_2.

3.3 Heterojunction band alignment model and discussion

3.3.1 Equilibrium heterojunction properties

Summarizing the results reported in the previous sections, we have observed that the formation of the interface between T6 and PDI-8CN_2 films produces a considerable enhancement of the hole current flowing into those heterostructures comprising continuous T6 films. Moreover, in comparison with the single layer T6 device, the values of holes field-effect mobility are largely improved in the T6/PDI-8CN_2 heterostructures (with T6 thickness of 7.5 and 15 nm) exhibiting well-defined hole-accumulation regions in the transfer-curves. This can occur in the case of heterostructures, as a consequence of the trap filling due to the accumulation of charges (see [79] for instance). Furthermore, even a T6 layer formed by disconnected islands (submonolayer coverage) has revealed to modify the density of free charge carriers in an unipolar n-type device.

All these experimental findings are likely to indicate an enrichment of the mobile charges in the organic double layer heterostructures, which can be explained taking into account the presence of an accumulation heterojunction. Indeed, a chemical reaction between T6 and PDI-8CN_2, like a formation of an intermixing layer, can be excluded by electrical and optical measurements. First of all, the current and the mobility of transistors with the co-evaporated active channel are lower than that one of the double-layer structures; moreover, even if the output curves reveal the presence of ambipolar transport, the blend structure exhibits a very poor current modulation driven by the field-effect, indicating that the density of free carriers (eventually due to the charge transfer effects) cannot be increased by the application of a gate voltage.

These results are very interesting since they remark the deep differences between the properties of the blend and the layered devices; the former, indeed, are expected to be much more disordered systems, with a wider Gaussian distribution of localized electronic states which can act as trapping centres being able to completely localize the charges [124]. The ambipolar behaviour suggests that the semiconductors form distinct percolative paths, while the non-zero

current at zero gate, and its slight variation with the gate-voltage, can be explained only by supposing that the density of carriers is increased by charge transfer, but that these charges are characterized by low mobility due to high degree of structural disorder. On the other hand, since in the layered heterostructures the electric behaviour is strongly gate-dependent, this excludes the presence of an intermixing layer at the interface.

The phenomena above discussed are consequently originated by a purely interfacial phenomenon, which can be explained only taking into account the presence of an accumulation heterojunction. Indeed, an increase in the density of, respectively, free holes at the HOMO and free electrons at LUMO level can justify the increase in current and mobility. Following a classical band structure picture, in an accumulation heterojunction the alignment of Fermi levels, which is simply a manifestation of a charge transfer at the organic/organic interface, implies the electron transfer from the maximum of the conduction band of the p-type semiconductor to the minimum of the valence band of the n-type one.

On the basis of our experimental results and on data reported in the literature (partly from measurements on the single molecules and partly from transport data) we can infer that the Fermi level of the two semiconductors before the formation of the interface lies in the centre of the forbidden gap for T6 and, due to its intrinsically doped nature [17], near the LUMO for PDI-8CN_2 respectively, We can consequently conclude that the T6 work-function (ϕ_P) is lower than the PDI-8CN_2 one (ϕ_N), even admitting that it is closer to the LUMO. As a consequence, the alignment of the Fermi levels implies the transfer of an electron from the HOMO level of the p-type semiconductor to the LUMO level of the n-type compound; this motion is accompanied by the formation of built-in local electric field which bends the electron and hole band (LUMO and HOMO levels) at organic/organic interface.

This mechanism in our case has been illustrated in the Fig. 3-9a, which reports the energy levels of the two semiconductors, while the picture described above is sketched in Fig. 3-9 b, where the equilibrium configuration of relevant energy levels of both T6 and PDI-8CN_2 has been depicted. For simplicity eventual contributions from interface dipole have been neglected, using the values reported in Fig. 3-9 a for electron affinity (χ) and ionization potential (I); the suffix "1" and "2" refer to T6 and PDI-8CN_2, respectively. In the figure, the z-axis is oriented normally to the interface, the SiO_2/T6 interface occurs at position z=0, while the thickness of T6 layer is indicated by L. For the sake of simplicity, the Fermi level position was assumed to

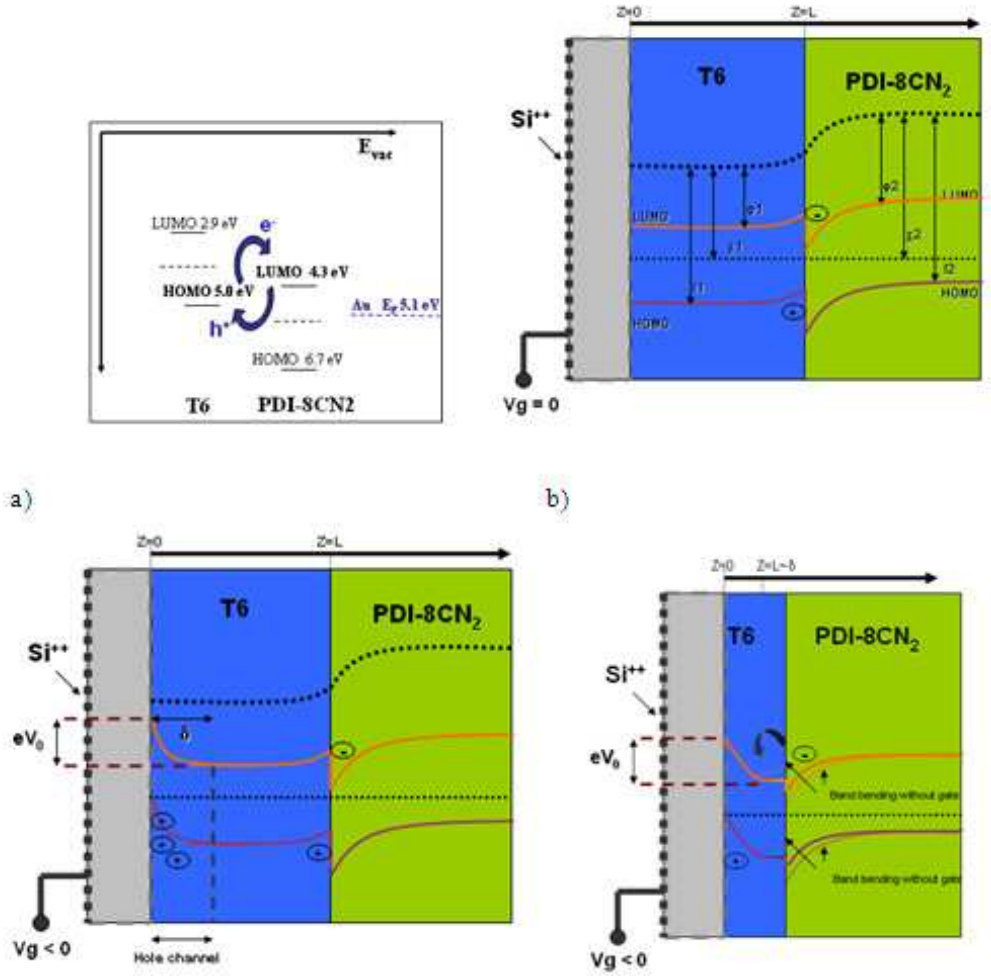

Figure 3-9: a) Charge transfer effect and band diagrams for T6/PDI-8CN2 heterostructures. b) Energy configuration at thermal equilibrium, where electron affinities (χ) and ionization potentials (I) indicated in Fig. 6A have been used. c) Energy configuration under applied negative gate, for T6 thickness larger than electric field penetration depth δ, d) Same but for the case of T6 thickness of the order of δ.

be at middle of HOMO-LUMO gap.

3.3.2 Gate voltage effect on heterostructure energetics: the NTC phenomenon

As already mentioned in the previous section, in the transfer curves at large negative V_{GS} values, the hole - dominated current unexpectedly begins to decrease and gives rise to a peak as magnified in the inset of fig. 3(b). This phenomenon is usually named negative transconductance (NTC) effect and is well known for inorganic devices based on semiconducting heterostructures [125] [126], while has been reported and discussed very rarely for organic based devices. A peculiar electrical behaviour with some similarities to our experimental findings has been recently observed in the transfer current–voltage characteristics of double-layered field-effect polymer transistors [127]. Indeed, it was shown that F8BT/TFB heterostructures exhibit an unusual plateau in the forward scan of the corresponding transfer-curve. Both the eventual presence and the magnitude of the transport current in the plateau regions were found to be dependent on the starting voltage of the forward gate voltage sweeping cycle. However, differently from Liu et al. [127], in our case no current plateau is observed, while instead a maximum current (i.e. a peak in transfer curve) followed by a net decrease in channel conductance at increasing negative values of gate voltage. We did not observe evident differences in the forward and backward scans of the transfer-curves. This excludes the possibility of a simply trapping and a subsequent de-trapping of charges at high gate voltages.

We consequently propose a different explanation for the NTC effect, according to the accumulation heterojunction picture, instead of trapping. The NTC effect is a phenomenon strongly gate-dependent, since the gate bias at which occurs varies monotonically with the T6 thickness; the absence of this effect in the coevaporated transfer curves, while instead is present in the reversed configuration device, represents consequently a further indication that this is basically an interfacial phenomenon, as discussed in the previous section.

The charge accumulation layers across the interface, sketched in Fig. 3-9 b, can be invoked from both electrical and optical characterization evidences. After the application of a negative gate voltage at Si electrode (Fig. 3-9 c) a transverse voltage profile builds up along the z direction. In figure 3-9 c, the voltage value at z = 0 is indicated by V_0, thus associated to an

additional (positive) potential energy -eV$_0$, corresponding to an upward bending of molecular levels in T6. Hole accumulation thus takes place at SiO_2/T6 interface, giving rise to the hole channel in the OFET.

Assuming that the thickness of the T6 layer (L) is larger than the hole accumulation length (indicated by δ in Fig. 3-9 c, so that the T6 film is able to accommodate the amount of charge needed to fully screen the external voltage (V_0), the molecular levels can be depicted as flat in the "bulk" of T6 (as in Fig. 3-9 c) and the electric field does not reach the interface. In the depicted condition, we can consequently infer that the application of the gate has no influence on the electronic structure of the region near to the interface between the two semiconductors.

The last statement holds no more once very thin T6 layers are considered, since the situation is here completely reversed. Indeed, in the case of L $\backsim$ λ or L$<\lambda$ the electric field penetrates inside the T6 up to the interface and hole accumulation extends throughout the whole T6 layer, resulting in a redistribution of both voltage profile and hole density also in the region close to the T6/PDI-8CN$_2$ interface. The redistribution implies that at largely negative V_{GS} the holes accumulated (due to the heterojunction effect) at the organic/organic interface spread indeed toward the SiO_2 interface, as shown in Fig. 3-9 d. In other words, the holes previously accumulated in the region close to the T6/PDI-8CN$_2$ interface are thus redistributed toward the SiO_2/T6 interfacial region in order to screen the external voltage. Consequently we have a flattening of the molecular bending of T6 levels at the heterojunction interface.

The application of a negative gate voltage consequently determines a decrease in the interface built-in field; the effective potential barrier confining the excess electrons in PDI-8CN$_2$ is lowered, facilitating the migration of electrons from PDI-8CN$_2$ to T6 where they can recombine with free holes, thus decreasing the density of mobile charge and the channel conductance. The phenomenon is schematically shown in Fig 3-9d, describing a T6 layer whose thickness is close to the hole accumulation length; here, the dashed lines indicate the band profile without any bias applied, in order to evidence the reduction of the band bending after the application of the gate.

This interpretation of NTC effect allows to qualitatively explain why the current drop in transfer curves occurs at larger gate voltages once the T6 thickness is increased. The results also indicate that charge accumulation in T6 occurs up to the third monolayer, in agreement with the findings of Dinelli et al. [122].

Interestingly enough, in similar heterostructures field-effect transistors in which charge transfer has been also observed [85] the NTC phenomenon is not present, even for thin bottom layer thicknesses. The explanation of this striking difference can reside in the peculiar electronic structure of PDI-8CN_2, which electrical behaviour resembles a doped semiconductor, showing for instance a negative threshold voltage [120] (n.d.r. in addition, our experimental findings on PDI-8, an n-type organic semiconductor with the same chemical structure except for the absence of the cyano groups, have not given the same results).

3.4 Conclusions

Sexithiophene (T6)/ N,N'-bis (n octyl)-dicyanoperylenediimide (PDI-8CN_2) heterostructures have been realized and studied as the active channel of field-effect transistors. Both layered, also with various layer thicknesses, and blend configurations have been fabricated through high vacuum evaporation. A complete electrical characterization and a morphological study have been performed in the different cases, highlighting interesting phenomena arising solely with the presence of an homogeneous interface between the two semiconductors.

Moreover, with the application of the gate, ambipolar transport and Negative Transconductance (NTC) phenomena (i.e. a decrease followed by an eventual nullification of the drain-source current at increasing gate voltages) have been observed.

A model has been proposed as a possible explanation of these phenomena describing the energetic levels at the heterointerface at the equilibrium and in presence of a field-effect, and accounting for the band bending promoted by the charge transfer at the interface. In this scenario, the NTC effect can be explained in terms of a further shift of the energetic levels at the interface due to the application of a gate voltage, which in favourable conditions, leads to recombination of charges.

Chapter 4

Schottky Gated Organic Heterostructures

Organic single crystals exhibit more reproducible and stable electrical performances, and consequently are the subject for an intense study devoted to the clarification of the fundamental issues of the charge transport in organic semiconductors. Here Schottky-gated heterostructures are used to probe the conducting layer that spontaneously forms at the interface between rubrene and PDI-FCN_2 single crystals, the materials that perform best in p- and n-channel organic single-crystal Field Effect Transistors (FETs). The resulting configuration resembles the one of a High Electron Mobility FET (HEMFET), which has been introduced in the first chapter and actually the physical response of the device reminds it in several aspects, such as for the formation of a 2D electron gas at the interface.

In this chapter I am presenting the electrical characterization on the samples I have made, but the conclusion take into account the results obtained from the whole group. The relization of the devices has been totally developed at the University of Geneva and the experimental results will be the subject of a scientific publication.

4.1 Device realization

Organic heterostructure devices can be realized accounting for different fabrication techniques and device architectures. The realization of a single crystal heterostructure can be accomplished

only through a delicate procedure which depends on the operator precision. Indeed, once the fragile organic single crystals are separately grown, they have to be laminated, aligned and assembled into micrometric devices by hand. Every damage in the crystals or in the metal used as a gate reduces or nullifies the performances of the devices.

Nevertheless, even if handling organic single crystals reveals to be a delicate task, focusing the attention on organic single crystals brings about several advantages. First of all, the intrinsic higher molecular ordering is responsible for the more reproducible performances, rendering them a perfect case study for the deepening of the physical mechanisms behind electronic conduction in organic semiconductors [53].

As discussed also in the previous chapters, the morphology and crystalline order of the organic thin films are instead very poorly reproducible, and so are the electrical properties [85]. This leads to a further complication in the realization of organic heterostructures, since it is expected that the molecular arrangement at the heterointerface, which cannot be easily controlled, will play a fundamental role into the transport properties at the interface. Separating the contribution of the morphology to that of the charge transfer at the heterointerface reveals a hard task which cannot be easily overcome.

Finally, in single crystals the effect of unintentionally present dopants in the bulk can be in general safely neglected [128], while in thin films the conduction through the bulk results more favored because of the high concentration of dopants. This renders more complicated in organic thin films the individuation of the region in which the charge transport actually occurs, since the conduction can equally arise at the interface or in the bulk.

Two device structures were realized, with two (Fig.4-1 a) or six probes (Fig.4-1 a). The first configuration brought the advantage of a simpler fabrication procedure but allowed only transfer and I-V curves measurements at low temperatures; the second one was instead purpose-made just for Hall effect measurements but also gave the opportunity to measure the four probe resistance, in order to investigate the possible effect of contact resistances on the behaviour of the interface.The materials chosen for the interface are rubrene as the p-type semiconductor and PDI-FCN_2 as the n-type one. Rubrene exhibits the highest mobility among p-type organic single crystals [129] and results consequently in one of the most studied organic single crystals. Its bulk [130] and surface [99] properties have been extensively studied; on different dielectrics, it exhibits a dependence of the mobility on the dielectric constant of the insulator material [100]. In a field

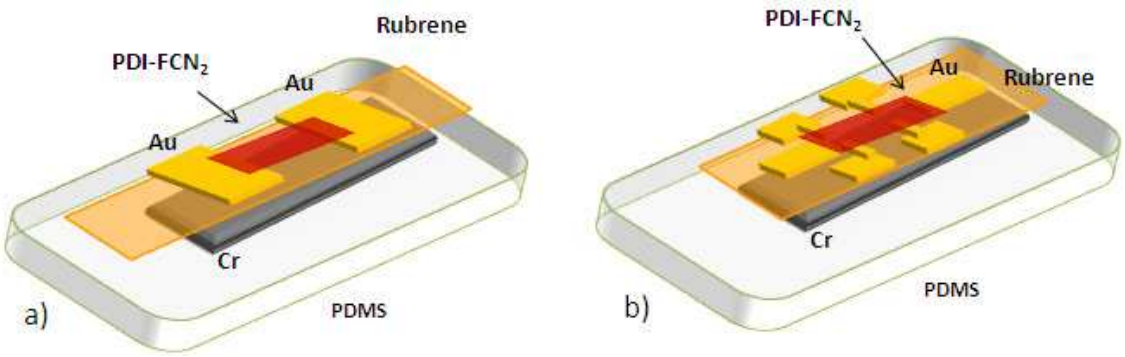

Figure 4-1: The Schottky Gated Organic Single Crystals Heterostructure: a) basic configuration; b) Hall effect measurement configuration.

effect configuration a gate-electric-field-induced crossover from thermally activated to nearly temperature-independent transport has been observed [131], while Hall effect measurements have demonstrated a band like behavior, with an increase of the mobility at lower temperatures [132]. Rubrene HOMO level is at 4.62 eV, while the LUMO at 1.14 eV, according to UPS measurements [133] and knowing that the gap is 2.3 eV [134].

PDI-FCN_2 is one of the most air stable, high mobility n-type semiconductors [11] [120] The best results with single crystals have been obtained in air gap field effect configurations, exhibiting a mobility of 5 cm^2/Vs [113] or even 6 cm^2/Vs [14]. In field effect devices with air gap configuration, a decreasing of the mobility until 175 K has been also observed [135]. The LUMO level has been determined as 4.5 eV by cyclic voltammetry measurements, while the HOMO level, 6.8 eV, has been obtained knowing that the optical gap of the material results to be 2.3 eV [17].

Different metals [104] have been demonstrated the formation of a Schottky barrier at the interface with rubrene or have been even used for the realization of organic MESFETs [49] [105]. In our case chromium has been chosen, since it was the simplest metal to handle, which exhibits a Fermi level of 4.5 eV; the formation of a Schottky barrier at the interface with rubrene is verified by experimental measurements.

In the following, we will expose the device realization procedure.

4.1.1 Device realization steps

The realization of the Schottky gated heterostructures was composed of several steps. The organic single crystals have been grown according to the procedure reported in the previous chapter, par. 2.1.2. The width of rubrene crystals used for the devices can vary between about 400 μm to more than 1 mm, in order to completely cover the underneath gate and avoid a possible short circuit with the source and drain electrodes. The length can range in the order of several hundreds of microns, sufficient to allocate the electrodes. The thickness of the crystals can be regulated to more than a mm depending on the time of growth (between 15 minutes and 48 hours); the transparency of the crystal gives an indication of the thickness. In our case, we used crystals about 2 μm thick or less, in order to have a depletion region covering the whole thickness of the crystal. Regarding instead the $PDIFCN_2$ crystals, the width was between 50 and 150 μm and the length between 100 and 400 μm. The time of growth was between 24 and 48 hours.

At first, the gate was evaporated by electron beam evaporation onto the substrate, a PDMS stamp (see Fig. 4-2 a) and Fig. 4-3 a)). Shadow masks were used to define a stripe of metal, with a width ranging between 200 and 400 μm. The continuity and uniformity of the layer were found to be basic requisites to guarantee the conductivity of the metal and were provided by deposition of four metal layers, in the following order and thicknesses: 3 nm of Ti, 22 nm of Au, 3 nm of Ti, 22 nm of Cr.

The micrometric organic crystals were manipulated with the aid of a hair. The crystal has been properly chosen without any optically visible defect and was then laminated through electrostatic bonding. A complete adhesion of the crystal on the Cr stripe was the requisite to fulfill in order to guarantee the formation of a Schottky barrier between the metal and the rubrene crystal (see Fig. 4-2 b) and Fig. 4-3 b)). The crystals adhere spontaneously on the substrate through electrostatic bonding, even though the quality of the adhesion greatly depends on the conditions of the substrate and of the crystal, and in several cases it was not successful. In the Fig. 4-3 b), for instance, it is possible to observe the presence of reflections on the surface of the crystal, which indicate an incomplete adhesion.

Au (15 nm) source and drain contacts were directly deposited on the rubrene crystal through electron beam deposition (see Fig. 4-2 c and e and Fig. 4-3 c and e). Handmade shadow masks

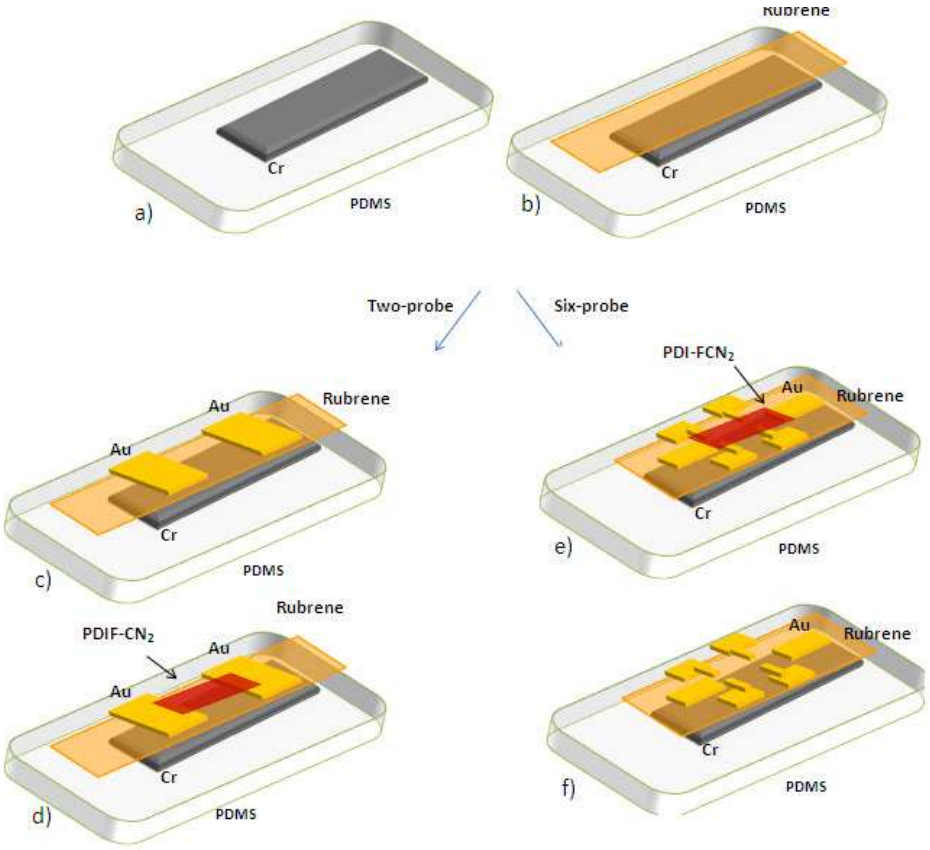

Figure 4-2: Panel showing the device fabrication steps both for a two (c and d) and a six (e and f) probes configuration. a) Chromium stripe on PDMS stamp; b) rubrene crystal laminated on the chromium stripe; c) and e) Au electrodes deposited on the rubrene crystal; d)and f) PDI-FCN_2 crystal laminated on the rubrene crystal and on the Au electrodes.

were used to shape the deposition areas in the case of a two probe configuration. For the six-probe devices SU-8 masks were instead fabricated by optical litography (Fig. 4-4 a). SU-8 was spinned on a clean silicon substrate, baked, exposed to UV light, post-baked and finally developed. The SU-8 was then lifted-off with an acqueous KOH solution. The alignment of the mask was performed under an optical microscope in order to guarantee that the Hall probes were perfectly aligned with the gate stripe (Fig. 4-4 b and c).

The PDI-FCN_2 crystal was chosen with criteria similar to those used for rubrene (see Fig. 4-2 d) 4-3 d) and 4-3 e)) and was then laminated under an optical microscope on the top of the rubrene crystal. The position of the crystal is very important especially in the fabrication of the four probe devices, since it has to be perfectly aligned with the Hall probes.

Finally, 25 μm diameter gold wires have been used to contact the gold source and drain electrodes, attached with about 250 - 300 nm diameter drops of solvent free silver epoxy paste (see Fig. 4-3 d)). Since the devices were extremely fragile, the devices had necessarily to be manually bonded.

4.2 Experimental results

Organic Schottky gated heterostructures need to exhibit the following features in order to be considered of good quality. The gate should be conductive, with a resistance lower than tens of kΩ and the Schottky gate should be rectifying for positive voltages applied to the metal gate (p-type semiconductor Schottky gate). The interface should be conductive even without the gate connected as a signature of the charge transfer at the interface; the output curves should exhibit a linear behavior, indicating a small effect of contact resistances. In the best devices, for positive voltages applied to the gate (i.e. when the Schottky gate is rectifying), the leakage current is at least an order of magnitude lower than the drain source voltage, with and without a gate applied. The gate field-effect should manifests itself through the increasing of the absolute drain source current with the absolute gate voltages more than the leakage current does.

The results shown here are my contribution to a research project developed in the framework of a collaboration with the prof. A.F. Morpurgo in the University of Geneva. The analysis and the interpretation discussed in this work are based on the totality of the results which are

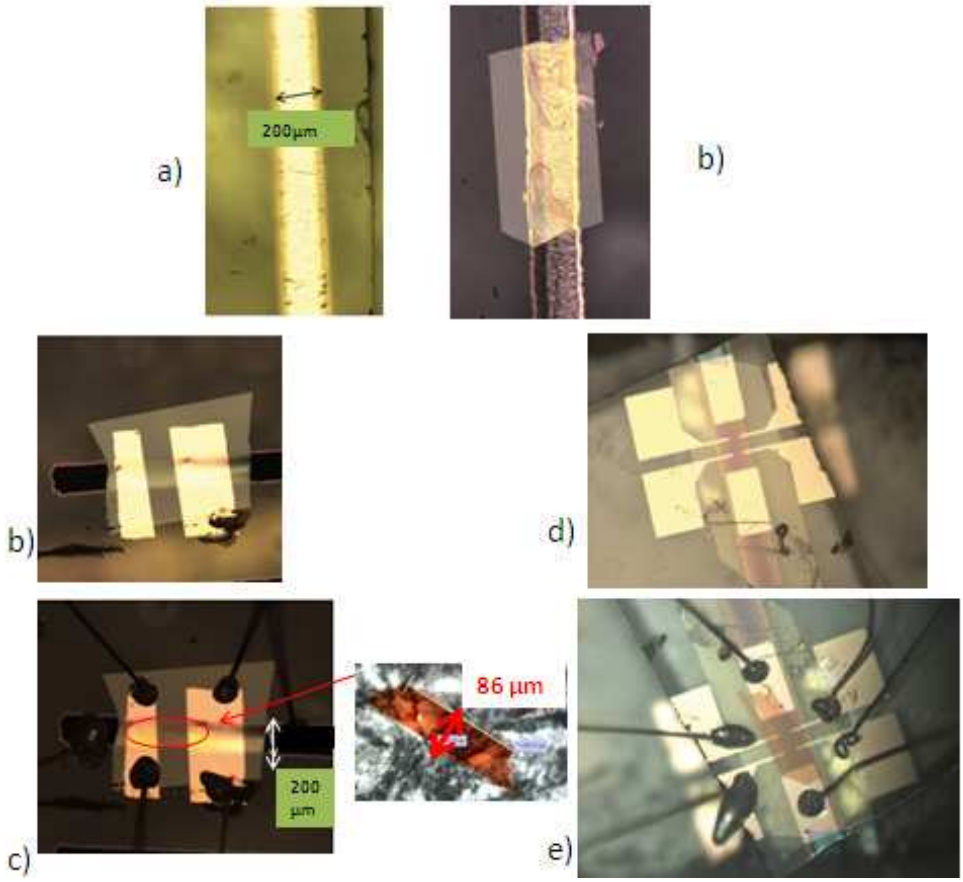

Figure 4-3: Panel showing pictures of the devices in different fabrication steps for both a two (c, d) and a six (e, f) probes configuration. a) a 200 m Cr stripe on PDMS; b) a rubrene crystal laminated on a Cr stripe (the waves indicate regions in which the adhesion is not good); c),e) Au electrodes deposited on rubrene; d),f) PDIF-CN_2 crystal laminated on the rubrene crystal and in the Au electrodes with a picture of a typical PDIF-CN_2 crystal (between c and e).

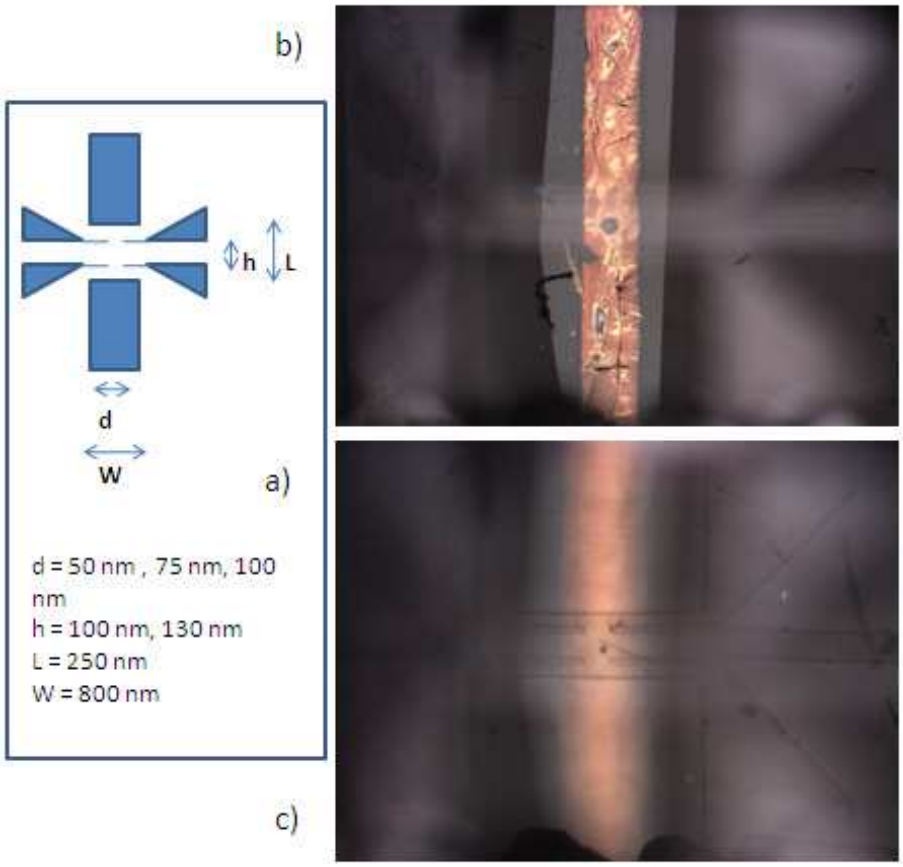

Figure 4-4: a) The typical configuration of the mask used to define the electrodes for Hall effect measurements with some typical sizes. Fig. b) and c) show the procedure of the SU-8 mask alignment with the Cr gate (b focus on the gate, c on the mask).

presented in [136]. I will present and comment in the following the electrical characterization of my best two devices realized; they have been indicated as "A" and "B", since they exhibit some different features. The electrical characterization has been performed from room temperature down to 50 K. The output curves and relative leakage currents have been recorded sweeping the source drain voltage between -10 V and 10 V and for different gate voltages applied (included zero). Transfer curves and relative leakage currents have been instead recorded sweeping the gate between -10 V and 80 V and applying different source drain voltages (including zero).

4.2.1 Electrical characterization

In order to verify the correct functioning of the gate voltage, the leakage currents of the transfer curves at zero source drain voltage have been considered. During the device operation they indeed basically correspond to the current that flows across the rubrene crystal through the Schottky barrier formed at the Cr – rubrene interface (Fig. 4-5). The device A does not show a rectifying behaviour, since the leakage current for positive voltages applied to the gate is higher than for negative ones (Fig. 4-5 a). Nevertheless, this does not affect dramatically the performances of the device, since the leakage current remains still lower than the drain one of three orders of magnitude. The occurrence simply implies that the leakage currents are unexpectdly high, probably depending on the impurities concentration in the rubrene crystal.

For the device B, as expected, the curves clearly exhibit a rectifying behavior, since the current magnitude depends on the bias polarity (Fig. 4-5 b). For positive voltages applied to the gate the carriers have to overcome the Schottky barrier and the current results lower. For negative voltage to the gate, the carriers do not encounter any barrier and the current flows through the rubrene crystal.In the Fig. 4-5 c the gate leakage current curves recorded at zero drain source voltage at several different temperatures have been shown for the device B. The current exhibits a quadratic dependence typical of a Space Charge Limited Current (SCLC) regime and experiences an exponential decrease with decreasing temperature, even for negative gate bias. This is characteristic of a thermally activated behavior of the carrier mobility, which indicates that the SCLC conduction takes place through states in the band gap of rubrene (traps) [137] [105].

From the curves reported in Fig. 4-5 c the variation of the current versus the temperature can be extracted (Fig. 4-5 d). From a fitting procedure, it is possible to determine the

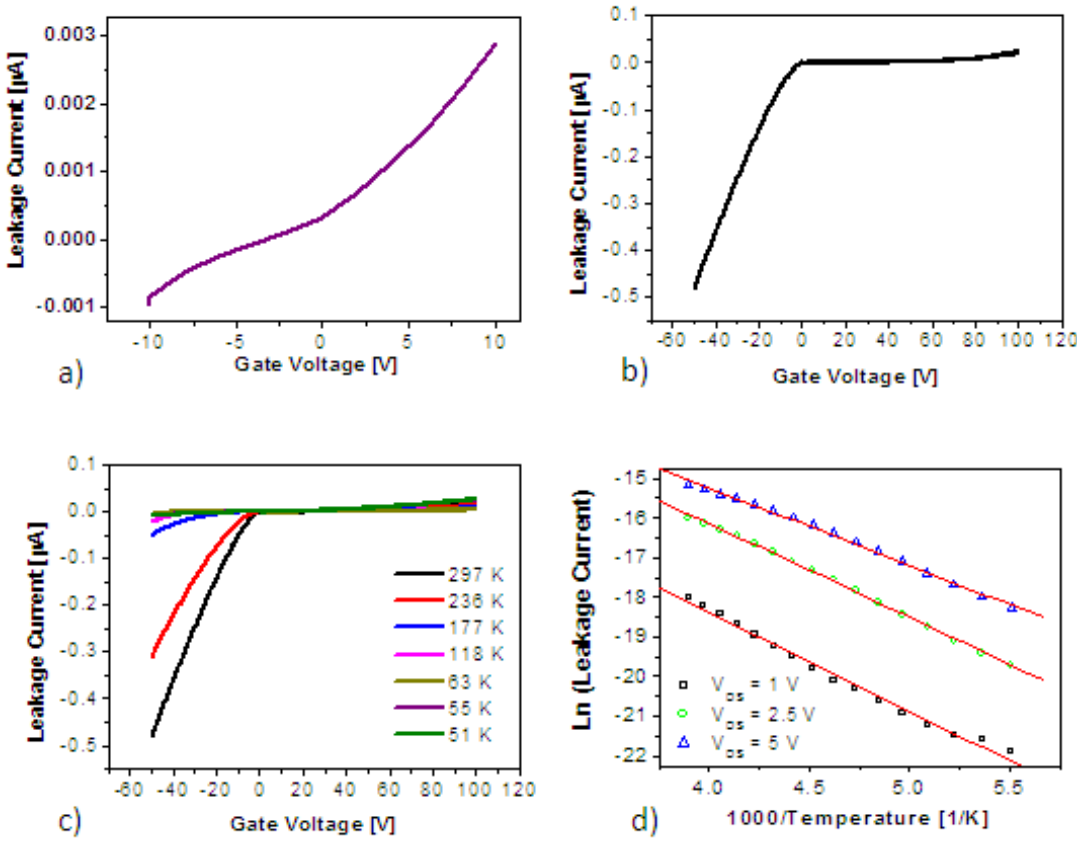

Figure 4-5: Gate leakage current curves recorded at zero drain source voltage at room temperature (a) for the device A and (b) for the device B several different temperatures. In c are instead reported gate leakage currents recorded at zero drain source voltage for the device B, from which the activation energy of the current is determined (d).

activation energy of the thermally activated mobility, which for the device under study results to be about 200 meV. Obviously the same analysis cannot be applied in the case of the device A, because of the absence of the rectifying behaviour.

The activation energy actually varies in a wide range depending on the specific device considered (between 250 and 400 meV [136]). Since it roughly corresponds to the difference between the Fermi level and the bottom of the valence band of rubrene, this suggest that the variations are due to the uncontrollable concentration of dopants unintentionally present in the rubrene crystal, different from device to device.

In Fig. 4-6 a and 4-6 b the output curves at room temperature are respectively reported for the device A and B. Fig. 4-6 c and 4-6 d show, instead, output at different temperatures for the two devices. For the device B, a non linear trend for high drain source voltage is evident and is typical of the presence of contact resistances. The non linearity is more evident at lower temperatures and at higher gates.

The square resistance extracted from the data in Fig. 4-6 results about 1.5 MΩ for the device A and 0.8 MΩ for the device B at room temperature (Fig. 4-7)). The device A exhibits an initial lowering of the resistance at high temperatures; the device B, instead first undergoes to an unexpected behavior characterized by a peak which origin is not totally clear at the moment. The other devices realized, indeed, only show a slight dependence on temperature, which can be either a decrease or an increase, depending on the device [136]. From about 120 K, instead, a further temperature decrease leads in all the cases to a rapid increase of the resistance.

The sign of the field in the transfer curves (Fig. 4-8) gives indication of an n-type behavior, which indicates that the current is carried by electrons. In Fig. 4-8 d it is possible to observe that the V_{ON} shifts versus more negative values at lowering temperatures.

The modulation of the current by the application of an electric field suggests the possibility to apply the same analysis currently used for transistors. The conductivity is given by the relation

$$\sigma(V_g) = n(V_g) e \mu_{FET} \tag{4.1}$$

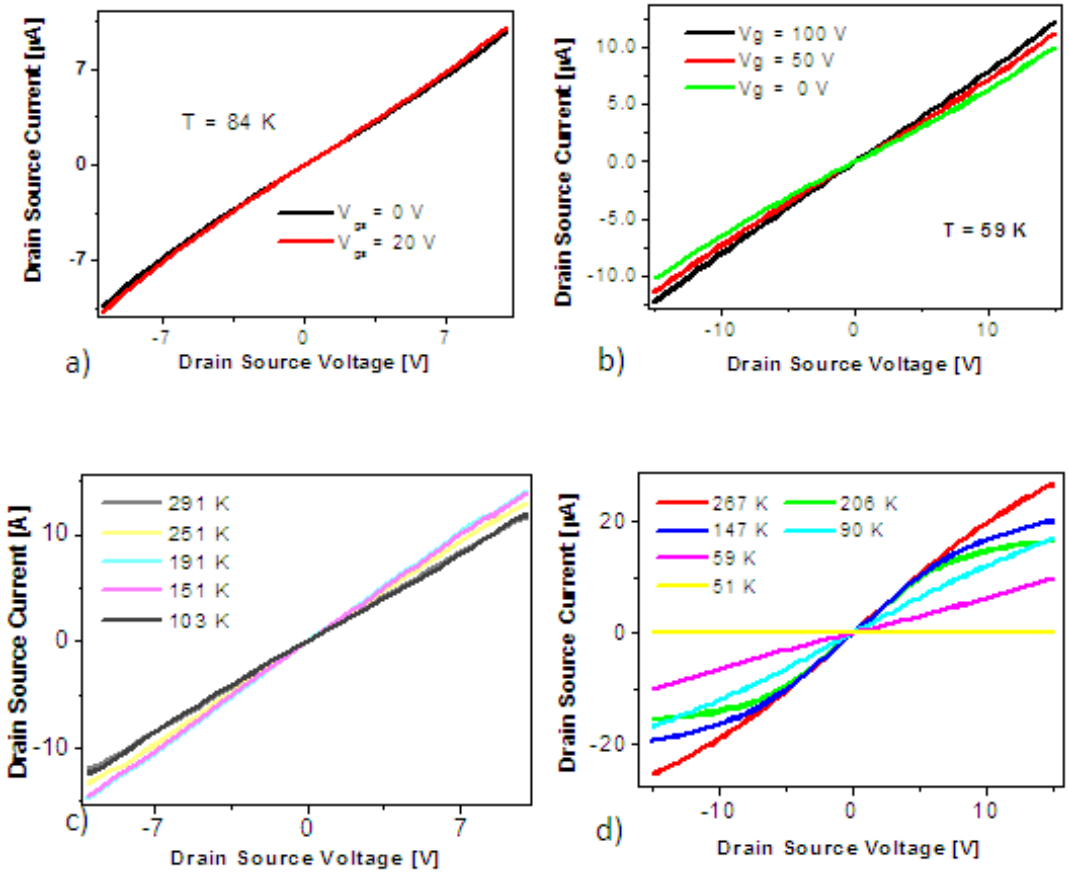

Figure 4-6: Output curves at zero gate voltage recorded at a) 84 K for the device A and b) 59 K for the device B. Output curves at zero gate voltage recorded at different temperatures for the c) device A and d) B.

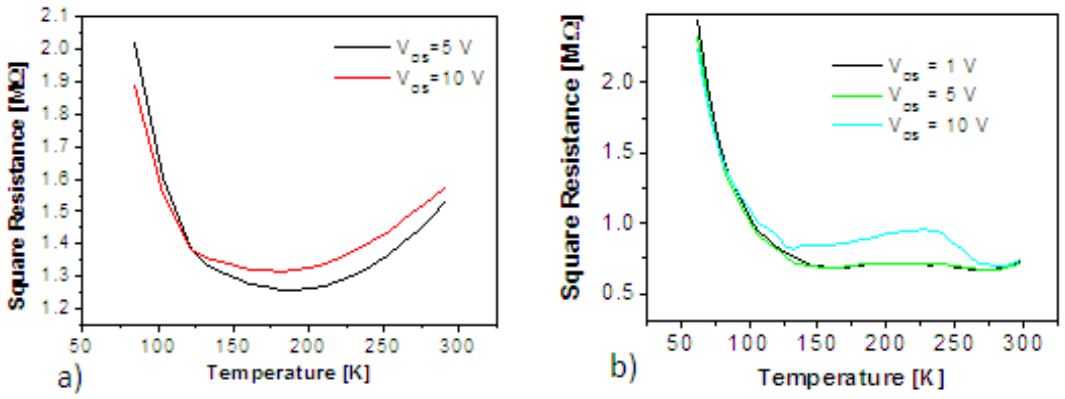

Figure 4-7: Square resistance versus temperature at zero gate voltage extracted from the output curves recorded at different temperatures for the device a) A and b) B.

where n(V_g) is the density of electrons at rubrene – $PDIFCN_2$ interface and is given by

$$n(V_g) = C(V_g - V_{th})/e \tag{4.2}$$

in the last relation, C = $\varepsilon\varepsilon_0/d$ is the capacitance per unit area between the interface and the gate, with d being the thickness of the rubrene crystal, measured by AFM analysis.

From the previous relationships the mobility can be consequently determined as:

$$\mu_{FET} = (L/CWV_{ds})dI/dV_g \tag{4.3}$$

where L is the channel length, W the channel width. The thickness of the rubrene crystal has been assumed 2 μm for the device A, while measured by AFM as 800 nm for the device B; inserting those values in the relation reported above, the mobilities can be easily evaluated. In the Fig. 4-9 is indeed showed the variation of the mobility extracted from the transfer curves at different temperatures for the two devices. We can observe that it increases down to about 120 K and then it decreases. For the device B, in the first region it undergoes to an atypical behavior, which origin is unclear at the moment.

The mobility value and trend with temperature have been compared with the case of transistors realized with PMMA as a dielectric, having the same dielectric constant of rubrene.

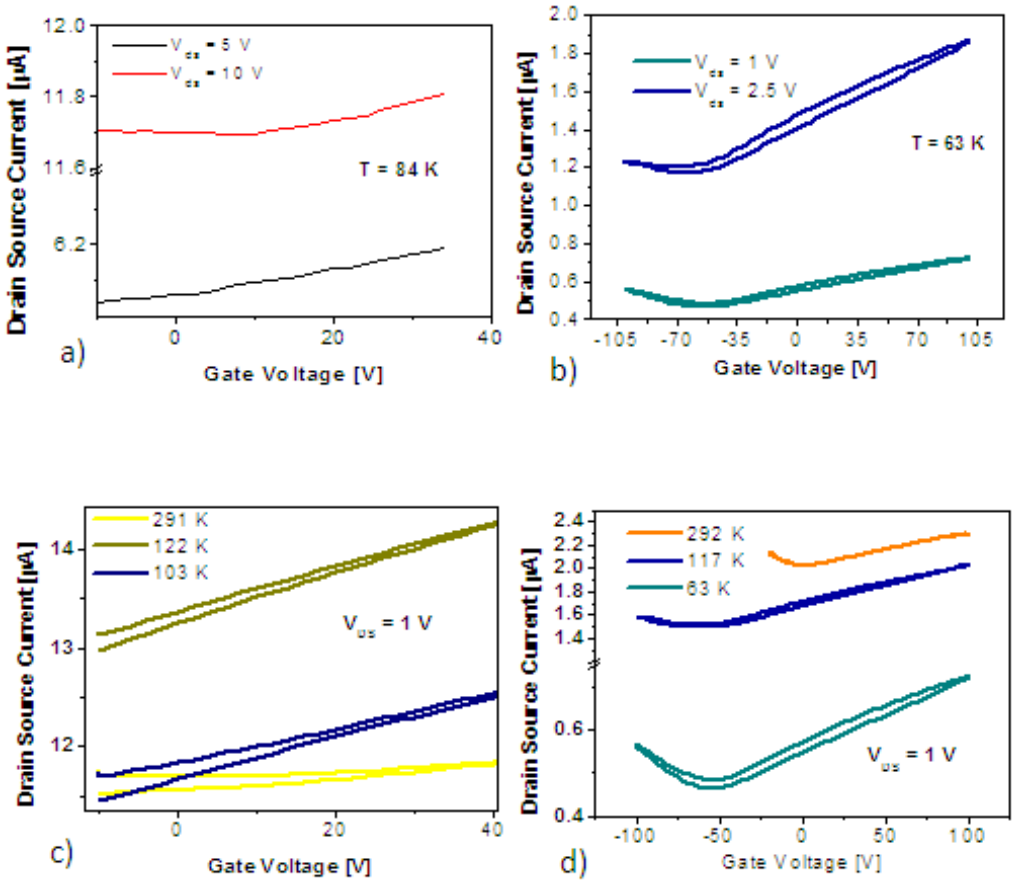

Figure 4-8: Transfer curves at different drain source voltages at a) 84 K for the device A and b) 63 K for the device B.

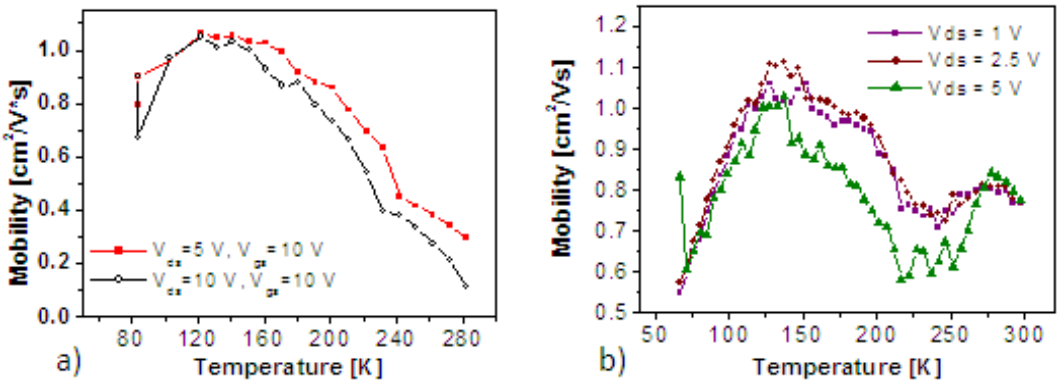

Figure 4-9: Mobility versus temperature extracted from the transfer curves at different temperatures a) for the device A and b) for the device B.

The similar mobility values at room temperature indicate that the analysis reported above is correct, also giving a further confirmation that the transport can be attributed to electrons. Moreover, this also suggests that crystals are not damaged during the fabrication procedure.

It is worth to underline that a band like behavior is also observable in the devices realized on air gap configuration, but that the range is less pronounced compared to the case of heterostructures, since the decrease is evident only up to 175 K [135].

Once determined the conductivity and the mobility, the density of carriers at zero gate can easily extracted by $n = \sigma/(\mu * e)$, simply dividing the two quantities. We can observe that it varies between 0.4 and 1.5 * 10^{13} cm^{-2} for the device A, while between 5 and 12 * 10^{13} cm^{-2} for the device B. In the device A the variation of the carrier density with temperature is minimal; the expected linear behaviour is verified only in the temperature range comprised between 130 K and 190 K, with a slope of 7.4*$10^{9}$$cm^{-1}K^{-1}$. For the device B the slope results instead 3.7*10^{10} $cm^{-1}K^{-1}$.

4.2.2 Hall effect measurements

Hall effect measurements are used in this work as an independent analysis to investigate the electrical behaviour of the devices realized, since the sign, the mobility and the density of charge carriers can be determined as a function of the temperature in addiction to the quantities extracted via field effect measurements. The configuration allowed the determination of both

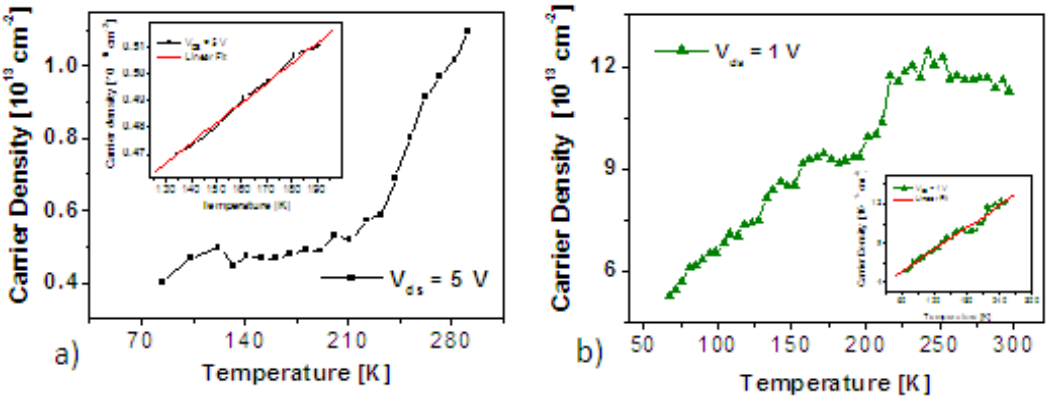

Figure 4-10: Carrier density determined from the square resistance at zero gate voltage and the mobility a) for the device A and b) B.

four probe and two probe resistance, which can be compared in order to exclude possible contact resistances effect. Hall effect measurements have been applied in the study of the carrier transport in organic semiconductors [102] [138], although the low density of carriers reduces the magnitude of the response to the application of the magnetic field and the high level of noise, especially at low temperatures, can mask it. Hall effect measurements on rubrene single crystals confirmed that charges can be highly delocalized in organic semiconductors, even if the mean free path is higher than the lattice constant; the Hall coefficient R_H resulted indeed equal to the induced surface charges estimated from the standard MOSFET model [138]. Also from Hall measurements on rubrene single crystals, a discrepancy between the field effect and the Hall mobility have been found between 175 and 250 K in rubrene single crystals. Since Hall effect gives the intrinsic mobility (i.e. trap free) it has been argued that at lowering temperatures the effect of the shallow traps underestimate the mobility values extracted by field effect measurements [102].

The contact configuration is reported in Fig. 4-11 a. A voltage (10 V) is applied to the drain in order to have current flowing in the channel, while the source is grounded. The magnetic field (sweeping between -6 and 6 T) is applied parallel to the sample. The probes 1 and 3 form an open circuit and are defined Hall probes. The potential difference between the two probes (V_3 - V_1) is the trasversal (Hall) voltage (V_H). In principle, also the couple of contact 2 and 3 can be used to measure the Hall voltage, but actually misalignment of the contacts

or disuniformities in the transistor channel can provoke the presence of voltage offsets. The potential difference between the probes 1 and 2 (longitudinal voltage) can be instead used to measure the four point resistance. The measured device clearly exhibits Hall effect, as can be observed for instance in Fig. 4-11 b, where the applied magnetic field is compared with the of the Hall voltage.

The extraction of the Hall voltage also requires the subtraction of the contribution due to the drift of the signal. The difference between the voltage values at the beginning and at the end of the measurement (both at zero magnetic field) gives an indication of the amount of drift; shaping the drift as a straight line, the relative contribution can be consequently easily calculated and subtracted.

The device was meaured down to 245 K; at lower temperatures the presence of a magnetoresistance effect [139] masked the Hall effect, rendering impossible the extraction of the Hall voltage and consequently of the other parameters. The origins of the magnetoresistance effect are not clear at the moment; a possible cause is a temperature gradient arising in the sample, such as in the case of the Nerst or the Righi-Leduc effects [140].

The sign of the Hall voltage confirms that the charge carriers are electrons. From the transversal voltage, the four point resistance is determined (Fig. 4-12 a). Both the two probe and the four probe resistance decrease with temperature, which indicates that the device is not affected by contact resistances. From the data reported in Fig. 4-11, the Hall mobility and the density of carriers are calculated (Fig. 4-12 b and c) from the following relationships [102]

$$R_H = \frac{1}{B}\frac{U_H}{l} \tag{4.4}$$

$$n_H = \frac{1}{eR_H} = \frac{Bl}{eR_H U_H} \tag{4.5}$$

$$\mu_H = R_H \sigma = \frac{1}{B}\frac{U_H}{l}\left(\frac{L^*}{H}\right) \tag{4.6}$$

n_H and μ_H monotonously increase and decrease with temperature, respectively. The density of carriers varies linearly with temperature, with a slope of $8{*}10^9 \mathrm{cm}^{-1}\mathrm{K}^{-1}$. This confirms the results obtained in the previous section, giving an independent measure of the same quantities and excludes the possibility of in the mobility extraction.

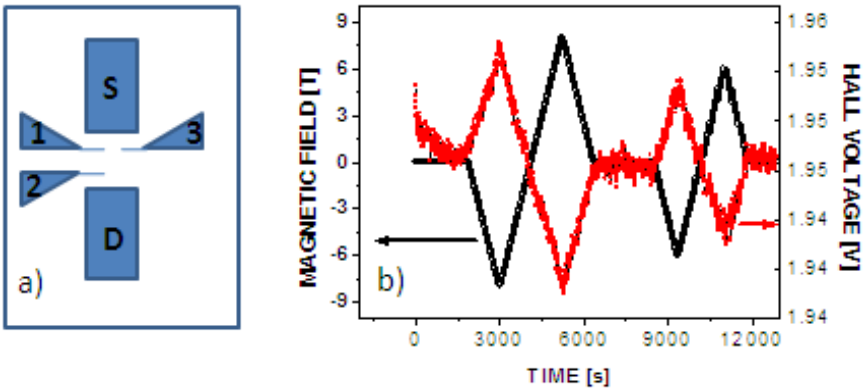

Figure 4-11: a) The contact geometry; S indicates the source while D the drain. The Hall voltage is determined as the difference between the voltage measured in 1 and 3 (Hall contacts) while 1 and 2 are the longitudinal contacts and are used to determine the four probe resistance. b) Hall measurements results at 291 K: the applied magnetic field (in black) and the measured Hall voltage (in red) versus time are plotted.

4.3 Band alignment in the Schottky Gated heterostructure

The extension of the range of band-like transport in PDI-FCN_2, the high density of carriers and its linear variation allow to conclude that the introduction of a Schottky gate causes an improvement of the charge transport properties of the devices, other than representing by itself an useful tool to tune of the carrier density and for the investigate of the fundamental physical properties at the heterointerface.

The slow variation of the carrier density with temperature suggest a completely different behavior respect to the previous ungated interfaces realized. Indeed, the interface between TTF-TCNQ exhibits a metallic behavior, with a constant or slightly decreasing resistance with temperature, which is easily explainable accounting for the overlapping of the valence and conduction band. A semiconducting behavior is instead attributed to the interface between TMTSF-TCNQ, exhibiting an exponentially increasing resistivity which activation energy corresponds to the gap between the LUMO level of TMTSF and the HOMO level of TCNQ (see Fig. 4-13).

The case of the Schottky gated heterostructures, with the slight dependence of the carrier density on the temperature, presents features that are ascribable to none of the previous ones,

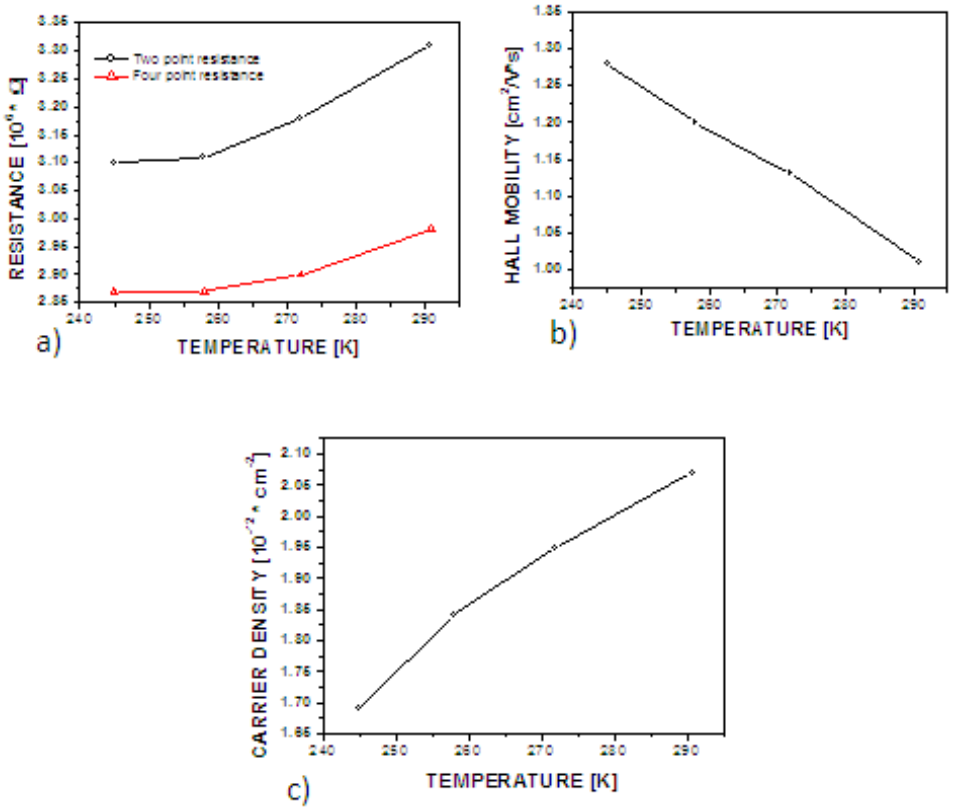

Figure 4-12: Some physical quantities extracted in function of temperature from the data in Fig. 4-11 a) Comparison between two point and four point resistance; b) Hall mobility; c) carrier density.

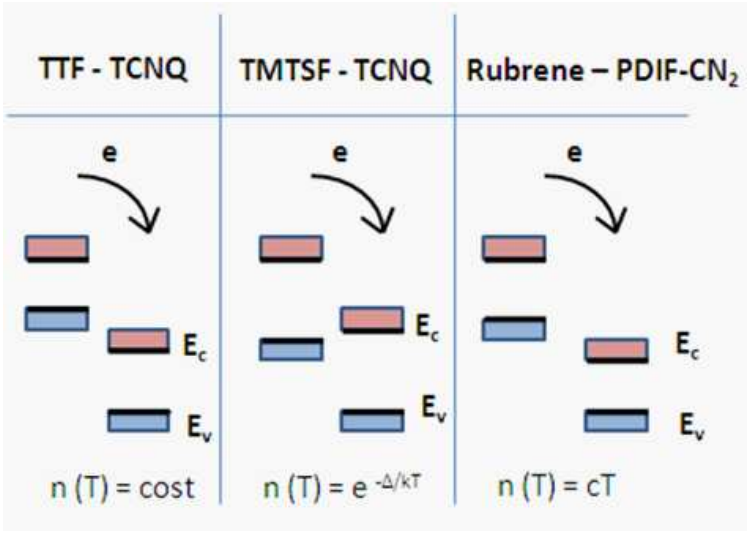

Figure 4-13: The comparison of the energetics of three different systems: TTF-TCNQ, TMTSF-TCNQ, rubrene-PDIF-CN_2.

accounting for the absence of a gap or the presence of a very small one. A realistic scenario explaining this occurrence can be easily depicted if we suppose that the HOMO level of rubrene and the LUMO level of PDI-FCN_2 were aligned before the two were put into contact. The scheme of the energy levels of the two semiconductors is reported in Fig. 4-13 in comparison with also TTF-TCNQ and TMTSF-TCNQ systems. Subsequently to the formation of the interface, a gap opens spontaneously as a consequence of the charge transfer, necessary to guarantee the uniformity of the chemical potential at the interface. An equal amount of charge carriers of both the charge types has to be transferred at the interface, in the first few layers of molecules or even only in the first one. This causes a dipole to arise, the opening of the energy gap being directly proportional to it.

Even if the presence of both electrons and holes is expected, only an n-type behavior has been observed in the transfer curves; this occurrence can be explained accounting for the presence of two contributes to the charge density, a surface and a bulk one. The first contribute is responsible for the formation of the dipole, while the other one arises from the uniformity of the chemical potential over the whole structure. The alignment of the chemical potential with that of chromium causes a redistribution of the bulk charge density and in particular an electron transfer from the PDI-FCN_2 to the rubrene, which fills the holes and reduces the hole density.

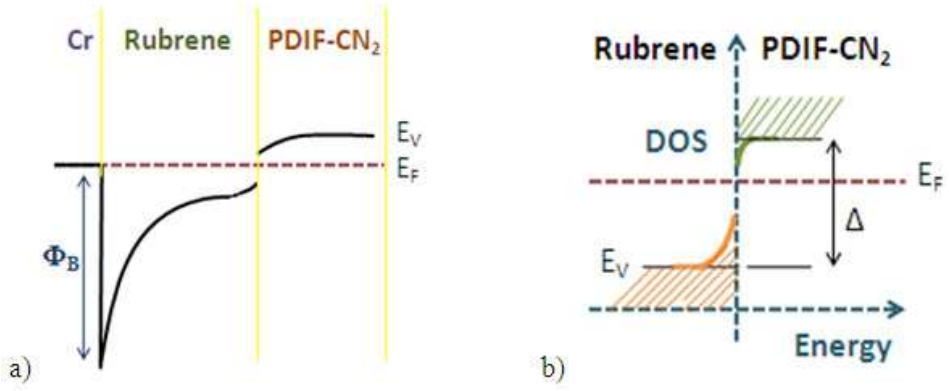

Figure 4-14: a) The energy bands in the device; b) a detail of the band bending at the heterointerface also reporting the dipole at the interface arising from the charge transfer ($\Delta = n_S e^2 d/\epsilon\epsilon_0$).

The resulting band diagram across the whole structure is the following one. The valence band of rubrene results to be far from the (common) Fermi level of a quantity that corresponds to the Schottky barrier that forms at the interface with chromium (0.8 – 1 eV). Far from the interface the distance between the conduction band in PDI-FCN_2 and the Fermi level reaches the bulk value, which depends on the concentration of unintentionally present dopants and can be estimated by measurements of the activation energy of the conductivity (about 100 – 120 eV).

The Fermi level of the structure will consequently result closer to the LUMO level of $PDIFCN_2$ than to the HOMO level of rubrene, and the electron conduction will result favored respect to the hole one.

At lowering temperatures, indeed, the carrier density transferred at the interface decreases and so the gap, directly proportional to it. On the other hand, the electron density in PDI-FCN_2 also decreases with temperature, pushing the LUMO level far from the chemical potential.

As a result, the LUMO level results close to the chemical potential even at lower temperatures, justifying the high mobility. The situation is different from the air gap FET, where a much larger decrease in mobility is observed with temperature, since in Schottky gated heterostructure the favorable energy level alignment at the interface maintain the position of the LUMO level in the region of shallow traps of PDI-FCN_2 even at low temperatures. The position of the PDI-FCN_2 LUMO level actually results "pinned" respect to the chemical potential, as

the high mobility at low temperatures suggests.

The conduction in the devices can be depicted in terms of the presence of an interface dipole (Δ) at the heterointerface, neglecting the contribute of the bulk charges. From simple electrostatic, the dipole at the interface is $\Delta = n_S e^2 d/\epsilon\epsilon_0$. The gap that forms after the two materials put into contact is equal to the potential arising from the presence of the dipole at the interface. Inserting this value into the expression of the charge carrier density as given in [56]

$$n_s = \int_{\Delta/2}^{\infty} 2N_S e^{-E/kT} dE \tag{4.7}$$

an equation for the charge carrier density is derived

$$n_s = 2N_S kT e^{-n_s e^2 d/\varepsilon\varepsilon_0 kT} \tag{4.8}$$

where N_S is the density of states at the surface per unit energy ($2*10^{15}$ $cm^{-2}eV^{-1}$) and is almost the same for rubrene and PDI-FCN_2. The equation reported can be solved self consistently. Defining

$$y = n_S/2N_S kT \tag{4.9}$$

we obtain an equation that is now independent by the temperature. Defining

$$y = e^{-N_S e^2 dy/\epsilon\epsilon_0}$$

if we now indicate with y* the solution of the previous equation, this gives the expression of the carrier density with time

$$n_s = y^* 2N_S kT \tag{4.10}$$

which actually predicts a linear temperature dependence of the carrier density. The equation gives an estimation of the slope of the carrier density versus temperature ($y^* = 0.029$) which is in good agreement with the experimental data (see the par. 4.2.1, in particular for the device A, the par. 4.2.2 and [136]). This indicates also that the transport properties at the interface are only determined by the band alignment.

The device B exhibits instead an atypical behavior respect to the other devices realized during the experimental project, since the mobility results indeed lower while the carrier density

higher. This behavior is actually expected if the thickness of the rubrene single crystal is thin enough to make the effect of the alignment with the cromium chemical potential more effective. This is indeed the case, since the thickness of the rubrene crystal results to be 800 nm, while in the other devices is closer to 2 μm [136].

The thinner the rubrene crystal, the lower is expected to lie the top of the rubrene valence band at the interface with PDI-FCN_2, since it falls deeper in the depletion region of the Schottky barrier with chromium. As a consequence, at the heterointerface holes are for sure completely depleted in the rubrene crystal, but a more pronounced band bending and a higher electron density is consequently expected.

It cannot be excluded that in favorable conditions (i.e. depending on the level of dopants unintentionally present in both the semiconductors) and with a thinner rubrene crystal, even a metallic behavior can be achieved.

4.4 Conclusion

Tuning of the charge carrier density at the interface between two organic semiconductors was achieved thanks to the realization of Schottky gated heterostructure transistors. My experimental work consisted in the realization of micrometric scale devices by a sequence of steps, including lamination of single crystals by hand on a flexible PDMS substrate, photolitography, bonding. The devices showed n-type behaviour, indicating an accumulation of electrons at the heterointerface which density have been modulated by applying a voltage to the Cr Schottky gate. They also exhibited a metallic-like behaviour, with a decreasing of the field effect mobility at lowering temperature; this suggests that the chemical potential of the structure is close to the PDI-FCN_2 LUMO level. The carrier density exhibited instead a linear variation with the temperature, which is an indication of the absence of the gap or the presence of a very small one.

Conclusive remarks

In this PhD work, the realization and characterization of organic thin film and single crystal heterostructure field effect devices have been devepoled. Given the high electrical instability of n-type semiconductors, a study of high performing perilene diimides compounds has been led, mainly devoted to the individuation of the most suitable compound.

N,N'- bis (n-octyl) -2- cyanonaphthalene -1,4,5,8- bis (dicarboximide) (NDI-8CN), N,N'- bis (n-octyl) -2,6- dicyanonaphthalene -1,4,5,8-bis (dicarboximide) (NDI-8CN_2) , N,N'-bis (n-octyl) -1,7- and N,N'- bis (n-octyl) -1,6- dibromoperylene -3,4:9,10-bis -(dicarboximide) (PDI-8Br_2), N,N'- bis(n-octyl) - 1,6,7,12 -tetrachloroperylene -3,4:9,10- bis(dicarboximide) (PDI-8Cl_4) have been considered. PDI-8 exhibits high electrical performances in vacuum, but the environmental conditions highly degrade the device response. PDI-8CN_2 and PDI-FCN_2 are instead both air-stable while also show high drain source current and mobility. PDI-FCN_2 has been used for the realization of thin film transistors with a mobility of 0.6 cm^2/Vs (the highest value found in the literature for top contact devices) and almost bias stress independent single crystal FETs (experiencing a I_{DS} decrease of much less than 1% after 5000 s) have been realized. Even if the best electrical performances belong to , it results affected by the substrate conditions (in thin film form, mainly) regarding morphological and electrical properties, hindering its use for thin film heterostructure, but not for single crystal interfaces.

Sexithiophene (T6)/N,N'-bis (n octyl)-dicyanoperylenediimide (PDI-8CN_2) thin film heterostructures have been used as the active channel in field effect transistors. The devices exhibited several interesting features, such as ambipolar behaviour and charge transfer at the heterointerface with a consequent improvement in the electrical performances and in particular in the conduction. A negative transconductance (NTC) effect consisting in a sudden decrease of the drain current for high negative gate voltages have been found and deeply investigated through different device configurations and varying the thickness of the lower layer of the heterostructure. The results have been corredated and confirmed by also X-ray and AFM analysis.

Schottky-gated heterostructures based on rubrene and PDI-FCN_2 single crystal interfaces have been fabricated. The formation of a depletion region due to the Schottky barrier covering the while rubrene thickness allows the injections by field effect of one type of charge carriers (electrons) at the interface. Evidences of band-like behaviour and a linear density of carrier

have been found through electrical analysis and confirmed by Hall effect measurements. The occurrence has been explained suggesting that a small gap forms as a consequence of the transfer of charges at the heterointerface and the equilibration of the potential in the whole device structure.

Bibliography

[1] Alan J. Heeger, Nobel Lecture: Semiconducting and metallic polymers: The fourth generation of polymeric materials, Rev.Mod. Phys., vol. 73 (2001).

[2] F. Garnier, A. Yassar, R. Hajlaoui, G. Horowitz, F. Deloffre, B. Servet,S. Ries, P. Alnot, J. Am. Chem. Soc. 115, 8716 (1993).

[3] A . Facchetti Materials Today 29 10 (2007).

[4] G. Horowitz, Organic Electronics, edited by H.Klauk, Wiley WCH Verlag GmbH e Co. KGaA.

[5] D.M. de Leeuw , M.M.J. Simenon, A.R. Brown, R.E.F. Einerhand, Synthetic Metals 87, 53 (1997).

[6] A.R. Brown, D.M. de Leeuw, E.J. Lous, E.E. Havinga Synthetic Metals 66, 257 (1994).

[7] Jana Zaumseil and Henning Sirringhaus Chem. Rev. 107, 1296 (2007).

[8] Christos D. Dimitrakopoulos and Patrick R. L. Malenfant Adv. Mater. 14, 2, (2002).

[9] http://www.trendsderzukunft.de/sony-armband-pc-mit-flexiblen-oled-touch-display/2010/05/26/.

[10] Lay-Lay Chua, Jana Zaumseil, Jui-Fen Chang, Eric C.-W. Ou, Peter K.-H. Ho, Henning Sirringhaus, Richard H. Friend 434, 194, (2005).

[11] Brooks A. Jones, Michael J. Ahrens, Myung-Han Yoon, Antonio Facchetti, Tobin J. Marks, and Michael R. Wasielewski, Angew. Chem. Int. Ed. 43, 6363 (2004).

[12] Brooks A. Jones, Antonio Facchetti, Michael R. Wasielewski, and Tobin J. Marks Adv. Funct. Mater. 2008, 18, 1329–1339 (2008).

[13] H. Z. Chen, M. M. Ling, X. Mo, M. M. Shi, M. Wang, and Z. Bao Chem. Mater. 2007, 19, 816.

[14] Anna S. Molinari, Helena Alves, Zhihua Chen, Antonio Facchetti and Alberto F. Morpurgo J.Am.Chem.Soc. 131 2462 (2009).

[15] R. Thomas Weitz, Konstantin Amsharov, Ute Zschieschang, Esther Barrena Villas, Dipak K. Goswami, Marko Burghard, Helmut Dosch, Martin Jansen, Klaus Kern, and Hagen Klauk. J. Am. Chem. Soc. 2008, 130, 4637.

[16] Mang-Mang Ling, Peter Erk, Marcos Gomez, Martin Koenemann, Jason Locklin, and Zhenan Bao Adv. Mater. 2007, 19, 1123.

[17] Brooks A. Jones, Antonio Facchetti, Michael R. Wasielewski, and Tobin J. Marks J. Am. Chem. Soc. 2007, 129, 15259.

[18] S.M. Sze, K.K. Ng, Physics of Semiconductor Devices, Wiley, 3rd edition.

[19] C. H. Ahn, A. Bhattacharya, M. Di Ventra, J. N. Eckstein, C. Daniel Frisbie, M. E. Gershenson, A. M. Goldman, I. H. Inoue, J. Mannhart, Andrew J. Millis, Alberto F. Morpurgo, Douglas Natelson, Jean-Marc Triscone Rev. of Mod. Phys. 78, (2006).

[20] H. Luth Surfaces and Interfaces of solids, Springer-verlag Second edition.

[21] R. Dingle, H. L. Stormer, A. C. Gossard, and W. Wiegmann 33, 665 (1958).

[22] Electronic Letters, 16, 667 (1980).

[23] Wei Chen, Dongchen Qi, Xingyu Gao, Andrew Thye Shen Wee Progress in Surface Science 84, 279 (2009).

[24] Y. Abe, T. Hasegawa, Y. Takahashi, T. Yamada, and Y. Tokura, Appl. Phys. Lett. 87 153507 (2005).

[25] Electronic Properties of Surfaces, M. Prutton, Adam Hilger Ltd, Bristol 1984.

[26] H. Ishii, K. Sugiyama, E. Ito, K. Seki, Energy level alignment and interfacial electronic structures at organic/metal and organic/organic interfaces, Adv. Mater. 11, 605, (1999).

[27] A. Kahn, N. Koch, W. Gao, Electronic structure and electrical properties of interfaces between metals and p-conjugated molecular films, J. Polym. Sci., Part B: Polym. Phys. 41, 2529 (2003).

[28] A.K.D. Cahen, Electron energetics at surfaces and interfaces: concepts and experiments, Adv. Mater. 15, 271 (2003).

[29] N. Koch, Organic electronic devices and their functional interfaces, Chem. Phys. Chem. 8 (2007) 1438–1455.

[30] N. Koch, A. Elschner, J.P. Rabe, R.L. Johnson, work function independent hole-injection barriers between pentacene and conducting polymers, Adv. Mater. 17, 335 (2005).

[31] G. Horowitz J. Mater. Chem., 9, 2021 (1999).

[32] Gilles Horowitz, Adv. Mater. 5, 365 (1998).

[33] G. Horowitz, J. Mater. Res., 7, 1946 (2004).

[34] Gilles Horowitz, Mohsen E. Hajlaoui, and Riadh Hajlaoui jap 87 4456 (2000).

[35] S. G. J. Mathijssen, M. Cölle, H.L. Gomes, E.C.P. Smits, B. de Boer, I. McCulloch, P.Bobbert, D. de Leeuw, Adv.Mat. 19, 2785 (2007).

[36] H.L. Gomes, P. Stallinga, F. Dinelli, M. Murgia, F. Biscarini, D. M. de Leeuw, M. Muccini and K. Mullen, Polym. Adv. Technol. 16, 227 (2005).

[37] T. Miyadera, S. D. Wang, T. Minari, K. Tsukagoshi, and Y. Aoyagi, Appl. Phys. Lett. 93, 033304 (2008).

[38] R.B. Wehrspohn, S.C. Deane, I.D, French, I. Gale, J. Hewett, M. J. Powell, J. Robertson, J. Appl. Phys. 87, 144 (2000).

[39] R. B. Wehrspohn, S.C. Deane, I.D. French, M.J. Powell, J. Non-Cryst. Solids 266, 459 (2000).

[40] D. Knipp, R.A. Street, A. Volkel and J. Ho, J.Appl. Phys. 93, 347 (2003).

[41] K.Suemori, S. Uemura, M. Yoshida, S. Hoshino, N. Takada, T. Kodzasa and T. Kamata, Appl. Phys.Lett. 93, 033308 (2008).

[42] A. Benor, A. Hoppe, V. Wagner, D. Knipp, Organic Electronics 8, 749 (2007).

[43] T. Richards and H. Sirringhaus, Appl.Phys.Lett. 92, 023512 (2008).

[44] S. D. Wang, T. Minari, T. Miyadera, Y. Aoyagi and K. Tsukagoshi, Appl.Phys.Lett. 92, 063305 (2008).

[45] A. Sharma, S. Mathijssen, E. Smits, M. Kemerink, D. de Leeuw, and P. Bobbert, Phys. Rev. B 82, 075322 (2010).

[46] A. Sharma, S. G. J. Mathijssen, T. Cramer, M. Kemerink, D. M. de Leeuw, and P. A. Bobbert, Appl. Phys. Lett. 96, 103306 (2010).

[47] B. Lee, A. Wan, D. Mastrogiovanni, J. Anthony, E. Garfunkel, and V. Podzorov, Phys. Rev. B 82, 085302 (2010).

[48] Mathijssen, S. G. J.; Kemerink, M.; Sharma, A.; Cölle, M.; Bobbert, P. A.; Janssen, R.A. J.; de Leeuw, D. M. Adv. Mater. 20, 975 (2008).

[49] Toshihiko Kaji, Taishi Takenobu, Alberto F. Morpurgo, and Yoshihiro Iwasa, Adv. Mater. 21, 3689 (2009).

[50] Herbert Kroemer Rev. of Mod. Phys. 73 783 (2001).

[51] H.Kroemer, G. Griffiths, ieee electron devices letter 1, 20 , 1983.

[52] H. Kroemer Surface Science 132 (1983) 543-576.

[53] S. Fratini and S. Ciuchi Phys. Rev. Lett. 103, 266601 (2009).

[54] A. Troisi and G. Orlandi, J. Phys. Chem. A, 110, 4065 (2006).

[55] H. Alves, A. S. Molinari, H. Xie & A. F. Morpurgo, Nature Materials 7, 574 (2008).

[56] M. Nakano, H. Alves, A. S. Molinari, S. Ono, N. Minder,and A. F. Morpurgo Appl. Phys. Lett. 96, 232102 (2010).

[57] A. Dodabalapur, H.E. Katz, L.Torsi, R.C. Haddon, Science 269, 1560 (1995).

[58] A. Dodabalapur, H.E. Katz, L.Torsi, R.C. Haddon, Appl. Phys. Lett. 68, 1108 (1996).

[59] N. Koch, C. Chan, A. Kahn and J. Schwartz, Phys. Rev. B, 67, 195330, (2003).

[60] Y. Harima, K. Yamashita, H. Ishii, and K. Seki, Thin Solid Films 366, 237 (2000).

[61] E. Ito, Y. Washizu, N. Hayashi, H. Ishi, N. Matsuie, K. Tsuboi, Y. Ouchi, Y. Harima, K. Yamashita, K. Seki, J. Appl. Phys. 92, 7306 (2002).

[62] H. Fukagawa, S. Kera, T. Kataoka, S. Hosoumi, Y. Watanabe, K. Kudo, and N. Ueno, Adv. Mater. 19, 665 (2007).

[63] S. Kera, Y. Yabuuchi, H. Yamane, H. Setoyama, K. K. Okudaira, A. Kahn, and N. Ueno, Phys. Rev. B, 70, 085304 (2004).

[64] P. S. Bagus,V. Staemmler and C. Woll, Phys. Lett. , 89, 096104-1, (2002).

[65] J. Hwang , A. Wan, A. Kahn, Materials Science and Engineering R 64,1 (2009).

[66] J. G. Champlain, Appl. Phys. Lett. 99, 123502 (2011).

[67] B. Crone, A. Dodabalapur, Y.-Y. Lin, R. W. Filas, Z. Bao, A. LaDuca, R. Sarpeshkar H. E. Katz & W. L NATURE, 403, 521 (2000).

[68] Dieter Bode, Kris Myny, Bregt Verreet, Bas van der Putten,Petar Bakalov, Soeren Steudel Steve Smout, Peter Vicca, Jan Genoe, and Paul Heremans Appl. Phys. Lett. 96, 133307 (2010)

[69] Tse Nga Ng , Sanjiv Sambandan, Rene Lujan, Ana Claudia Arias,Christopher R. Newman, He Yan , and Antonio Facchetti Appl. Phys. Lett. 94, 233307 (2009).

[70] Jeremy Smith, Richard Hamilton, Martin Heeney, Dago M. de Leeuw, Eugenio Cantatore, John E. Anthony, Iain McCulloch, Donal D. C. Bradley, and Thomas D. Anthopoulos, Appl.Phys.Lett 93, 253301 (2008).

[71] W. S. C. Roelofs,S. G. J. Mathijssen, J. C. Bijleveld, D. Raiteri, T. C. T. Geuns, M. Kemerink, E. Cantatore, R. A. J. Janssen, and D. M. de Leeuw, Appl. Phys. Lett. 98, 203301 (2011).

[72] Eiji Kuwahara, Yoshihiro Kubozono, Tomoko Hosokawa,Takayuki Nagano, and Kosuke Masunari, Akihiko Fujiwara, Apl 85 4765 (2004).

[73] G. Paasch and Th. Lindner, C. Rost-Bietsch, S. Karg, and W. Riess, S. Scheinert, J. of Appl. Phys. 98, 084505 (2005).

[74] Y. Wen and . Liu, Adv. Mater. 22, 1 (2010).

[75] Rost, C.; Karg, S.; Riess, W.; Loi, M. A.; Murgia, M.; Muccini, M. Appl. Phys. Lett. 85, 1613 (2004).

[76] R. Schmechel, M. Ahles, H. von Seggern, J. of Appl. Phys. 98 084511 (2005).

[77] Zaumseil, J.; Friend, R. H.; Sirringhaus, H. Nat. Mater. 5, 69 (2006).

[78] Haibo Wang and Donghang Yan NPG Asia Mater. 2, 69 (2010).

[79] H. Wang, J. Wang, H. Huang, X. Yan, D. Yan, Organic Electronics 7, 369 (2006).

[80] K. M. Lau, J. X. Tang, H. Y. Sun, C. S. Lee, and S. T. Lee Donghang Yan Appl. Phys. Lett. 88, 173513 (2006).

[81] Feng Zhu, Haibo Wang, De Song, Kun Lou, and Donghang Yan Appl. Phys. Lett. 93, 103308 (2008).

[82] ShanYuQuan, LinmeiYang, FengTeng, ZhengXu, Yongsheng Wang Physica B 405 469 (2010).

[83] Tomo Sakanoue, Toru Irie, and Chihaya Adachi J. of Appl. Phys. 105, 114502 (2009).

[84] Steffen Duhm, Georg Heimel, Ingo Salzmann, Hendrik Glowatzki, Robert L. Johnson, Antje Vollmer, Jürgen P. Rabe, Norbert Koch, Nature Materials 7, 326 (2008).

[85] Jianwu Shi, Haibo Wang, De Song, Hongkun Tian, Yanhou Geng, and Donghang Yan Adv. Funct. Mater. 17, 397 (2007).

[86] R. Hayakawa, M. Petit, T. Chikyow, and Y. Wakayama, Appl. Phys. Lett. 93, 153301 (2008).

[87] M.F. Calhoun, J. Sanchez, D. Olaya, M.E. Gershenson, V. Podzorov, Electronic functionalization of the surface of organic semiconductors with self-assembled monolayers, Nat. Mater. 7, 84 (2008).

[88] J. L. Yang, D. H. Yan Chem Soc.Rev. 38, 2634 (2009).

[89] Lizhen Huang, Feng Zhu, Chengfang Liu, Haibo Wang, Yanhong Geng, Donghang Yan Organic Electronics 11 (2010) 195–201

[90] H. Wang, F. Zhu, J. Yang, Y. Geng, D. Yan Adv. Mater. 19 2168 (2007)

[91] Feng Zhu, Haibo Wang, De Song, Kun Lou, and Donghang Yan Appl. Phys.Lett. 93, 103308 (2008).

[92] Feng Zhu, Kun Lou, Lizhen Huang, Jianbing Yang, Jidong Zhang, Haibo Wang, Yanhou Geng, and Donghang Yan Appl. Phys. Lett. 95, 203106 (2009).

[93] Nobuya Hiroshiba, Ryoma Hayakawa, Matthieu Petit, Toyohiro Chikyow, Kiyoto Matsuishi, Yutaka Wakayama, Organic Electronics 10 1032 (2009).

[94] Colin Reese and Zhenan Bao Materials Today, 10, 20 (2007).

[95] R. W. I. de Boer, M. E. Gershenson, A. F. Morpurgo, and V. Podzorov phys. stat. sol. (a) 201, No. 6, 1302 (2004).

[96] Alejandro L. Briseno, Ricky J. Tseng, Mang-Mang Ling, Eduardo H. L. Falcao, Yang Yang, Fred Wudl, and Zhenan Bao Adv. Mater. 18, 2320 (2006).

[97] V. Y. Butko, X. Chi, D. V. Lang, and A. P. Ramirez, Appl. Phys. Lett. 83, 4773, (2003).

[98] R. W. I. de Boer T. M. Klapwijk, and A. F. Morpurgo Appl. Phys. Lett. 83, 4345 (2003).

[99] V. Podzorov, V. M. Pudalov, M. E. Gershenson, Appl. Phys. Lett. 82, 1738 (2003).

[100] A. F. Stassen, R. W. I. de Boer, N. N. Iosad, and A. F. Morpurgo, Appl. Phys. Lett. 85, 3899, (2004).

[101] I. N. Hulea, S. Fratini, H. Xie, C. L. Mulder, N. N. Iossad, G. Rastelli, S. Ciuchi, A. F. Morpurgo Nature Materials, 5, 982 (2006).

[102] V. Podzorov, E. Menard, A. Borissov, V. Kiryukhin, J. A. Rogers, and M. E. Gershenson Phys. Rev. Lett. 93 086602-1 (2006).

[103] Iulian N. Hulea,Saverio Russo, Anna Molinari, and Alberto F. Morpurgo Appl. Phys. Lett. 88, 113512 (2006).

[104] Anna Molinari, Ignacio Gutiérrez, Iulian N. Hulea, Saverio Russo, and Alberto F. Morpurgo, Appl. Phys. Lett. 90, 212103 (2007).

[105] D.Braga, M.Campione, A. Borghesi, G. Horowitz, Adv. Mater. 22, 424 (2010).

[106] C. D. Dimitrakopoulos, P. R. L. Malenfant Adv. Mater. 14, 99 (2002).

[107] Organic Field-Effect Transistors. Edited by Zhenan Bao and Jason Locklin. CRC Press 2007.

[108] F. Biscarini, P. Samorı, O. Greco, and R. Zamboni Physical Review Letters, vol. 78, 2389, 1997.

[109] G. Palasantzas, Physical Review B, vol. 48, p. 14472, 1993

[110] M. Riccio, A. Irace, G. Breglio, L. Rossi, M. Barra, F.V. Di Girolamo and A. Cassinese Appl. Phys.Lett. 93, 243504 (2008).

[111] F.V. Di Girolamo, C. Aruta, M. Barra, P. D'Angelo, A. Cassinese Appl Phys A 96, 481 (2009).

[112] R. A. Laudise, Ch. Kloc, P. G. Simpkins and T. Siegrist, J. Cryst. Growth 187, 449 (1999).

[113] S. Ono, N. Minder, Z. Chen, A. Facchetti, and A. F. Morpurgo, Appl. Phys. Lett. 97, 143307 (2010).

[114] M. P. Walser, W. L. Kalb, T. Mathis, and B. Batlogg, Appl. Phys. Lett.

[115] M. Barra, F. V. Di Girolamo, F. Chiarella, M. Salluzzo, Z. Chen, A. Facchetti, L. Anderson, A. Cassinese J. Phys. Chem. C 114, 20387 (2010).

[116] F. Chiarella, M. Barra, A. Cassinese, F.V. Di Girolamo, P. Maddalena, L. Santamaria, S. Lettieri Appl Phys A 104, 39 (2011).

[117] R. Häuserman, B. Battlogg, Appl. Phys Lett. 99, 083303 (2011).

[118] AC. Hosokawa et al., Appl. Phys. Lett. 62, 3228 (1993).

[119] F.V. Di Girolamo, M. Barra, F. Chiarella, S. Lettieri, M. Salluzzo, A. Cassinese, Ambipolar transport and charge transfer at the interface between Sexithiophene (T6) and N,N'-bis (n-octyl)- dicyanoperylenediimide (PDI-8CN_2) films, submitted to Physical Review B.

[120] T. Jung, B. Yoo, L. Wang, A. Dodabalapur, B. A. Jones, A. Facchetti, M. R. Wasielewski, and T. J. Marks, Appl. Phys. Lett. 88, 183102 (2006).

[121] V. Tkachenko, F. V. Di Girolamo, F. Chiarella, A. Cassinese, and G. Abbate, in press in Thin Solid Films, DOI: 10.1016/j.tsf.2011.09.075.

[122] F. Dinelli, M. Murgia, P. Levy, M. Cavallini, F. Biscarini, D.M. DeLeeuw, Phys. Rev. Lett.92, 116802 (2004).

[123] F.V.Di Girolamo, M.Barra, P.V. Capello, M.Oronzio, C. Romano and A.Cassinese, J. Appl. Phys. 107, 114508 (2010).

[124] G. Garcia-Belmonte, P. P. Boix, J. Bisquert, M. Lenes, H. J. Bolink, A. La Rosa, S. Filippone, and N. Martín J. Phys. Chem. Lett. 1, 2566, 2010.

[125] K.R. Kim, H.H. Kim, K.-W. Song, J.I Huh, J.D. Lee, IEEE Trans. of Nanotechnology 4, 317 (2005).

[126] K.R. Kim, D.H. Kim, K.-W. Song, J. Baek, H.H. Kim, J.I Huh, J.D. Lee, IEEE Electr. Dev. Lett. 25, 439 (2004).

[127] C. Liu, H. Sirringhaus, Organic Electronics 11 558 (2010).

[128] I. Gutierrez Lezama and A. F. Morpurgo Phys. Rev. Lett. 103, 066803 (2009).

[129] M. Yamagishi, J. Takeya, Y. Tominari, Y. Nakazawa, T. Kuroda, S. Ikehata, M. Uno, T. Nishikawa, and T. Kawase, Appl. Phys. Lett. 90, 182117 (2007).

[130] D. Braga, N. Battaglini, A. Yassar, and G. Horowitz Phys. Rev. B 77, 115205 (2008).

[131] V. Y. Butko, J. C. Lashley, and A. P. Ramirez Phys.Rev.B 72, 081312 (R), (2005).

[132] V. Podzorov, E. Menard, J. A. Rogers, and M. E. Gershenson, Phys. Rev. Lett. 95, 226601 (2005).

[133] J.H Seo, T.M. Pedersen, G.S. Chang, A. Moewes, K. – H. Yoo, S. J. Cho. C. N. Whang, J. Phys. Chem. B 111, 9513 (2007).

[134] Zhang Z.L. Jiang X.-Y., Xu S.-H., Nagatomo T., Omoto O., J.Phys. D: Appl.Phys. 31, 32 (1998).

[135] Minder, N., Ono, S., Facchetti, A. & Morpurgo, A. F. Band-like transport in n-type organic field-effect transistors. Submitted to Advanced Materials.

[136] Ignacio Gutiérrez Lezama, Masaki Nakano, Zhihua Chen, Flavia V. Di Girolamo, Antonio Facchetti and Alberto. F. Morpurgo, Transport Properties and Electronic Structure of Organic Charge-Transfer Interfaces probed using Schottky-Gated Heterostructures. Submitted to Nature.

[137] M. Kaya, H. Cetin, B.Boyarbay, A. Gok, E. Ayylidiz, J. Phys.: Condes. Matter. 19 406205 (2007).

[138] Jun Takeya, Kazuhito Tsukagoshi, Yoshinobu Aoyagi, Taishi Takenobu and Yoshihiro Iwasa Jap. J. of Appl. Phys. (2005).

[139] M. Nishioka, Yeon-Bae Lee, A. M. Goldman, Yu Xia, and C. D. Frisbie, Appl. Phys. Lett. 91, 092117 (2007).

[140] O. Lindberg Proceedings of the I.R.E. 1414 1952.

Acknowledgments

My PhD work has been developed thanks to the collaboration and the support of a large group of people, who have influenced in different ways my personal and scientific improvement.

I would like to thank Antonio Cassinese, because as my PhD tutor he did everything was possible to give me the opportunity to get in touch with different scientific realities and widen my points of view. Mario Barra has always accompained me for coffees and "philosophical" discussions, indefatigably corrected my hypothesis, my thesis, my articles, my abstracts, my contributions, my posters, my speechs, suggested me articles and books (not only scientific!). Marco Salluzzo has for sure represented the "most physical side" of my thesis, a great help for me, being not a phisicist at all...but maybe it could understand me much better than other because he has "the enemy" (a material engineer, like me) in his house, Daniela Stornaiuolo ! Roberto Di Capua has instead been my "confessor" and introduced me to football and other various board and not-board games, included the one that is commonly named "team work". Stefano Lettieri has been so patient with my stubborn doubts on semiconductor physics, Fabio Chiarella with the Atomic Force Microscopy, Gabriella Maria De Luca with x-ray and Vladimir Tkachenko with optical measurements. Furthermore, I have always felt from above the supervision of Ruggero Vaglio, even when his duties took him far from Naples.

Angelica Grimaldi, Daniele Preziosi and Francesca Santoro have been worthy fellow travellers in part of this way, and I hope that we will always be, even in different manners and places. Guido Celentano has always been an impeccable, hard working, affable referement.

Part of this work has been developed at the Department of Condensed Matter Physics of the University of Geneva, in collaboration with Prof. Alberto Morpurgo, Ignacio Gutierrez Lezama and Nikolas Minder. Without their help and their support the realization of PDI-FCN_2 Single Crystal Transistors and Schottky gated heterostructures would have never been

possible. Alberto Morpurgo has not even being my tutor, but he always gave me clear and patient suggestions and explanations, he always supported me and the presence, but mostly for being exacting, hard and impatient when necessary. I thank Nacho for the things I am aware of, but mostly for those I am not...and of course, for piñacolada! Niko...I'll tell you what I though to write personally... Sandra for her never stopping, never giving up, her constant support and encouragement. Anya for her imagination, for the coffees together and for being the main responsible of my restyling... Nuno for at the right time saying the right thing, doing the right thing, being at the righ place....and also when he was not. Daniele for reminding where do I come from. Ki for his infinite patience and Jo for his questions. Fabio because...he has "stolen" my "first place" in Geneva. And of course, Alex, mostly for his "trip-organizing" skills.

I thank my sister, simply because she shared my same room and my complainings for years. I thank my whole family always showing me unconditional support. I thank my old and new friends, Paolo, Miriam, Giorgio, Simone, Daniela Di Rienzo, Davide (I promise to always try to do good things, as you asked), Angela e Fo, the guys of the Orchestra Antonio Izzo, Rinascita Calena, Libreria 80 mq, La Città del Sole, Annalisa and Marco, Lella and Gino, Giovanna and Valerio. I will alway keep in mind the nice memories shared in the foyer with Enrica, Emmanuele e Giancarlo, MartAle, Giusy e Remy, Jelica, Rim, Swansen, Henan....I thank all the people I have met in the stations, trains, airports, planes, buses, streets, during my trips forth and back.

Last but not least, I thank Ketty, because she unexpectedly understood being my only possible company in these long nights writing this thesis.